UNIVERSITÀ DI PARMA

UNIVERSITA' DEGLI STUDI DI PARMA

DOTTORATO DI RICERCA IN

"*Medicina Molecolare*"

CICLO XXXIV

Set-up and characterization of an iPSC-derived neurocardiac co-culture model

Coordinatore:

Chiar.mo Prof. Prisco Mirandola

Tutore:

Chiar.mo Prof. Donatella Stilli

Dr. Alessandra Rossini

Dr. Alessandra Zanon

Dottoranda: Giada Cattelan

Anni Accademici 2018-2021

The data, results, methods and other information contained and/or described in this doctoral thesis shall be subjected to a 24-months embargo period from the date of its deposit in “Dspace Unipr” as they are part of a larger study already initiated by Eurac Research. The entire thesis shall however to be considered strictly confidential from the beginning of its revision also by the designated reviewers.

1 INDEX

1.1 Table of Contents

1.2 Table of Figures

1.3 Tables

2 ABBREVIATION LIST

2D: two-dimensional

3D: three-dimensional

AA: ascorbic acid

ACM: arrhythmogenic cardiomyopathy

AF: atrial fibrillation

ANS: autonomic nervous system

AP: action potential

APh: alkaline phosphatase

ATP: adenosine triphosphate

BCA: Bicinchoninic Acid

BMP: bone morphogenetic protein

BSA: bovine serum albumin

c_iPSCs: Commercial iPSC line

Ca_{2+}: calcium

cAMP: cyclic-AMP

CANS: cardiac autonomic nervous system

cDNA: complementary DNA

CMs: cardiomyocytes

CPTV: catecholaminergic polymorphic ventricular tachycardia

cTnI: cardiac Troponin I

Cu_{1+}: cuprous cation

$CuSO_4$: copper sulfate

CX43: Connexin 43

DBH: dopamine beta hydroxylase

DBH: dopamine beta hydroxylase

DMSO: Dimethyl Sulfoxide

dNTPs: deoxy-nucleotide-tri-phosphate

EBs: embryoid bodies

ECG: electrocardiogram

ECM: extra cellular matrix

ECs endothelial cells

ECT: engineered cardiac tissue

END-2: endoderm-like stromal cells

ESCs: embryonic stem cells

FBs: fibroblasts

FGF: fibroblast growth factor

FPD: field potential duration

GFP: green fluorescent protein

GP: ganglionated plexi

HRP: horseradish peroxidase

I_{CaL}: Ca2+ channels L-type

I_{CaT} : Ca2+ channels T-type

I_{Kr}: rapid delayed rectifier potassium current

I_{KS}: slow delayed rectifier potassium current

I_{Na}: inward sodium current

iPSCs: induced pluripotent stem cells

LQTS: long QT-syndrome

MAP2: Microtubule-associated protein 2

MDP: maximal diastolic potential

MEA: multi electrode array

mRNA: messenger RNA

MSCs: mesenchymal stem cells

MYH7: Myosin Heavy Chain 7

nAChR: inotropic nicotinic acetylcholine receptors

NEPs: neuroepithelial cells

NMPs: neuromesodermal progenitor

NMVMs: neonatal mouse ventricular myocytes

NP: neural plate

NPCs: neural progenitor cells

NPY: neuropeptide Y

O.D.: optical density

ON: overnight

P/S: Penicillin/ Streptomycin

PAGE: polyacrylamide gel electrophoresis

PBMCs: peripheral blood mononuclear cells

PBS phosphate-buffered saline

PCR: Polymerase Chain Reaction

PDL: Poly-D-Lysin

PFA: paraformaldehyde

PHOX2B: paired-like homeobox 2b

PKA: Protein kinase A

PMP: purmorphamine

PSN: parasympathetic neurons

PVDF: polyvinylidene difluoride

PVI: pulmonary vein isolation

RA: retinoic acid

RMP: resting membrane potential

RT-PCR: Real-Time Polymerase Chain Reaction/quantitative PCR

SAPs: sympathoadrenal progenitors

SCFs: superior cervical ganglia

SDS: sodium dodecyl sulfate

SeV: Sendai virus

SHH: Sonic Hedgehog

SNs: sympathetic neurons

SsTnI: skeletal Troponin I

TBS-T: Tris- buffered saline-tween

TdP: Torsade de Pointes

TFs: transcription factors

TGF-β: transcription growth factor-β

TH: Tyrosine hydroxylase

TTNI3: Troponin I 3

VIP: vasoactive intestinal polypeptide

VSMCs: vascular smooth cells

WB: Western Blot

Y: Rho-associated protein kinase inhibitor Y-27632

αMHC: α- myosin heavy chain

βMHC: β- myosin heavy chain

3 ABSTRACT

The autonomic nervous system (ANS) regulates the heart rate, conduction velocity, force of contraction, myocyte cohesion and relaxation of the heart. The elucidation of how ANS and the cardiac system interact and cooperate is at the basis of the comprehension of the mechanisms that participate in the development of many different cardiac diseases. The branch of Neurocardiology studies the co-participation of the cardiac system and the ANS in the development of cardiovascular disorders such as atrial fibrillation, long QT syndrome, Brugada syndrome, ventricular tachyarrhythmia and arrhythmogenic cardiomyopathy. However, the difficult obtainment of human neurons and cardiac cells makes extremely hard to study the interaction between these two cell types in ex-vivo and *in vitro* systems.

For this reason, the aim of this thesis is to develop an *in vitro* neurocardiac cell-model suitable for the study of the interaction between the ANS and the heart. To achieve this aim, the avantgarde technology of induced Pluripotent Stem Cells (iPSCs) represents the perfect strategy for the development of a neurocardiac cell-model thanks to the possibility to differentiate iPSCs in any cell type, including neurons and cardiomyocytes.

In this work, iPSC-derived CMs and iPSC-derived SNs were produced starting from the same line of iPSCs. Human iPSC-derived CMs, obtained with a protocol well established in our laboratory, showed spontaneous beating activity and expressed typical cardiac markers such as α-actinin, troponin I and myosin heavy chain 7, as evident by gene and protein analysis. iPSC-derived SNs, obtained reproducing a protocol available in literature, were in depth characterized by RT-PCR, Flow cytometry, Western Blot, immunofluorescence and multi electrode array analyses. The results confirm the derivation of sympathetic neuronal lineage cells, showing the expression of the noradrenergic markers Paired-like homeobox 2b (PHOX2B), Tyrosine Hydroxylase (TH) and Dopamine Beta Hydroxylase (DBH). The characterized cells were then employed for the creation of a neurocardiac model. The co-culture conditions were optimized including medium composition, cell densities, coating strategy and spatial distribution. After 3-5 days of co-culture with CMs, iPSC-derived SNs formed TH-positive axonal prolongation toward the cardiac population and showed positivity for the marker Synapisin where connections with iPSC-derived CMs were formed. Preliminary functional experiments seem to indicate that the presence of iPSC-derived SNs might increase the beating rate of iPSC-derived CMs when co-cultured for a period of two weeks.

The establishment of this co-culture methodology and the preliminary observations collected in this work provide a promising *in vitro* cell model for a deeper investigation of the neurocardiac interconnection and future insights in the modelling of many cardiac disorders.

4 INTRODUCTION

4.1 Cardiac Autonomic Nervous System

4.1.1 Autonomic regulation of cardiac functions

Early in 1628, William Harvey underlined the connection between brain and heart in a book written in Latin, reporting that "For every affection of the mind that is attended with either pain or pleasure, hope or fear, is the cause of an agitation whose influence extends to the heart" (Shen and Zipes, 2014b). In 1794, Antonio Scarpa published a collection of tables in which he presented the result of over 20 years of research on the *nervous system*, describing for the first time the path of several cranial nerves including the vagus nerve and the innervation of the heart (Kuder and Nowak, 2015). The strong interest of scientists in the cardiac autonomic nervous system found deeper basis in the 19th century, when, thanks to experiments inspired by Galvani's and Volta's studies, it became evident that the heart is able to beat independently of the nervous system, even though it can be influenced by the vagus and the intercostal nerve (Piccolino and Bresadola; Bayliss and Starling, 1892). The first paper related to this latter assessment was written in 1845 by the brothers Ernst Heinrich and Eduard Weber, heightening the antagonistic activity of the sympathetic and parasympathetic system on the heart using an electromagnetic rotation apparatus first on frogs and later on birds and on mammals as well (Ernsberger and Rohrer, 2018). In the same period, other scientists such as Langley, Gaskell, Bayliss and Starling contributed with many publications in increasing the knowledge in this field. With the deep investigation on the cardiac nervous system performed in the subsequent centuries and the precise definition of the cardiac innervation, the foundation of the new discipline called Neurocardiology took place in 1994 (Ardell and Armour, 2016). Nowadays many steps have been made ahead. In addition to the main regulations performed by the autonomic nervous system (ANS) on the heart in physiological conditions, it is now clear that the interconnection between the heart and ANS already starts during the developmental stage (Coskun and Lombardo, 2016) (Duraes Campos et al., 2018) (Hanna et al., 2017). Different subtypes of neural interplayers collaborate for the regulation of the cardiac control creating a complex multilevel neural network and conferring to this cardiac innervation the expression of "little brain" (Armour, 2008).

4.1.2 Anatomy and function of the cardiac autonomic nervous system (CANS)

The cardiac autonomic nervous system (CANS) is strictly connected to the heart's function because it is able to constantly modulate heart's mechanical and electrical activities by acting on the properties of single cardiomyocytes (CMs) such as size and structure (O'Connell et al., 2003) (Levy, 1990; Chow et al., 1993; Crick et al., 1994; Shen and Zipes, 2014a). In particular, the major features controlled by the CANS are (Hanna et al., 2017): heart rate (*chronotropy*), conduction velocity (*dromotropy*), force of contraction (*inotropy*), myocyte cohesion (*adhesiotropy*) and relaxation (*lusitropy*) (Fedele, 2020). The neural control over the heart is hierarchically performed through a dense and intricate coverage of different neurons, distributed along the cardiac innervation. Categorizing the distribution of neural innervation, it is possible to divide the CANS in two different but interconnected parts: the extrinsic CANS (innervation between the central

nervous system and the heart) and in the intrinsic CANS (innervation entering in the pericardial sac (Shen, 2014) (Figure 1).

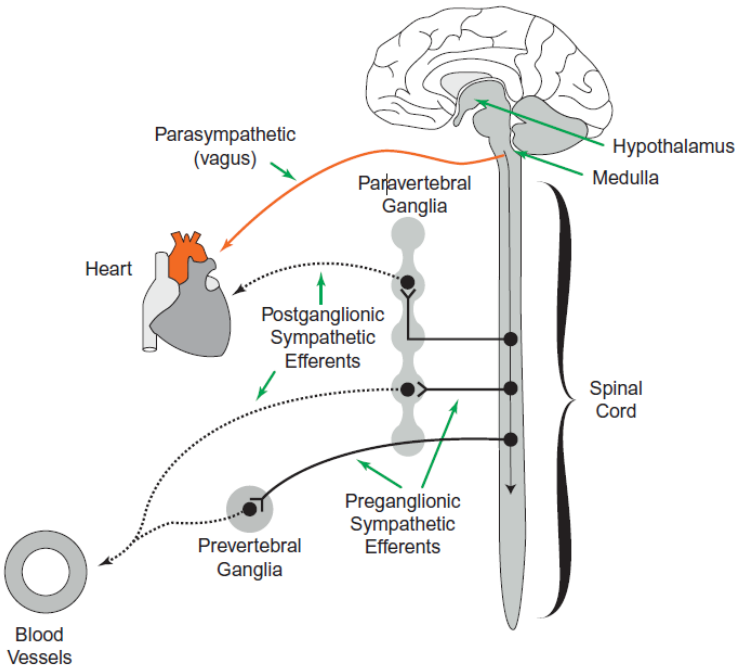

Figure 1: Schematic view of the autonomic innervation divided in extrinsic and intrinsic innervation. Reproduced with permission from Drew - Elsevier Inc. – 2012 (Drew and Sinoway, 2012).

4.1.2.1 Extrinsic Innervation

The extrinsic heart functions are mainly regulated by the intercellular communication between the sympathetic nervous system and the heart. (Prando et al., 2018). The extrinsic innervation is composed of the two antagonist systems: the sympathetic and parasympathetic innervation (Hanna et al., 2017).

4.1.2.1.1 Extrinsic Sympathetic Innervation

The sympathetic system reacts to the "fight or flight" response of the body. When it is activated, it increases the cardiac frequency and the ventricular contraction (Hamill and Shapiro, 2004; VanPatten and Al-Abed, 2017), while tuning the conduction velocity of myocardial tissue (Casella and Taglietti, 1993).

The sympathetic preganglionic efferents originate in the cervical and spinal cord, entering in the stellate ganglia (sympathetic chain) and mediastinal ganglia (Hopkins and Armour, 1984; Janes et al., 1986; Kawashima, 2005) (Figure 2). These ganglia house the majority of cell bodies of postganglionic sympathetic neurons (SNs), whose axons project to the sino-atrial node, the atrio-ventricular node, the His bundle, the ventricular myocardium and to a defined population of the intrinsic cardiac adrenergic neurons (Figure 3) (Casella and Taglietti, 1993; Shen and Zipes, 2014a; Hanna et al., 2017). When the preganglionic efferents are activated, they release the

neurotransmitter acetylcholine (Jamali et al., 2017), which binds the nicotine receptors of the postganglionic adrenergic efferents. The postganglionic efferents release norepinephrine (noradrenaline) (Jamali et al., 2017), which activates β-adrenergic receptors at synapses level (Drew and Sinoway, 2012), increasing intracellular cyclic-AMP (cAMP) (Zaccolo and Pozzan, 2002; Rochais et al., 2004) and modulating calcium handling (Burton et al., 2019) (Figure 5). In general, norepinephrine is the principal neurotransmitter of cardiac SNs. SNs use adenosine triphosphate (ATP), neuropeptide Y (NPY) and galanin as neurotransmitters (Ernsberger, 2001; Protas et al., 2003), with the main function of decreasing acetylcholine from parasympathetic terminals (Herring et al., 2008; Herring et al., 2012) and acting as a vasoconstrictor (Robertson and Biaggioni, 2012).

4.1.2.1.2 Extrinsic Parasympathetic Innervation

The parasympathetic system reacts to the "rest and digest" response of the body, inducing a general inhibitory response of the cardiac activity. Conversely to the sympathetic system, the activation of the parasympathetic innervation leads to the decrease of the cardiac frequency, of the ventricular contraction and of the atrio-ventricular conduction (Casella and Taglietti, 1993; Hamill and Shapiro, 2004; VanPatten and Al-Abed, 2017). Preganglionic ParaSympathetic Neurons (PSNs) originate in the nucleus ambiguous and dorsal motor nucleus of the medulla oblongata, whose axons project along the vagus nerve directly to postganglionic efferent PSNs located in the atrial intrinsic cardiac ganglia (Standish et al., 1995) (Figure 2), in particular in the sino-atrial node (innervated by the right vagus nerve) and in the atrio-ventricular node and His bundle (innervated by the left vagus nerve) (Figure 3) (Casella and Taglietti, 1993). In canine models, it has been shown that the majority of the PSNs are located in the ganglionated plexi close to the right pulmonary vein-atrial junction and in the region of the inferior vena cava- inferior left atrium junction (Randall and Ardell, 1985). The major part of the postganglionic PSNs converges at the intramural third fat pad of epicardium, between the superior vena cava and the aorta, following the path of sinus and atrioventricular nodes (Chiou et al., 1997). The principal neurotransmitter of PSNs is acetylcholine (Hasan, 2013; Jamali et al., 2017), which activates muscarinic receptors in the sinoatrial and atrioventricular nodes (Drew and Sinoway, 2012) (Figure 5). Together with acetylcholine, cardiac PSNs use as neurotransmitter vasoactive intestinal polypeptide (VIP), being a nitric oxide (Conlon et al., 1996).

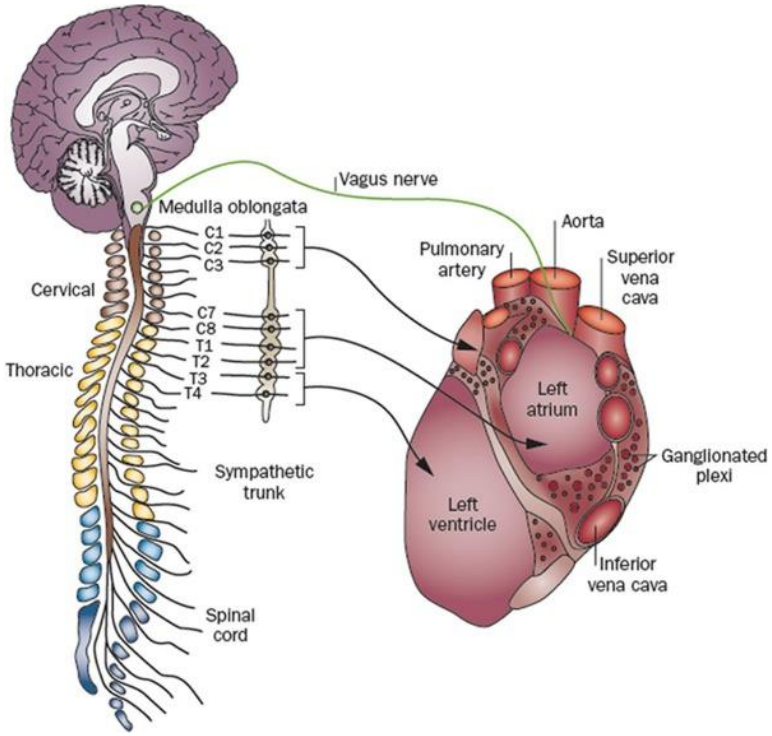

Figure 2: The targets of the cardiac autonomic system: the sympathetic system innervates the sino-atrial node, the atrio-ventricular node, the His bundle, ventricular myocardium and a defined population of the intrinsic cardiac adrenergic neurons; the parasympathetic system projects directly to the sino-atrial node, the atrio-ventricular node and His bundle. Reproduced with permission from Shen – Circulation Research – American Heart Association Journal - 2014 (Shen and Zipes, 2014a)

4.1.2.1.3 The functional balance between sympathetic and parasympathetic innervation

The relationship between the sympathetic and parasympathetic systems is functional thanks to the reciprocal "accentuated antagonism" between them (Vanhoutte and Levy, 1980; Levy, 1990; Choate et al., 1993).

Heart rate is reduced by the parasympathetic system, through the hyperpolarization of the nodal tissue (Hasan, 2013), but at the same time, the activation of the sympathetic system increases rapidly the heart rate (Khemani and Mehdirad, 2020). Post-ganglionic parasympathetic axons are close by the post-ganglionic sympathetic axons in pacemaker regions. Their proximity creates axo-axonal synapses formation, promoting the reciprocal modulation of heart rate with acetylcholine and norepinephrine release (Ehinger et al., 1970; Vanhoutte and Levy, 1980; Manabe et al., 1991). Even though the parasympathetic modulation of the sinus node is predominant over the sympathetic control, the latter stimulates the vagally induced bradycardia (Hasan, 2013). β-adrenoreceptors, in particular the β-1 receptors, are the responsible of the chronotropic effect in the cells of the sino-atrial node, regulating the pacemaker rate through the membrane currents driven by HCN4 and NCX (Stieber et al., 2003; DiFrancesco, 2010). In detail, alterations of inward currents due to solely cAMP or cAMP/Protein kinase A (PKA) are responsible for the diastolic depolarization in the sino-atrial node (Stieber et al., 2003).

Stimulation of β-adrenoreceptors leads to a positive inotropic effect. PKA activates cAMP, which leads to the phosphorylation of calcium (Ca^{2+}) (Bers, 2008). The phosphorylation of Ca^{2+} handling proteins, L-type Ca^{2+} channels, Phopholamban, and Ryanodine receptor 2 increases the amount of Ca^{2+} available for the contraction (Rochais et al., 2004; Bers, 2008). Furthermore, the CMs size is strictly associated with innervation density (Hirsch et al., 2013). In conclusion, the only existence of a functional and equilibrate autonomic innervation makes possible the preservation of the cardiac structure (Zaglia and Mongillo, 2017).

4.1.2.2 Intrinsic CANS

The intrinsic cardiac innervation is located in the cardiac ganglia. A ganglion can be composed by a different number of neurons, with groups of one to few neurons and other groups constituted of around 200 to 1000 neurons of different subtypes: motor neurons (sympathetic and parasympathetic) (Armour et al., 1997; Pauza et al., 2000), afferent neurons, and interconnecting local circuit neurons (Armour, 2008). The cardiac ganglia are located in zones called ganglionated plexi (GP), abundantly situated in the intramural epicardial fat wall of the atria and ventricles (Randall et al., 1986; Singh et al., 1996; Kapa et al., 2010; Lachman et al., 2011; Hanna et al., 2017). For instance, the GPs are associations between cardiac ganglia and connecting nerves (Duraes Campos et al., 2018). In general, an average of 550 ganglia (458 ± 43 in atria and 88 ± 7 in ventricles) have been found in the human heart, varying in their dimensions and associated with 14.000 neurons (Armour et al., 1997). Armour and colleagues created an elaborate map of intrinsic CANS, as reported in Figure 3 (Armour et al., 1997). The majority of GP is localized in 5 specific zones in atria and 5 in the ventricles. The atrial ganglionated plexus are: superior right atrial ganglionated plexus, superior left atrial ganglionated plexus, posterior right atrial ganglionated plexus, posteromedial left atrial ganglionated plexus and interatrial septal ganglionated plexus (Armour et al., 1997; Pauza et al., 2000; Kawashima, 2005; Hou et al., 2007; Armour, 2010) (Tan et al., 2006). An additional and small atrial plexus has been found in the posterior lateral surface of the left atrial base called posterolateral left atrial ganglionated plexus. The majority of ventricular GPs are embedded in fat around the aortic root and in general, they are found at the origins of the vessels (Armour et al., 1997; Armour, 2010). The five ventricular GPs are: aortic root ganglionated plexus (containing the largest collection of ventricular neurons), posterior descending ganglionated plexus, anterior descending ganglionated plexus, obtuse marginal ganglionated plexus, right acute marginal ganglionated plexus (Armour et al., 1997).

GPs act as an integration center, able to modulate the relationship between extrinsic and intrinsic ANS (Hou et al., 2007) and cardio-cardiac reflexes (Hanna et al., 2017). In particular, intrinsic cardiac ganglia connect with the extrinsic intrathoracic cardiac ganglia through the cardiopulmonary nerves and small mediastinal nerves (Armour et al., 1997).

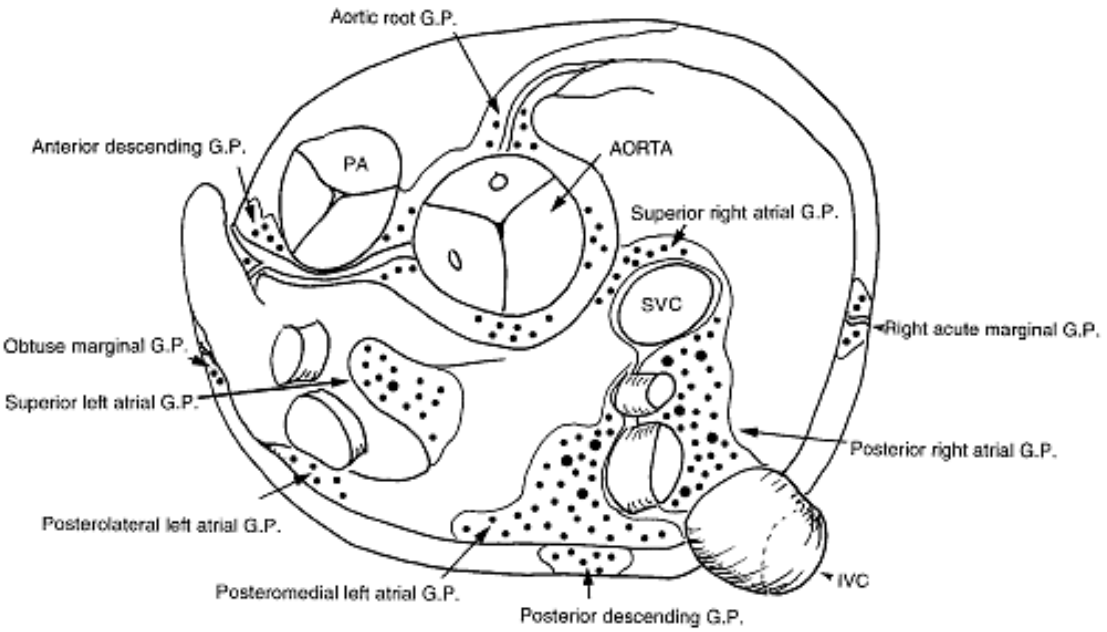

Figure 3: Scheme of ganglionated plexi in heart: superior view. Reproduced with permission from Armour - The Anatomical Record - Wiley-Liss, Inc. - 1997 (Armour et al., 1997)

4.1.3 Neuro-cardiac junctions

It is important to determine the modality of intercommunication between ANS and CMs in order to understand how the information is delivered to the final cardiac target. Thanks to ultrastructural analysis of section of heart specimens, it was possible to elucidate the interconnection between the neural and the cardiac cells (Hirst et al., 1996). Even though the neuro-cardiac communication was described for long time as non-specialized junction (Burnstock, 2008; 2009), new evidences highlight that the neuro-cardiac communication is quasi-synaptic, similar to the communication of neuromuscular junction (Zaglia and Mongillo, 2017; Di Bona et al., 2020). From different experiments it was possible to classify the neuro-cardiac junctions in three different types: the intimate junctions with <20 nm distance, the close junctions with a distance included between 20 and 100 nm and the separated junction with a distance bigger than 100 nm (Thaemert, 1970; Kikuchi, 1976; Klemm et al., 1992; Choate et al., 1993). The majority of the junctions of the sympathetic and parasympathetic innervation has a gap of <100nm distance connecting the post-ganglionic efferents with the sino-atrial node (Klemm et al., 1992; Choate et al., 1993).

4.1.3.1 Sympathetic-cardiac junctions

Sympathetic nerves release norepinephrine which is detected by the adrenergic receptors situated in heart. Three types of adrenergic receptors are distinguishable, although all associated with G protein-coupled receptors: the β1 (localized in sarcolemma), the β2 and the β3 (both localized in ventricular T-tubules). β1 receptor is the most abundant in heart and it is associated with G_s, leading to an increase in cAMP and to the stimulation of the downstream effector

proteins (Finlay et al., 2017). Instead, β2 receptors, coupled with G_s and G_i, are able to influence β1 receptors activity with a reduction of cAMP. β3 receptors, initiating eNOS (endothelial nitric oxide synthase), are able to stimulate the production of cGMP. Cardiomyocytes present another type of receptors: the α1 and α2 adrenoreceptors bot coupled with $G_{q/11}$ and producing a positive inotropic effect (Finlay et al., 2017).

When SNs processes spread through the myocardial interstitium, they extend in a parallel-way to capillary vessels, displaying a peculiar shape (Ieda et al., 2007; Kimura et al., 2012) (Figure 4A). The characteristic shape exhibited by sympathetic processes is a pearl necklace morphology, where the "pearls" or enlargements are called varicosities, where the neuroexocytosis apparatus is localized (Figure 4B). The sympathetic neurotransmitters, including norepinephrine, ATP, and NPY are released at the level of varicosities (Thaemert, 1966; Sosunov et al., 1997). Recently, it was demonstrated that the neuronal processes present in the heart result in a proportion similar to the capillary-CMs ratio (Anversa et al., 1989; Hirsch et al., 2013; Zaglia and Mongillo, 2017). Thanks to two-photon microscopy methodology, also the smallest processes are detectable. In rodent heart, it is evident that CMs are in contact with many varicosities from the same neuronal processes and, at the same time, building contact with processes of different neurons, resulting in CMs that are within short range of SNs processes (Freeman et al., 2014) (Figure 4C). This complex capillary innervation network created by SNs promotes the control of cardiac function in a cell-specific fashion, with precision, and with a wide range effect (Zaglia and Mongillo, 2017).

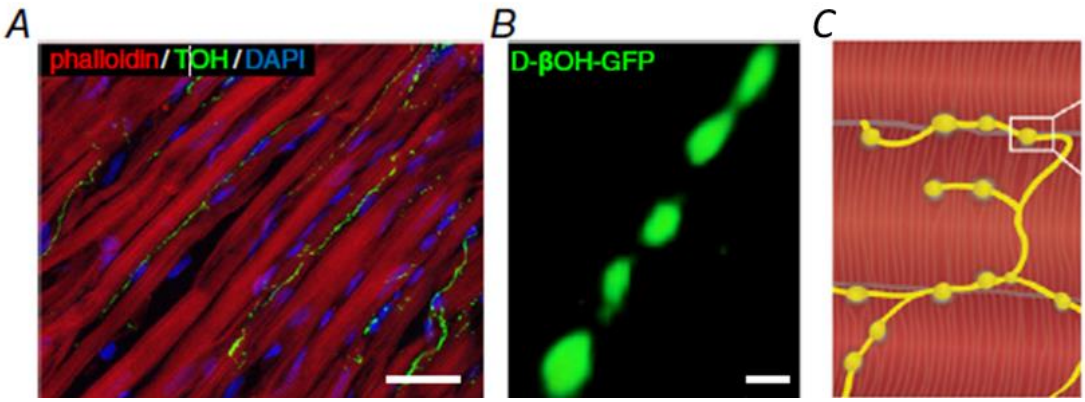

Figure 4: Spreading of sympathetic processes. ***A:*** *sympathetic processes spread in a parallel way to capillary vessel.* ***B:*** *Varicosities displaying the typical pearl necklace morphology.* ***C:*** *Different CMs are in contact with many varicosities from the same neuronal processes. Reproduced with permission from Zaglia - The Journal of Physiology - John Wiley & Sons, Inc., - 2017. Modified (Zaglia and Mongillo, 2017)*

4.1.3.2 Parasympathetic-cardiac junctions

In the case of the parasympathetic innervation, the nerve terminals release acetylcholine which is detected by the metabotropic muscarinic acetylcholine receptors. These muscarinic receptors are divided into M1 to M5, where M2 is the most abundant expressed in the cardiac tissue and coupled to G_i, leading to a decrease in cAMP signaling (Fedele and Brand, 2020). It is also possible to find the receptors M1 and M3 in the cardiac tissue, coupled with $G_{q/11}$ and activating the PLC

pathway (Finlay et al., 2017). Acetylcholine or vagal stimulation decreases the beating rate. In details acetylcholine alone provokes action potential shortening together with an increase in peak potential and membrane hyperpolarization, while the vagal stimulation triggers membrane depolarization without altering the peak potential (Hartzell, 1980; Bywater et al., 1989; Campbell et al., 1989). In the cleft of the parasympathetic-cardiac junctions, acetylcholine is cleaved by the hydrolytic enzyme acetylcholinesterase localized both in pre- and postjunctional membranes. Through a reuptake mechanism, the resulting choline is reabsorbed in the neurons and reconverted again in acetylcholine ready to be one more time released (Rump et al., 1995). The enzyme acetylcholinesterase is found at high level in the area of the sino-atrial node in comparison to atria and ventriculi (Loffelholz and Pappano, 1985). (Figure 5).

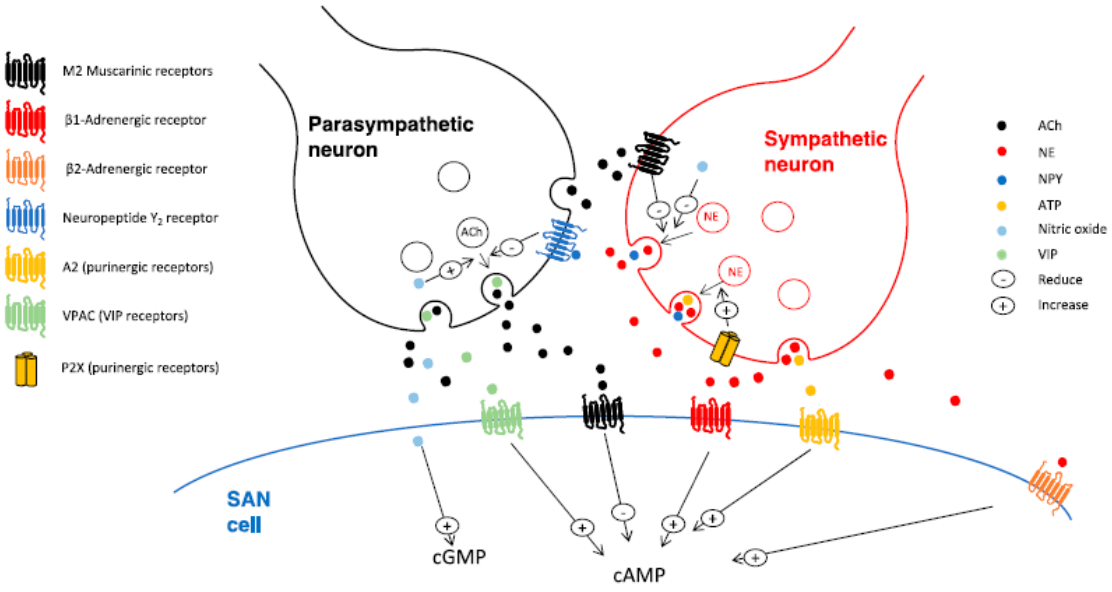

Figure 5: Schematic representation of neuro-cardiac junctions with the interaction of sympathetic and parasympathetic branches in the sino-altrial node and the release of the different types of neurotransmitters. Reproduced with permission from Fedele – Journal of Cadiovascular Development and Disease – MDPI – 2020. (Fedele and Brand, 2020)

4.1.4 Neurocardiology

The efforts made in understanding and characterizing the cardiac autonomic innervation has brought to light the neuronal components involved in heart control (Julian and Sheridan, 1978), giving rise to a new discipline called neurocardiology (Ardell and Armour, 2016). The interaction between the ANS and the heart is clear in the pathophysiology of many cardiovascular disorders (Hanna et al., 2017). In fact, ANS alterations have an impact on cardiac pathologies, including sudden cardiac death, heart failure, atrial fibrillation, ventricular tachycardia, and inherited cardiomyopathies (Hasan, 2013; Fedele and Brand, 2020; Khemani and Mehdirad, 2020). The role of ANS in the arrhythmogenesis has been demonstrated over >80 years (Shen and Zipes, 2014a).

4.1.4.1 Atrial fibrillation

Already in 1978, Coumel demonstrated that atrial arrhythmias are associated with cardiac ANS activities (Coumel et al., 1978). Later on, the atrial fibrillation (AF), the most common arrhythmia, was correlated to the unbalance between the sympathetic and parasympathetic systems (Bettoni and Zimmermann, 2002; Amar et al., 2003; Tomita et al., 2003). An increased calcium transient is caused by sympathetic activation, while the activation of parasympathetic innervation leads to a reduction of the effective refractory period (Wijffels et al., 1995; Bers, 2002). The discrepancy between action potential (AP) duration and calcium transient increases the forward Na/Ca exchanger current, which, in turn, can generate early afterdepolarization (Patterson et al., 2006) as potential source of arrhythmic events. AF is frequently observed during sleep as well, caused by a parasympathetic dominance (Scherlag and Po, 2006; Chen and Tan, 2007; Jamali et al., 2017) and proved by some works in patients with sleep apnea (Asirvatham and Kapa, 2009; Ghias et al., 2009; Verrier and Josephson, 2009). The incidence of the predominance of the sympathetic or parasympathetic AF depends on comorbidities (Kapa et al., 2010). Furthermore, in a canine model, the parasympathetic neurotransmitter VIP was linked to the AF initiation (Liu et al., 2013). If it is clear that extrinsic ANS is crucial for the onset of AF, the cooperation with intrinsic innervation was unknown (Shen and Zipes, 2014a) until Choi and collaborators demonstrated that the 11% of AF is triggered by intrinsic innervation alone (Choi et al., 2010). Since the discovery that AF can spontaneously arise from enhanced activity in the pulmonary vein ostia (Jais et al., 1997; Haïssaguerre et al., 1998), pulmonary vein isolation (PVI), a widely used ablation technique (Haïssaguerre et al., 1998), resulted in an effective technique for patients with AF (Haïssaguerre et al., 2000). It consists of the disruption of innervation around the pulmonary vein (Jamali et al., 2017). However, the PVI alone cannot be sufficient to treat the pathology (Shen and Zipes, 2014a) and a more successful method was developed. It consists of the autonomic denervation of the atrial GP (Katritsis et al., 2011; Jamali et al., 2017), preserving the sinus rhythm in the majority of the cases (Platt et al., 2004; Scherlag and Po, 2006). GP ablation, in combination with PVI, leads to a helpful strategy for the treatment of AF patients (Shen and Zipes, 2014a).

4.1.4.2 Ventricular tachyarrhythmias

Under the term of ventricular tachyarrhythmias, it is possible to attribute some cardiac pathologies, including sudden cardiac death, ventricular arrhythmias, and ventricular fibrillation (Shen and Zipes, 2014a). An enhanced sympathetic activity leads to modification in electrocardiogram (ECG) repolarization, stimulating the onset of ventricular fibrillation (Yanowitz et al., 1966). Furthermore, ventricular fibrillation happens even more in presence of cardiac ischemia and myocardial infarction (Opthof et al., 1991), which results in the perfect triggering substrate for arrhythmia, due to cardiac remodeling (Tomaselli and Zipes, 2004) and innervation heterogeneity (Barber et al., 1983). Foci of ventricular arrhythmia are frequent in fibrosis zones, characterized by discontinuous electrical impulse and hypersensitivity to catecholamine (Hasan, 2013). After a myocardial infarction, at the border of the not-damaged myocardium, there is a heterogeneous distribution of the sympathetic innervation, causing sources of electrical impulses (contractions) due to heterogeneities in AP propagation (Hasan, 2013) and for consequence giving rise to tachyarrhythmia (Lavery et al., 1997). The heterogeneous innervation is principally caused

by nerve sprouting (new nerve growth) (Cao et al., 2000; Chen et al., 2001) in denervated zones. An increasing nerve sprouting is demonstrated at the border of normal myocardium and scar tissues in patients with diagnosed ventricular arrhythmias (Cao et al., 2000). In myocardial infarction, there is an upregulation of nerve growth-related proteins, such as nerve growth factor, growth-associated protein 43, and synaptophysin in the damaged area (Zhou et al., 2004) and in the upstream bilateral stellate ganglia (Han et al., 2012). The new nerves suppress $I_{(to)}$ and $I_{(K1)}$, decreasing heart rate variability, and increase the sensitivity to ventricular fibrillation (Cao et al., 2000; Chen et al., 2001; Ren et al., 2008).

To reduce the ventricular tachyarrhythmias, β-blockers have been shown to fortify the sympathetic innervation (Steinbeck et al., 1992; Antz et al., 1995). However, for patients with drug-resistance the sympathectomy technique, the direct ablation of sympathetic nerves including α-receptors interruption, has been used (Shen and Zipes, 2014a). In fact, the elimination of bilateral stellate ganglia and/or upper thoracic ganglia help drug-resistant patients with ventricular fibrillation (Estes and Izlar, 1961) (ZIPES et al., 1968)

4.1.4.3 Long QT Syndrome

This cardiomyopathy is characterized by the prolonged QT interval of EGC, torsade de pointes, and sudden cardiac death (Moss et al., 1991; Zipes, 1991). The syndrome can present different abnormalities whether in the potassium or sodium channels (Verrier and Antzelevitch, 2004). The early afterdepolarizations and the correlated stimulated sympathetic activity are the primary triggers of arrhythmogenicity (Shen and Zipes, 2014a). The increased sympathetic activity enhances the spontaneous inward current in l-type calcium channels, stimulating the early afterdepolarization development and initiation of reentry (Shimizu and Antzelevitch, 1998; Huffaker et al., 2004). Even though the patient with QT syndrome are extremely susceptible to the autonomic stimulation, it seems that the sympathetic activation depends on the type of the QT syndrome (Verrier and Antzelevitch, 2004).

4.1.4.4 The Brugada syndrome

This is an autosomal-dominant inherited cardiomyopathy, characterized by right bundle branch block and persistent ST-segment elevation with a high risk of sudden cardiac death and ventricular arrhythmias (Brugada and Brugada, 1992; Wilde et al., 2002). In the Brugada syndrome it seems that an imbalance of the sympathetic and the parasympathetic branches is highly involved in the development of the disease (Matsuo et al., 1999). An increased parasympathetic activity (vagal tone) during rest and sleep plays a crucial role in episodes of ventricular fibrillation in Brugada-patients (Matsuo et al., 1999; Takigawa et al., 2008). In fact, heart rate analysis demonstrated the stimulation of parasympathetic activity just before ventricular fibrillation episodes (Kasanuki et al., 1997). It has been observed that in patients with Brugada syndrome there is a presynaptic sympathetic dysfunction of heart (Wichter et al., 2002). This sympathetic dysfunction could affect protein phosphorylation and spatial heterogeneity of transient calcium currents may resulting in arrhythmia.

4.1.4.5 Arrhythmogenic Cardiomyopathy (ACM)

This cardiomyopathy was first observed in 1970 in young patients and it is characterized by sudden cardiac death in young patients and ventricular arrhythmias (Thiene et al., 1988). In this arrhythmia, there is a stimulated sympathetic innervation due to physical activities or mental stress (Wichter et al., 1992). The downregulation of increasing firing of efferent sympathetic innervation causes density reduction of myocardial β-adrenergic receptors, suggesting the key role of sympathetic hyperactivity in triggering arrhythmias in ACM patients (Wichter et al., 2000).

4.2 Induced pluripotent stem cells

4.2.1 Induced Pluripotent Stem Cells

A valid source of human material is essential for the study of genetic diseases. Obtaining a proper source of biomaterial from humans (for example tissues like heart or brain) can be difficult in terms of invasive methods for the collection and in terms of legal issue regarding ethical problems. To bypass this problem, a reliable and reproducible method has been developed for the generation of an unlimited source of human materials. Indeed, in 2006 Yamanaka and co-workers were able to report the conversion of adult somatic cells back to a pluripotent state through the introduction of four reprogramming factors: Oct-4, Sox-2, Klf-4, and c-Myc (the OSKM factors), giving rise to the so-called Induced Pluripotent Stem Cells (iPSCs) (Takahashi and Yamanaka, 2006). They selected 24 genes identified as candidates reprogramming factors and they inserted them in mouse embryonic fibroblasts with retroviral transduction. 22 colonies survived to antibiotic selection and resembled to ESCs (embryonic stem cells). In order to reduce the candidates only to the key genes, they tested 24 combinations of reprogramming factors, removing in each experiment 1 different factor from the group of 24. When the obtained colonies still resembled ESCs, the 24th removed factor can be definitely excluded by the list of the essential factors. They were able to reduce the list to 10 genes and in a second round they were able to determine the four essential factors crucial for the generation of iPSCs (Takahashi and Yamanaka, 2006). After that they applied the technique to human cells and they succeed in the generation of human iPSCs (Takahashi et al., 2007) with transgene-free methods (Okita et al., 2011). Thanks to this revolutionary discovery, in 2012 Shinya Yamanaka was awarded with the Nobel Prize in Physiology or Medicine. Since then, the fields of science and medicine has been revolutionized by iPSCs technology, representing a new tool for disease modelling, drug discovery/screening and the regenerative medicine. The new strategy of iPSCs represent an incredible tool to obtain with a limitless amount any type of human cells and in a patient-specific manner.

4.2.2 Definition and Features of iPSCs

iPSCs are a type of pluripotent cells directly obtained from a forced reprogramming of adult cells into a pluripotent status, forcing the expression of four stemness factors: Oct-3/4, Sox2, c-Myc, and Klf4 (Takahashi and Yamanaka, 2006). iPSCs resemble human ESCs in terms of proliferation rate, morphology, ability to differentiate into three-germ layers, teratoma formation, promoter activities and expression of specific markers (Takahashi and Yamanaka, 2006). The ethical concerns associated with the obtaining human ESCs and related to the destruction of the embryos, are bypassed with the artificial production of iPSCs (Sommer and Mostoslavsky, 2010). The study of transcription factors was essential for the discovery of iPSCs. They are able to drive the cellular identity during the entire developmental process, by expressing or suppressing some genes characteristic of the different lineages (Stadtfeld and Hochedlinger, 2010). Oct4 is a homeodomain transcription factor, belonging to the POU family and responsible for the self-renewal of undifferentiated embryonic stem cells. Sox2 is a member of the Sox family of transcription factors. The two factors work together binding DNA at non-palindromic sequences, activating the transcription of pluripotency genes and contributing at the same time to the

suppression of genes involved in cell differentiation (Masui et al., 2007).
Klf4 is a zinc finger DNA-binding protein, part of the family of the Krüppel-like family of transcription factors (Ghaleb et al., 2008). This factor has different functions like regulation of cell proliferation, cell differentiation, apoptosis, and somatic cell reprogramming. The role of this factor can switch from pro-cell survival to pro-cell death only under particular conditions (Wang et al., 2015).
c-Myc is a regulatory gene encoded for a pleiotropic transcription factor (Guo et al., 2009) and specialized in the modulation of the progression of cell cycle between growth and differentiation (Martinez-Fernandez et al., 2010). Of note, c-Myc is able to promote the pluripotency through the activation of a class of stemness genes, binding to a huge number of pluripotency genes (Kidder et al., 2008). Unfortunately, C-Myc is an oncogene and its dysregulation lead to cancer development (Izumo et al., 1988). The use of the OSKM factors was used for the first generation of iPSCs, but further studies have been done to improve the reprogramming phase, increasing efficiency and bypassing the use of oncogenes (Takahashi et al., 2007; Yu et al., 2007; Okita et al., 2011).
In any case, the first combination of the four factors given by Yamanaka (Takahashi and Yamanaka, 2006), remains the most adapted and utilized.

4.3 Reprogramming approaches

Many are the different techniques used for the development of iPSCs generation and it is possible to distinguish between two groups of different approaches: the Integrating Vectors (retrovirus, lentivirus, and transposons) and the Non-Integrating Vectors (excisable vectors, adenovirus, Sendai-virus, episomal vectors, and proteins/RNA delivery) (Zhou and Zeng, 2013).

The original technique used for the generation of iPSC consisted in the transient expression of exogenous pluripotency factors through a retroviral vector (Takahashi et al., 2007). After insertion in the cell, the retrovirus releases the reprogramming genes, which integrate in the host genome (Stadtfeld et al., 2008). A higher reprogramming efficiency has been achieved with lentivirus, which works with the same principle as retrovirus (Yu et al., 2007; Wernig et al., 2008). Anyway, both vectors are associated with the higher efficiency of transduction with the stable genomic integration. However, the outbreak of malignancies, due to insertional mutagenesis and/or silencing of viral vectors may prevent full cell reprogramming (Okita et al., 2007). Transposons represent another approach for reprogramming, consisting in transposable elements of DNA that can change their position in the genome, leading to consequent alterations in the genetic sequence. Alterations in 5% of transposition events have been reported (Wang et al., 2008) and transposase expression could lead to alteration in cellular functions, such as the normal differentiation process. (Stadtfeld and Hochedlinger, 2010).
Many efforts have been made to improve the protocols without the integration of exogenous DNA into cellular genomes; adenovirus and Sendai virus are two examples of a non-integrating approaches. Adenoviruses are non-enveloped and replication-incompetent viruses able to affect replicating and non-replicating cells. Due to their non-integrating features, they are used for the targeted gene therapy and for the generation of iPSCs in both mice and humans. The probability

of tetraploid cell formation of the adenoviral vectors-based delivery system is characterized by a very low yield around the 0.0001 and the 0.001%) (Zhou and Zeng, 2013).

Fusaki and colleagues proposed the Sendai virus (SeV) as another non-integrative viral strategy to create iPSCs (Fusaki et al., 2009). SeV replicates in form of single-stranded RNA in the host cell cytoplasm (Sommer and Mostoslavsky, 2010). Even though this can be considered the safest method in the category of the viral reprogramming (Fusaki et al., 2009; Nishimura et al., 2011) the method has some limitations, including the high sensitivity of the viral replicase to the nature of the transgenic sequences and the difficulty in the elimination of Sendai virus from the host cells because of their constitutive replication (Macarthur et al., 2012).

An alternative reprogramming without genome integration can be done with proteins or mRNA. However, both methods result much more complicated than others (Zhou and Zeng, 2013) because they have to be repeated more times (Zhou et al., 2009). In the reprogramming with synthetic RNA, where mRNAs are synthesized *in vitro*, the reprogramming factors are encoded by modified nucleotides, which synthetized the RNA (Warren et al., 2010). Due to the rapid turnover of mRNAs and the maximal protein expression, it is necessary a daily transfection (Karagiannis et al., 2019).

Last, integration-free episomal plasmids are commercially available tools now used by many laboratories around the world (Okita et al., 2011) (Meraviglia et al., 2015). Through a single transient transfection, this cost-effective viral-free approach leads to the reprogramming of human somatic cells. These vectors are derived from a portion of the Epstein-Barr herpesvirus, and transfected without the viral packaging, undergoing stable extrachromosomal replication only once per cell cycle (Zhou and Zeng, 2013). The simplicity of this strategy, using elementary procedures, confers to episomal plasmid an easily access to any lab (Si-Tayeb et al., 2010). Despite the good quality of the reprogramming using episomal plasmids, the efficiency of this method is lower than other integrating strategies (Yu et al., 2009).

4.3.1 Starting material for iPSC production

The biomedical research was revolutionized by the discovery of iPSC technology and the consequent production of patient-specific cell lines. Despite different cells' morphologies and functionalities, all the cells of the human body present the same genome and genetic background. Given that, the identification of an easily accessible source of cells from patients is a crucial choice for the starting material. The most popular donor cell type until now are skin fibroblasts (Takahashi et al., 2007; Okita et al., 2011). Other examples of cells employed in the reprogramming into iPSCs are: keratinocytes (Aasen et al., 2008), dental pulp cells (Beltrao-Braga et al., 2011), adipose stromal cells (Miyoshi et al., 2011), hair follicles (Wang et al., 2013) and bone marrow mesenchymal stem cells (Streckfuss-Bomeke et al., 2013). The isolation of these starting materials requires invasive surgical procedures. Alternative and less invasive starting materials (because of the easily access) and are cord blood (Giorgetti et al., 2009) and peripheral blood, specifically peripheral blood mononuclear cells (PBMCs) (Staerk et al., 2010). PBMCs require a minimal expansion *in vitro* before reprogramming experiments, thus reducing of about 3-4 weeks

the time needed for the production of iPSCs compared to other sources, like fibroblasts (Loh et al., 2009). Moreover, iPSCs derived from PBMCs display an epigenetic signature more similar to hESCs than those obtained from mesenchymal stem cells (MSC)/fibroblasts (Kim et al., 2009). For this reason, it is important to evaluate the right starting material (adult cell) for each experiment, because iPSCs have a memory of the original epigenetic status, which can affect the further differentiation capacity. The epigenetic memory can be attenuated or eliminated with a prolonged time in culture (Kim et al., 2010; Karagiannis et al., 2019) or by a second reprogramming (Polo et al., 2010).

4.4 iPSC Differentiation

4.4.1 Cardiomyogenic differentiation

The human heart has a limited regenerative capacity because it is a terminally differentiated organ (Steinhauser and Lee, 2011). This always had a great impact on both basic and clinical research. After the iPSC breakthrough, the disease modelling, drug screening, cell-based therapies and cardiac tissue engineering had a great momentum, based on the iPSC ability to be indefinitely expanded *in vitro* and differentiated into all the cardiovascular cell types (Di Baldassarre et al., 2018). Producing differentiated cardiomyocytes from iPSCs is a fundamental step in the cardiac research, as iPSC-derived cardiomyocytes represent one of the most promising tools for regenerative medicine (Fujiwara et al., 2011) and have been demonstrated to be a good model for many cardiac diseases, ranging from cardiomyopathies as the arrhythmogenic cardiomyopathy (Caspi et al., 2013; Kim et al., 2013; Ma et al., 2013a) and hypertrophic cardiomyopathy (Tanaka et al.; Lan et al., 2013; Liang et al., 2013b) to long QT-syndrome (LQTS-1 (Moretti et al., 2010a; Egashira et al., 2012; Liang et al., 2013b); LQTS-2 (Itzhaki et al., 2011; Matsa et al., 2011; Lahti et al., 2012a); LQTS-3 (Ma et al., 2013c; Terrenoire et al., 2013); LQTS-8 (Yazawa et al., 2011)), catecholaminergic polymorphic ventricular tachycardia (Itzhaki et al., 2012; Jung et al., 2012; Kujala et al., 2012; Di Pasquale et al., 2013a; Lodola et al., 2016; Sasaki et al., 2016) and atrial fibrillation (Benzoni et al., 2020; Grandi and Dobrev, 2020). In the last decades different types of strategies have been accurately developed for the differentiation of iPSCs into CMs. What is essential in the development of a new protocol for the cardiomyogenic differentiation is the recapitulation of the essential *in vivo* cardiac developmental stages (Di Baldassarre et al., 2018). Two important steps consist in the activation of the canonical Wnt pathway in an early phase of the development for the induction of the mesoendoderm and the subsequent inhibition of the same pathway, in order to specify the cardiac mesoderm (Burridge et al., 2012; Sirabella et al., 2015). Several methods for cardiomyogenic differentiation are: A) differentiation per Inductive co-culture, B) differentiation in suspension and in 3D via Embryoid Body formation, C) two-dimensional monolayer differentiation and D) dynamic cell culture in suspension in spinner flask and/or bioreactors for a large-scale production (Di Baldassarre et al., 2018).

A) Inductive co-culture differentiation was the first method used for the cardiomyogenic differentiation and it consists in the co-culture of iPSCs with mouse visceral endoderm-like stromal cells (END-2) (Burridge et al., 2012). The role of visceral endoderm is essential concerning the release of factors and molecules responsible for the induction of cardiogenic precursor's

differentiation. This method is relatively inefficient because of the low yield of cardiomyocytes with an immature phenotype (less than 10%, but usually around 1%) (Passier et al., 2005). Also, cardiac differentiation is driven by partially unknown chemical factors produced by END-2 cells and the mechanisms underlying the differentiation are poorly characterized. However, the advantage of the co-culture method is the fact that is simple, rapid and cost-effective (Mummery et al., 2012).

B) Differentiation in suspension is performed through the formation of 3D non-adherent spherical agglomerates, called embryoid bodies (EBs) that mimics early embryonic development leading to the differentiation into the three germ layers (mesoderm, endoderm, and ectoderm). The EBs are spheroidal aggregates variable in structures and composition (multi-cellular) able to differentiate also in spontaneously contracting region containing cardiomyocytes in presence of fetal bovine serum (Itskovitz-Eldor et al., 2000; D'Amico et al., 2016).
A more efficient protocol by Yang et al., suggested the elimination of the serum component and proposed the implementation of the medium with the following cytokines: Activin A, BMP4, VEGF, DKK1 and β-FGF (Yang et al., 2008). A further improvement of the latter protocol was given by Karakikes with the addition of small molecules to further ameliorate the efficiency of the protocol (Karakikes et al., 2014). In particular, the small molecule IWR-1 is able to provide to all differentiating CMs a ventricular-like phenotype and DKK, on the contrary, leads to the formation of an heterogenous population of CMs. A limitation of this method is the lack of control over the shape and size of EBs, leading to a frequent agglomeration of EBs in large aggregates with negative effects on cell proliferation and differentiation and an asynchronous beating of them (Rungarunlert et al., 2009). To circumvent this issue, new approaches have been developed to force the aggregation, like Spin EBs (Burridge et al., 2007), Microwell EBs (Mohr et al., 2010) and Micropattern EBs (Bauwens et al., 2008). All these methods are high-throughput approaches for the formation of aggregates of cells all characterized by identical size. The disadvantage of these approaches is the need for appropriate technologies, which are not always commercially available. Moreover, the strategy via EBs formation is characterized by the low efficiency of cardiomyogenic differentiation (about 5% of cardiomyocytes) and cardiomyocytes display an immature phenotype (Mummery et al., 2012; Di Baldassarre et al., 2018).

C) Two-dimensional monolayer protocols are based on the use of small molecules and growth factors added to the medium in a controlled manner, to induce differentiation into cardiomyocytes. Several works have demonstrated that these techniques are more reproducible and scalable than EBs formation and co-culture, leading to a more efficient cardiomyogenic differentiation (Mummery et al., 2012), and it can be also considered for clinical purposes (Di Baldassarre et al., 2018). This method reduced the differentiation variability between the cell lines, also reducing the quality and quantity variation of CMs during different experiments (Di Baldassarre et al., 2018). Moreover, monolayer protocols produce more mature cardiomyocytes with features of different subtypes (ventricular, atrial, or pacemaker cardiomyocytes). In the last few years, several 2D monolayer differentiation techniques have been developed to increase the

yield of cardiomyocytes (85%–95%) and to decrease the cost by reducing the number of media components (Mummery et al., 2012).

The first monolayer differentiation protocol has been reported in 2007 by Laflamme et al. (Laflamme et al., 2007) . They cultured hESCs on Matrigel coating in MEF-conditioned medium until a high confluence in the wells (Laflamme et al., 2007). When the cells reached the perfect confluence, they were cultured with RPMI media+B27 supplement (RPMI-B27). The first day the cells were supplemented with Activin-A and after four days with BMP4. The cells started beating spontaneously after 12th day, obtaining a final population of about 30% of cardiomyocytes. Unfortunately, studies on this method revealed inconsistent results for different cell lines (Paige et al., 2010). To improve the strategy, a Matrigel-sandwich was applied to the culture in order to facilitate the epithelial-to mesenchymal transition. This method consisted in the application of a second layer of Matrigel on the cells on the day before the addition of the differentiation medium. This strategy increased the differentiation efficiency up to 98 % (Zhang et al., 2012a).

In 2012, Lian and colleagues were able to obtain CMs demonstrating the regulation of the differentiation process through the modulation of the Wnt canonical pathway (Lian et al., 2013). They noted the essential importance of the timing and of the dose regulation of Wnt pathway for effective development of CMs. Their protocol proposed a stimulation of the Wnt signaling pathway at the beginning of the differentiation from day 0 to 1 and then the suppression of it from day 3 to 5, with a GSK3-inhibitor and a Wnt-inhibitor respectively. The protocol has been validated on different cell lines of both iPSCs and ESCs, yielding a final cardiomyocytes' differentiation efficiency of 82-92 % (Lian et al., 2013).

In 2014, Burridge and coworkers optimized fully defined media in order to reduce the possibility of dysfunctionality in the protocols (Burridge et al., 2014). For the differentiation, CHIR99021, the GSK3-inhibitor, has been used for two days, followed by treatment with WNT-inhibitor, WNT-C59, for the next two days. After that, the cells were cultured with CDM3 for the maintenance of cardiomyocytes. CDM3 is a medium composed by only three components: RPMI 1640 basal medium, recombinant albumin and L-ascorbic-acid. These are the only three components essential for complete differentiation of cardiomyocytes. The obtained cardiomyocyte population yielded the 85-95% of efficiency (Burridge et al., 2014). Besides, they showed that laminin-511 and laminin-521 allowed reliable pluripotent growth and long- term attachment of the CMs (Bird et al., 2003). A cheaper substitute for these factors could be Vitronectin, even though cells need to be passaged every 15 days (Burridge et al., 2014). The differentiated cardiomyocytes, obtained with differentiation protocols, correspond to three specific subtypes, atrial, ventricular, or nodal cardiomyocytes, which are recognizable by electrophysiological analysis.

D) Dynamic cell culture in suspension in spinner flask and/or bioreactors for a large-scale production of CMs is adopted in case of cell transplantation. This is because the number required for a transplantation is around the 10 billion of clinical grade hiPSC-derived CMs (Di Baldassarre et al., 2018). The protocol developed for the large-scale production derived from the already

tested protocol. One example is given by the method of the culture of hESC aggregates with a defined size obtained from suspension bioreactor combined with the micro-contact printing technique. This method gives rise to 50% of beating aggregates and results in a more efficient methods compared to the static culture (Niebruegge et al., 2009; Jing et al., 2010). The technique used by Kempf and coworkers leads to the production of 40 million of hiPSC-derived CMs (Kempf et al., 2014b). iPSCs were cultured as floating aggregates and differentiated in cardiomyocytes. Cells were transferred to a rotating Erlenmeyer flask and then to 100 ml stirred bioreactors perfused for feeding (Kempf et al., 2014b).

Table 1: A summary of the different protocol strategies published for the production of iPSC-derived CMs

Strategy	**Author**	**Title**	**Efficiency**	**CMs subtype**	**Reference**
EBs in static suspension culture	Lei Yang, Mark H Soonpaa, Eric D Adler, Torsten K Roepke, Steven J Kattman, Marion Kennedy, Els Henckaerts, Kristina Bonham, Geoffrey W Abbott, R Michael Linden, Loren J Field, Gordon M Keller	Human cardiovascular progenitor cells develop from a KDR+ embryonic-stem-cell-derived population	40-50% cardiac Troponin	Mixed atrial and ventricular	(Yang et al., 2008)
EBs in static suspension culture	Ioannis Karakikes , Grant D Senyei, Jens Hansen, Chi-Wing Kong, Evren U Azeloglu, Francesca Stillitano, Deborah K Lieu, Jiaxian Wang, Lihuan Ren, Jean-Sebastien Hulot, Ravi Iyengar, Ronald A Li, Roger J Hajjar	Small molecule-mediated directed differentiation of human embryonic stem cells toward ventricular cardiomyocytes	90% cardiac Troponin 100% beating	ventricular	(Karakikes et al., 2014)
EBs in static suspension culture	David A Elliott, Stefan R Braam, Katerina Koutsis, Elizabeth S Ng, Robert Jenny, Ebba L Lagerqvist, Christine Biben, Tanya Hatzistavrou, Claire E Hirst, Qing C Yu, Rhys J P Skelton, Dorien Ward-van Oostwaard, Sue Mei Lim, Ouda Khammy, Xueling Li, Susan M Hawes, Richard P Davis, Adam L Goulburn, Robert Passier, Owen W J Prall, John M Haynes, Colin W Pouton, David M Kaye, Christine L Mummery, Andrew G	NKX2-5(eGFP/w) hESCs for isolation of human cardiac progenitors and cardiomyocytes	96% beating 27% Nkx2.5	Not shown	(Elliott et al., 2011)

	Elefanty, Edouard G Stanley				
EBs in static suspension culture	Miao Zhang, Jan Sebastian Schulte, Alexander Heinick, Ilaria Piccini, Jyoti Rao, Roberto Quaranta, Dagmar Zeuschner, Daniela Malan, Kee-Pyo Kim, Albrecht Röpke, Philipp Sasse, Marcos Araúzo-Bravo, Guiscard Seebohm, Hans Schöler, Larissa Fabritz, Paulus Kirchhof, Frank Ulrich Müller, Boris Greber	Universal cardiac induction of human pluripotent stem cells in two and three-dimensional formats: implications for *in vitro* maturation	50% cardiac Troponin 100% beating	ventricular	(Zhang et al., 2015)
Monolayer- sandwich	Jianhua Zhang , Matthew Klos, Gisela F Wilson, Amanda M Herman, Xiaojun Lian, Kunil K Raval, Matthew R Barron, Luqia Hou, Andrew G Soerens, Junying Yu, Sean P Palecek, Gary E Lyons, James A Thomson, Todd J Herron, José Jalife, Timothy J Kamp	Extracellular matrix promotes highly efficient cardiac differentiation of human pluripotent stem cells: the matrix sandwich method	90% cardiac Troponin	Mixed atrial and ventricular	(Zhang et al., 2012a)
Monolayer	Michael A Laflamme, Kent Y Chen, Anna V Naumova, Veronica Muskheli, James A Fugate, Sarah K Dupras, Hans Reinecke, Chunhui Xu, Mohammad Hassanipour, Shailaja Police, Chris O'Sullivan, Lila Collins, Yinhong Chen, Elina Minami, Edward A Gill, Shuichi Ueno, Chun Yuan, Joseph Gold, Charles E Murry	Cardiomyocytes derived from human embryonic stem cells in pro-survival factors enhance function of infarcted rat hearts	50% Myosin Heavy Chain	Not shown	(Laflamme et al., 2007)
Monolayer	Miao Zhang, Jan Sebastian Schulte, Alexander Heinick, Ilaria Piccini, Jyoti Rao, Roberto Quaranta, Dagmar Zeuschner, Daniela Malan, Kee-Pyo Kim, Albrecht Röpke, Philipp Sasse, Marcos	Universal cardiac induction of human pluripotent stem cells in two and three-dimensional formats: implications for *in vitro* maturation	90% cardiac Troponin	ventricular	(Zhang et al., 2015)

	Araúzo-Bravo, Guiscard Seebohm, Hans Schöler, Larissa Fabritz, Paulus Kirchhof, Frank Ulrich Müller, Boris Greber				
Monolayer	Xiaojun Lian, Xiaoping Bao, Misha Zilberter , Mattias Westman, André Fisahn , Cheston Hsiao, Laurie B Hazeltine , Kaitlin K Dunn , Timothy J Kamp , Sean P Palecek	Chemically defined, albumin-free human cardiomyocyte generation	98% cardiac Troponin	Mixed atrial and ventricular	(Lian et al., 2015)
Monolayer	Paul W Burridge, Elena Matsa, Praveen Shukla, Ziliang C Lin , Jared M Churko, Antje D Ebert, Feng Lan, Sebastian Diecke, Bruno Huber, Nicholas M Mordwinkin , Jordan R Plews , Oscar J Abilez, Bianxiao Cui, Joseph D Gold, Joseph C Wu	Chemically defined generation of human cardiomyocytes	90% cardiac Troponin	Mixed atrial and ventricular	(Burridge et al., 2014)
Monolayer	Shan S Parikh, Daniel J Blackwell, Nieves Gomez-Hurtado, Michael Frisk, Lili Wang, Kyungsoo Kim, Christen P Dahl, Arnt Fiane , Theis Tønnessen, Dmytro O Kryshtal , William E Louch, Bjorn C Knollmann	Thyroid and Glucocorticoid Hormones Promote Functional T-Tubule Development in Human-Induced Pluripotent Stem Cell-Derived Cardiomyocytes	80% colocalization a-actinin and Junctophilin 2	Mixed atrial and ventricular	(Parikh et al., 2017)
Suspension Large Scale Matrix-dependent aggregate/ Rocker culture	Sherwin Ting, Allen Chen, Shaul Reuveny , Steve Oh	An intermittent rocking platform for integrated expansion and differentiation of human pluripotent stem cells to cardiomyocytes in suspended microcarrier cultures	65% cardiac Troponin	Not shown	(Ting et al., 2014)
Suspension Large Scale Matrix-dependent aggregate-EBs/Spinner flasks	Allen Kuan-Liang Chen, Xiaoli Chen, Andre Boon Hwa Choo, Shaul Reuveny, Steve Kah Weng Oh	Critical microcarrier properties affecting the expansion of undifferentiated human embryonic stem cells	80 % beating	Not shown	(Chen et al., 2011)

Suspension Large Scale Matrix-independent aggregate/Erlenmeyer Flask and bioreactor	Henning Kempf, Ruth Olmer, Christina Kropp, Michael Rückert, Monica Jara-Avaca, Diana Robles-Diaz, Annika Franke, David A. Elliott, Daniel Wojciechowski, Martin Fischer, Angelica Roa Lara, George Kensah, Ina Gruh, Axel Haverich, Ulrich Martin and Robert Zweigerdt	Controlling expansion and cardiomyogenic differentiation of human pluripotent stem cells in scalable suspension culture	84% cardiac Troponin	80-90% ventricular	(Kempf et al., 2014a)
Suspension Large Scale Matrix-independent aggregate/ Spinner flask	Hananeh Fonoudi, Hassan Ansari, Saeed Abbasalizadeh , Mehran Rezaei Larijani, Sahar Kiani , Shiva Hashemizadeh , Ali Sharifi Zarchi , Alexis Bosman, Gillian M Blue, Sara Pahlavan, Matthew Perry, Yishay Orr, Yaroslav Mayorchak , Jamie Vandenberg, Mahmood Talkhabi, David S Winlaw, Richard P Harvey, Nasser Aghdami , Hossein Baharvand	A Universal and Robust Integrated Platform for the Scalable Production of Human Cardiomyocytes From Pluripotent Stem Cells	>90% cardiac Troponin	Not shown	(Fonoudi et al., 2015)

4.4.2 Neural differentiation

As already described for the heart, also studying brain mechanisms and neurodegenerative diseases is difficult without a proper cell source. In fact, collect brain tissue or neurons from the neural system of one subject is very risky and it can create damage to its integrity and healthy status. In addition, neurons are post-mitotic cells, therefore cannot be expanded for long time in order to obtain a high quantity of material (Corti et al., 2015). The advent of iPSCs and their differentiation capability to any cell type is a powerful tool potentially able to solve these problems. As already pointed out for cardiomyocytes, iPSCs are an infinite source of autologous patient material that can be easily expanded for long time *in vitro*. When stimulating their differentiation toward the neural fate, iPSC-derived neurons provide an efficient tool for studying neural functions and/or development and they represent cell models specific for different neurological diseases, able to recapitulate the mechanisms underlying the different pathologies (Mertens et al., 2016; Tao and Zhang, 2016).

In vitro neural differentiation is possible thanks to the exhaustive studies of the last years on mammalian brain development (Mertens et al., 2016; Pons-Espinal et al., 2017). Indeed, the *in vitro* neural differentiation follows each step of the *in vivo* developmental stages driven by

different signaling pathways and cues in a time-controlled manner (Young, 2011). The differentiation is characterized by the unidirectionality of the process and the loss of the multipotency of the neural progenitors cells (NPC), making feasible the definition of the neuronal subtype characteristics (Burney et al., 2013). The induction of neuroepithelial cells (NEPs), also called neural induction, is the initial step for the generation of a subset of neurons derived from iPSCs. This process corresponds to the *in vivo* specialization of the ectoderm toward the neural fate. NEPs work as neural progenitor cells able to produce all the post-mitotic mature neurons under the exposure of environmental cues (Willardsen and Link, 2011). The most common method for the derivation of NEPs is in monolayer cultures. Usually, it is possible to obtain the NEP induction through the initial inhibition of transcription growth factor-β (TGF-β) and bone morphogenetic protein (BMP) pathways. The inhibition of both pathways is performed blocking SMAD, one key player of both pathways. SMAD is inhibited using two antagonist molecules Noggin (BMP-inhibitor) and SB431542 (TGF-β-inhibitor) (Chambers et al., 2009; Fei et al., 2010; Corti et al., 2015; Tao and Zhang, 2016; Vieira et al., 2018).

After the neural induction, cells define their neural subtype fate with the *in vivo* formation of the neural tube, where the neural plate (NP) fold itself (Tao and Zhang, 2016). The *in vitro* subtype specification of the neural progenitors is coordinated spatially and temporarily by morphogens and mitogens molecules along the axes. Together with signaling pathways, transcription factors (TF) as well are key-regulators and controllers of the neural differentiation (Urbán and Guillemot, 2014), defining the final response of the signal pathways (Osório, 2016). Signaling pathways are manipulated through the use of different morphogens and mitogens molecules, obtaining an enriched population of a specific neural subtype and conferring to them their regionalization and final identity (Chambers et al., 2009; Fasano et al., 2010; Maury et al., 2015; Tao and Zhang, 2016). Morphogens are molecules secreted in different regions of the dorsal-ventral and anterior-posterior axes which, during their secretion time, create a gradient in the axes, specifying the expression of specific neurons only in defined regions (Vieira et al., 2018) and defining their transcriptional code (Tao and Zhang, 2016). Some of the most important morphogen pathways are: Sonic Hedgehog (SHH) signaling as ventralizing factor, BMP signaling as dorsalizing factor, WNT signaling as caudalizing and dorsalizing factor, fibroblast growth factor (FGF) and retinoic acid (RA) as anteroposterior factors (Ciani and Salinas, 2005; Liu and Niswander, 2005; Fuccillo et al., 2006; Maden, 2007; Mason, 2007).

4.4.2.1 Sympathetic neural differentiation: in vivo vs. in vitro

First studies conducted *in vitro* for SNs differentiation were still based on the initial induction of the neural crest. One of the first group studying sympathetic neural differentiation was the one led by Lee (Lee et al., 2007; Lee et al., 2010). Human PSCs were differentiated inducing the neural rosette progenitors and isolating them manually. Neural crest cells were spread out from these neural rosette progenitors and isolated using flow cytometry (Lee et al., 2007; Lee et al., 2010). In 2014 Zeltner et al. increased the efficiency of the differentiation protocol and adapted the culture to feeder-free conditions (Zeltner et al., 2014). A further improvement of the protocol was achieved by another research group differentiating hPSCs directly in neural crest precursors through WNT activation(Menendez et al., 2011; Menendez et al., 2013) and SMAD inhibition

(Chambers et al., 2009), thus preventing the neural rosette formation and the sorting steps . Given the fact that the induction of Menendez at al. did not clarify the subtype of neural crest cells, Mica et al. optimized the neural crest induction adding BMP treatment later on WNT activation and SMAD inhibition (Mica et al., 2013).

4.4.2.2 Strategies for sympathetic neural differentiation

In the last 15 years, several attempts from many research groups have been made to generate cells with sympathetic like characteristics starting from different cell sources and with different strategies. However none of them was able to provide an exhausting neural characterization (Wu and Zeltner, 2019) of the novel obtained cell population. Recently, the panorama of differentiation of cells into sympathetic neurons has grown and now many groups provided paper-protocols and research-papers indicating a clear strategy for the development of stem cell derived sympathetic neurons. Among the well-studied protocols there are the ones proposed by Oh et al. (Oh et al., 2016) and Zeltner et al. (Zeltner et al., 2016; Saito-Diaz et al., 2019; Saito-Diaz and Zeltner, 2019; Wu and Zeltner, 2020), both focused on the derivation of trunk neural crest cells, and by Abu-Bonsrah et al. (Abu-Bonsrah et al., 2018), Frith et al.(Frith et al., 2018; Frith and Tsakiridis, 2019), and Kirino et al.(Kirino et al., 2018), based on the generation of NMP progenitors and the following induction of neural crest cells.

In 2016, Lee's group proposed a differentiation protocol followed by a detailed characterization of the obtained cells (Oh et al., 2016). To monitor the differentiation progression, the group created two hiPSC reporter lines, expressing green fluorescent protein (GFP) from the loci of *ASCL1* (SAP marker) and *PHOX2B* (SNs marker). The first step of the differentiation protocol consisted in the induction of the neural crest cells with the SMAD inhibitors LDN193189 and SB431542 (Chambers et al., 2009). To increase the neural crest induction, the three inhibitor molecules CHIR99021, DAPT, PD173074 (MEK inhibitor), were used (Oh et al., 2016). It has been shown that it is essential to activate the WNT pathway with CHIR99021 one day before SHH activation, to achieve a higher expression of ASCL1 and PHOX2B. To further increase this expression of these two key transcription factors, SHH was used in combination with purmorphamine (PMP), a SHH agonist, and BMP4. The PHOX2B reporter line was sorted at day 14 of the differentiation in order to isolate a pure population of sympathetic neuronal precursors. The maturation of the cells was performed for other 15 days, cultivating the cells in presence of the following factors: cAMP, ascorbic acid, NGF, BDNF and GDNF. The maturation of hPSC-derived SNs was confirmed by the gene expression of *ASCL1, PHOX2A/B, INSM1, ISL1, TH* and *DBH*, by electrophysiological measurements using Ca^{2+} and Na^{+} channel blockers, reactivity to nicotine and release of dopamine and norepinephrine. Further maturation was provided to hPSC-derived SNs by coculturing with primary cardiomyocytes (Oh et al., 2016).

In the same year, starting from the same approach of the neural crest induction, Zeltner et al. published a protocol of SN differentiation generated from iPSCs (obtained from fibroblasts) of patients with mild/severe Familial Dysautonomia, recapitulating the disease-related phenotypes (Zeltner et al., 2016). After SMAD inhibition, they added CHIR99021 until day 11 inducing neural crest cells. At day 11 cells are sorted for the cell surface marker α 4-integrin/CD49D and positive

cells for this marker were put in culture in form of floating spheroids. Spheroids were cultured for additional 4 days with CHIR99021 and FGF2 factors in order to recover the cells and to enlarge the neural crest progenitor's population. This step is important also for the posteriorization of the neural crest cells and to pave the way for the further sympathetic differentiation. After day 15, the spheroids have been plated and maturated with cAMP, ascorbic acid, NGF, BDNF and GDNF and a low concentration of retinoic acid. The cells expressed high levels of ASCG10, TH, SCL1, PHOX2A and DBH. However, this cell population was not able to release norepinephrine, thus resulting immature in comparison to the SN neurons obtained by Oh et al. (Oh et al., 2016).

Always using the strategy of floating spheroids, Kirino's group developed an alternative protocol for the development of hiPSC-derived SNs starting with the NMP induction (Kirino et al., 2018). Kirino et al. together with Frith et al. (Frith et al., 2018; Frith and Tsakiridis, 2019) were the first two groups able to recapitulate *in vitro* the induction of trunk- neural crest cells starting from NMP. Before the beginning of the differentiation protocol, cells were aggregated (10.000 cells/well). In the initial step (the first 3 days of differentiation) of the protocol proposed by Kirino et al. there is the stimulation of the differentiation of NMP-like cells using CHIR99021 and SB431542. For the neural crest progenitors' induction, they performed a treatment of 7 days with FGF2, BMP4 and retinoic acid (until day 10). At this point, cell aggregates are dissociated for sorting ($CD49d^{+}eGFP^{+}$) and reaggregated in spheroids (100.000 cells/well) cultured on ultra-low attachment plates to induce SAP using the factor BMP4, EGF and FGF2 in neurobasal medium supplemented with B27 for 7 days. The maturation of the hPSC-derived SNs was conducted on ultra-low attachment plates under the stimulation of NGF, GDNF and BDNF factors for two weeks. For the validation of the protocol a reporter line linking GFP to PHOX2B was created to confirm the efficiency of the protocol. They sorted the cell for the report line and cultured them until day 30 of differentiation. The 80% of hPSC-derived SNs positively expressed PRPH, TH, DBH and PHOX2B markers. The researcher group confirmed the possibility to reproduce the protocol for the derivation of SNs without the need of reporter lines and sorting procedure; it is only necessary to dissociate and replate the cells at day 10 of differentiation and further cultivate them on ultra-low attachment plates (250.000 cells/well) as described above. The efficiency of the differentiation protocol is verified by flow cytometry analysis, confirming the production of ca. 80% of hPSC-derived SNs (Kirino et al., 2018; Wu and Zeltner, 2019).

Another protocol deriving SNs starting from the NMP induction is proposed by Frith's group (Frith et al., 2018; Frith and Tsakiridis, 2019). They stimulated hPSCs for NMP induction with CHIR99021 and FGF2 for 3 days; this is the conventional and most used approach for the induction of NMP (Henrique et al., 2015). The use of FGF2 by Frith et al. (Frith and Tsakiridis, 2019) is different from the use proposed in the differentiation method by Kirino et al. (Kirino et al., 2018). Frith et al. used FGF2 for the NMP induction and not after the NMP induction like Kirino et al. (Frith and Tsakiridis, 2019). The later use of FGF2 by Kirino et al. (Kirino et al., 2018) could be ascribable to the effective induction of trunk-neural crest. On the contrary Frith et al. (Frith and Tsakiridis, 2019) used CHIR99021, SB431542, BMP4 (moderate) and the BMP4 receptor type I inhibitor DMH1. The combination of a BMP4 agonist and antagonist seems contrasting but this strategy could finely

modulate BMP levels and increase differentiation consistency among experiments (Hackland et al., 2017). For the SAP induction, BMP4 concentration was increased at day 8 of differentiation and the factors SHH and PMP were added, as in Oh et al. (Oh et al., 2016). Starting from day 12 of differentiation, cells were maturated with NGF, GDNF and BDNF factors for one week. During the differentiation protocols, the sympathetic fate evolution was confirmed by FACS analysis. Cells obtained at day 12 of differentiation and at the end of the protocol showed a comparable level of PHOX2B, ASCL1, GATA2/3 and ISL1. Instead, only the cells obtained at the end of the differentiation (day 19) displayed a higher level of PHOX2A, TH and DBH, confirming the mature phenotype of these neurons. In general, the protocol for the derivation of SNs has an efficiency around the 50% and it is the shortest protocol in comparison to the previous proposed by Oh et al. Zeltner et al. and Kirino et al (Oh et al., 2016; Zeltner et al., 2016; Kirino et al., 2018).

Table 2: A summary of the different protocol strategies published for the production of iPSC-derived SNs

Year	Author	Title	Strategy	Cell Types	Ref
2016	Oh Y, Cho GS, Li Z, Hong I, Zhu R, Kim MJ, Kim YJ, Tampakakis E, Tung L, Huganir R, Dong X, Kwon C, Lee G.	Functional Coupling with Cardiac Muscle Promotes Maturation of hPSC-Derived Sympathetic Neurons	Neural crest induction	PHOX2B::eGFP / OCT4::eGFP/ SOX10::eGFP / ASCL1::eGFP reporter hESC lines	(Oh et al., 2016)
2016	Zeltner N, Fattahi F, Dubois NC, Saurat N, Lafaille F, Shang L, Zimmer B, Tchieu J, Soliman MA, Lee G, Casanova JL, Studer L.	Capturing the biology of disease severity in a PSC-based model of familial dysautonomia	Neural crest induction	PSC derived from fibroblasts	(Zeltner et al., 2016)
2018	Kirino K, Nakahata T, Taguchi T, Saito MK.	Efficient derivation of sympathetic neurons from human pluripotent stem cells with a defined condition	NMP and Neural crest induction	hESC lines KhES1 and KhES3; iPSC lines 409B2 and 604A1	(Kirino et al., 2018)
2019	Frith TJR, Tsakiridis A.	Efficient Generation of Trunk Neural Crest and Sympathetic Neurons from Human Pluripotent Stem Cells Via a Neuromesodermal Axial Progenitor Intermediate	NMP and Neural crest induction	hPSCs	(Frith and Tsakiridis, 2019)
2020	Wu HF, Zeltner N.	Efficient Differentiation of Postganglionic Sympathetic Neurons using Human Pluripotent Stem Cells under Feeder-free and Chemically Defined Culture Conditions	Neural crest induction	hPSCs	(Wu and Zeltner, 2020)
2019	Saito-Diaz K, Wu HF, Zeltner N.	Autonomic Neurons with Sympathetic Character Derived From Human Pluripotent Stem Cells	Neural crest induction	hESC WA09; hESC SOX10::GFP; hiPSCS	(Saito-Diaz et al., 2019)

2018	Frith TJ, Granata I, Wind M, Stout E, Thompson O, Neumann K, Stavish D, Heath PR, Ortmann D, Hackland JO, Anastassiadis K, Gouti M, Briscoe J, Wilson V, Johnson SL, Placzek M, Guarracino MR, Andrews PW, Tsakiridis A.	Human axial progenitors generate trunk neural crest cells *in vitro*	NMP and Neural crest induction	hPSC lines: a Shef4-derived Sox2-GFP reporter hESC line; H9-derived T-VENUS; SOX10-GFP; PHOX2B-GFP reporter hESC lines; MSGN1-VENUS reporter hiPSC line ; wild type Mastershef7 hESC line; iPSC line (MIFF-1) derived from healthy individual	(Frith et al., 2018)
2016	Huang M, Miller ML, McHenry LK, Zheng T, Zhen Q, Ilkhanizadeh S, Conklin BR, Bronner ME, Weiss WA.	Generating trunk neural crest from human pluripotent stem cells	Neural crest induction	ESC (H1) and iPSC (WTC) line	(Huang et al., 2016)
2018	Carr-Wilkinson J, Prathalingam N, Pal D, Moad M, Lee N, Sundaresh A, Forgham H, James P, Herbert M, Lako M, Tweddle DA.	Differentiation of Human Embryonic Stem Cells to Sympathetic Neurons: A Potential Model for Understanding Neuroblastoma Pathogenesis	Neural crest induction	H9 hESCs	(Carr-Wilkinson et al., 2018)
2018	Herrmann M, Anders S, Straub RH, Jenei-Lanzl Z.	TNF inhibits catecholamine production from induced sympathetic neuron-like cells in rheumatoid arthritis and osteoarthritis *in vitro*	Human synovial adipose cells	Human synovial adipose tissue-derived stem cells (sASC)	(Herrmann et al., 2018)

4.4.3 iPSC Application

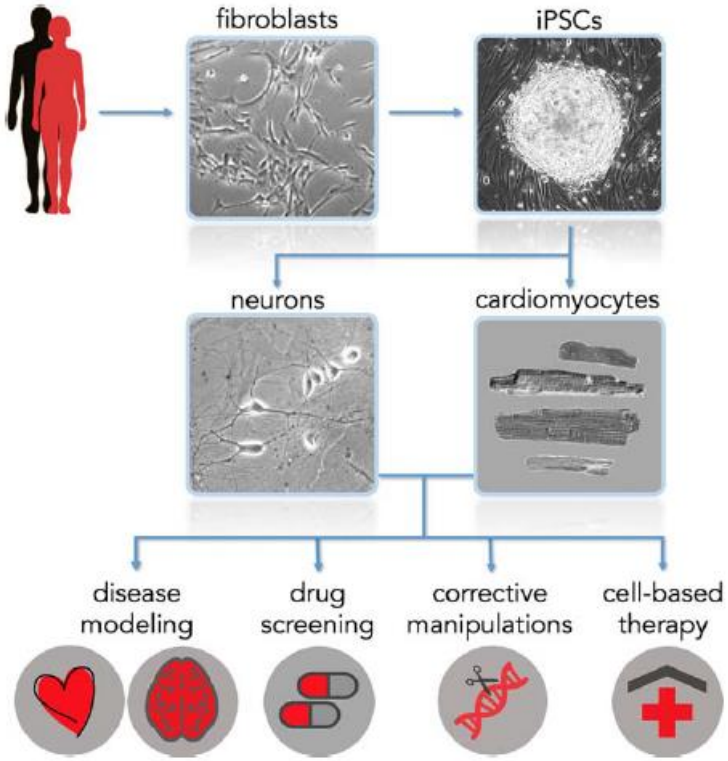

Figure 6: iPSC Applications. Reproduced with permission from Coskun - Journal of Neuroscience Research - John Wiley & Sons, Inc., - 2016. (Coskun and Lombardo, 2016)

All the cells of the body possess the same genetic material, therefore, if one individual carries a mutation, all the cells of his body carry the same mutation (Yang et al., 2008). iPSC and iPSC-derived cells maintain the same genetic background of the origin patients, thus helping the scientist in the recapitulation of phenotype of genetic diseases and in the elucidation of the molecular basis of pathologies, leading also the creation of library of patient-specific iPSCs (Karagiannis et al., 2019) and iPSC bank (Ohnuki and Takahashi, 2015; Di Baldassarre et al., 2018). The iPSC patient specificity is a fundamental characteristic of iPSCs, which turns out to be extremely useful in iPSC applications as disease modeling, drug screening and cell-based therapy.

4.4.3.1 Disease models

In the past, animal models have been used for the study of the disease' mechanisms and they enormously contributed to the elucidation of different pathologies. However, animal models have the big disadvantage that present considerable differences with the human models (Ohnuki and Takahashi, 2015). An important application of iPSC-derived cells is the development of disease models, in order to study the molecular mechanisms, underlying the pathogenesis of the diseases and the interactions with the environment (Liang et al., 2019). Thanks to the direct derivation of iPSCs from a patient and the consequent exact maintenance of the genetic background and variations, with the iPSC-model it is possible to create a connection between the phenotype and

the genotype. Deriving the iPSC line from a whole family helps to reduce the genetic differences and bias between the patients and controls recapitulating the complexity of the disease with more precise results. Big advantages of iPSCs are the easy reproducibility, low costs, non-time consuming and the higher amount of cell production (Del Alamo et al., 2016), resulting in an important source for generation of iPSC line specific for each disorder. Since then, several groups have used iPSCs as cell models to study inherited cardiomyopathies and neurological disorder and a growing number of patient-specific iPSC lines of genetically inherited cardiovascular diseases and neural disorder have been generated (Imaizumi and Okano, 2014; Tanaka et al., 2015). Some example are the models of long QT syndrome (LQTS) (Moretti et al., 2010b) (Matsa et al., 2014) (Ma et al., 2013b) (Yazawa et al., 2011), catecholaminergic polymorphic ventricular tachycardia (CPVT) (Fatima et al., 2011; Di Pasquale et al., 2013b), ACM (Kim et al., 2013; Ma et al., 2013a), Alzheimer's disease (Yagi et al., 2011; Israel et al., 2012; Kondo et al., 2013), Parkinson's disease (Devine et al., 2011; Nguyen et al., 2011; Seibler et al., 2011; Imaizumi et al., 2012; Jiang et al., 2012; Liu et al., 2012; Sánchez-Danés et al., 2012; Rakovic et al., 2013; Reinhardt et al., 2013), amyotrophic lateral sclerosis (Mitne-Neto et al., 2011; Bilican et al., 2012; Egawa et al., 2012) , Huntington's disease (Park et al., 2008; Zhang et al., 2010; An et al., 2012; Camnasio et al., 2012; Jeon et al., 2012; Juopperi et al., 2012), schizophrenia (Brennand et al., 2011; Chiang et al., 2011; Pedrosa et al., 2011; Paulsen Bda et al., 2012), familial dysautonomia (Lee et al., 2009; Lee et al., 2012), Down syndrome (Li et al., 2005; Park et al., 2008; Weick et al., 2013).

4.4.3.2 Drug screening and Toxicity test

Around 89% of drugs successfully pass the *in vitro* and *in vivo* animal model tests, but when they late arrive at their human target in the clinical trials, they are withdrawn (Kola and Landis, 2004). The major cause of drugs withdrawn from the market is the unpredictable cardiovascular toxicity, resulting in 33% of drug failure (MacDonald and Robertson, 2009). The principal collateral effects of these drugs are the risk of arrhythmias (QT prolongation), life-threatening polymorphic ventricular tachycardia or Torsade de Pointes (TdP) (Mandenius et al., 2011). In fact, TdP was traditionally evaluated as the arrhythmic potential in the preclinical test of new drugs (Callaghan et al., 2019). A long period of prediction, studies, hypotheses precedes the identification of targets and the strategies for the development of the new drug proposal, which can be useless if the final drug has unpredictable effects (Del Alamo et al., 2016). The unsuccess during the drug testing reflects also in a big loss of money (Khan et al., 2013) and a waste of time (Khan et al., 2013). For instance, iPSCs represent the new paradigm for an early introduction of the human part in the discovery pipeline (Del Alamo et al., 2016). The development of differentiated cardiomyocytes from iPSCs opens a new frontier in the safety testing and validation of new drugs to evaluate toxicity and side effects. (Weinberger et al., 2017). The possibility to create a disease specific cell-models allows the screening of already established and new drugs. With the peculiarity of the contraction functionality, iPSC-derived CMs respond immediately to cardioactive drugs (Laustriat et al., 2010), resulting in a high throughput tool for drugs screening process (Lian et al., 2010; Csöbönyeiová et al., 2016). The double potential of drug development and toxicological screening is especially relevant for large-scale production of iPSC-derived CMs (Csöbönyeiová et al., 2016).

4.4.3.3 Stem cell-based therapy for cardiac disease

In the clinical field, the advent of iPSCs kicks off new therapeutic strategies involving the injection of iPSCs and/or iPSC-derived cells in the patients, trying to ameliorate their pathological condition. As already mentioned previously in this introduction, iPSCs are easy to produce, can be derived from a non-invasive procedure and do not rise any ethical concern. They also have a potential for clinical application as they can be produced in significant high number and in feeder-free and xeno-free condition (elimination of all the animal and viral components in the material used to produce them) (Okita et al., 2011; Ohnuki et al., 2015). Furthermore, the autologous production of cells directly from the patient itself reduces the risk of immune rejection or infection (Araki et al., 2013; Guha et al., 2013)(Okita et al., 2011). The small capacity of regeneration of heart suggests the scientists that other unconventional approaches, like the cell-based therapy, can be taken into consideration for the management of the damaged myocardium. With their high cardiomyogenic potential, stem cells are considered a safe source for a potential non-traditional therapy for heart injuries (heart failure, ischemic heart and myocardial infraction) (Assmus et al., 2006; Schächinger et al., 2006; Kim et al., 2018; Mardanpour et al., 2019).

Among all effects triggered by the introduction of stem cells, the paracrine effect is the major contributor in the cell-therapy. In fact, cell therapy appears to be functional for myocardial infraction treatments thanks to the modulation of the paracrine effect, either in an autologous or allogenic injection of cells (Tao et al., 2016). The beneficial effect of new-injected cells consists in the recovery of dormant mechanisms of heart, improving the general conditions of the myocardium, reducing the infarcted area and enhancing angiogenesis (Gnecchi et al., 2006; Tao et al., 2016). The real mechanisms behind the paracrine effect are still not well completely understood, but it is believed that it does not influence a direct de novo cardiomyogenesis through the new engrafted stem cells; instead, the real capacity of stem cells is to stimulate a broad range of chemo-attractant molecules, vesicles, growth factors released by the secretome of stem cells to activate the self-healing capacity of heart, including angiogenesis, reducing heart remodeling, decreasing apoptosis and regulating homeostasis (Gnecchi et al., 2006; Di Baldassarre et al., 2018). However, some limitations can be attributable to the high cost and the long period to generate the cells.

4.4.4 Limitations of iPSC-derived CMs

Although the innumerable positive effects of iPSC-derived CMs, a big disadvantage is still evident: their immaturity. iPSC-derived CMs resemble fetal CMs (Mummery et al., 2003), appearing much more similar to 16-weeks fetal CMs (Weinberger et al., 2017) than to adult CMs. As for adult CMs that require many years to become fully mature (Peters et al., 1994), it has been demonstrated that prolonged time in culture of iPSC-derived CMs can improve their maturity but never leading to the complete maturity (Laflamme and Murry, 2011). iPSC-derived CMs, as fetal CMs in the physiological condition, are small round-shaped cells and with a long-term culture they can increase in size starting from an area of 400-500 μm^2 within 30-40 days from the start of the differentiation, enlarging until the area of 600-1700 μm^2 in 90-100 days of culture (Lundy et al., 2013; Robertson et al., 2013; Yang et al., 2014). Despite this augmentation in size, the morphology of iPSC-derived CMs remain still immature. Adult CMs are cells with an area of 1500 μm^2 and they

appear with an elongated rod-like shape and aligned anisotropically in comparison to iPSC-derived CMs, which *in vitro* maintain their irregular-circular and chaotic form and spread in all directions (Gerdes et al., 1992; Bird et al., 2003; Mummery et al., 2003; Zhang et al., 2009). The number of nuclei consists of another difference between iPSC-derived CMs and adult CMs. In fact, iPSC-derived CMs are mononucleated like fetal CMs, but in contrast with adult CMs, where the cells are binucleated (Snir et al., 2003) (Smolich, 1995).

iPSC-derived CMs are also different from adult CMs in terms of sarcomeric organization, gene expression, ultrastructure (e.g. T tubules and mitochondria), metabolism and electrophysiological properties.

iPSC-derived CMs have a scarce sarcomeric organization, with short and disorganized sarcomeres, with only variable Z-discs and I-bands formed and low myofibril density and orientation, resulting in a reduced force of contraction and poor organized contractile machinery (Snir et al., 2003; Lundy et al., 2013; Robertson et al., 2013). This organization is similar in fetal CMs, with myofilaments distributed randomly in the cell, low myofibril density and lacking M and H bands (Kim et al., 1992), but with a general more ordered alignment and an increase in the production of contractile materials. Adult CMs display a fully organized and aligned structure with all components of the sarcomere (Z-disc, M-, I-, H- and A bands) with a sarcomere length of 1,8 µm *in vitro* (in iPSC-derived CMs 1,6 µm) (Kim et al., 1992; Bird et al., 2003; Lundy et al., 2013). While in adult CMs the localization of gap-junctions is in the intercalated discs (Chen et al., 2009), in iPSC-derived CMs and in fetal CMs is all around the circumference of the cells, determining a slower conduction velocity (Denning et al., 2016).

Diverse level of gene expression is found in adult CMs vs. iPSC-derived CMs, and it is used to evaluate the level of maturity of cardiomyocytes. Adult CMs express a high level of: *MYH7* (βMHC), *SERCA2A, TNNI3, ITPR3, CAV3, RYR2, CASQ2, COAX6A2, S100A1, SCN5A, MYOM2/3*. On the contrary, iPSC-derived CMs have a low expression of the reporter genes, in particular: *MYH6* (αMHC), *CASQ2, RYR2, SERCA2A*, *TNNI1* and *PLN* (Denning et al., 2016; Machiraju and Greenway, 2019). Also, different myofibrillar protein isoforms are subjected to a switch. For example in iPSC-derived CMs (and in fetal CMs too) it is possible to find the expression of: titin elastic N2BA isoform (Opitz et al., 2004), slow skeletal Troponin I (ssTnI) (Metzger et al., 2003), more α- myosin heavy chain (αMHC) (Xu et al., 2009) and MLC2a (Hailstones et al., 1992) in comparison to adult CMs, where the following isoforms are expressed: cardiac titin stiffer N2B (Lahmers et al., 2004), cardiac Troponin I (cTnI) (Bhavsar et al., 1991), more β- myosin heavy chain (βMHC) (Xu et al., 2009) and MLC2v (Hailstones et al., 1992).

The fundamental element of the excitation-contraction coupling is the T-tubule network, which is perfectly developed and functioning in adult CMs, but is missing in the iPSC-derived CMs. T-tubules are essential in CMs because they regulate the contraction of the entire cell, transmitting the electric excitation and triggering the sarcoplasmic reticulum calcium release (Lieu et al., 2009). The lack of this key component in the iPSC-derived CMs produces a lower excitation-contraction

coupling, non-uniform calcium dynamics, and transients with a greater calcium peak in the sarcolemma (Fu et al., 2006; Itzhaki et al., 2006; Binah et al., 2007).

The number of mitochondria in the adult heart is high, around 20-40% of the total cell size, due to the high energy demand of the heart and they are distributed in all the cells, in a crystal-like lattice pattern with lamellar cristae (Denning et al., 2016). This is in contrast with the low number in iPSC-derived CMs, occupying a small volume of the cell, with a perinuclear localization (Denning et al., 2016) and a low oxidative capacity (Lopaschuk and Jaswal, 2010; Robertson et al., 2013). Different metabolisms are used: iPSC-derived CMs follow the glycolysis path for the production of energy, but the adult CMs' metabolism is based on the fatty acid oxidation with a high level of oxidative phosphorylation (Karakikes et al., 2015; Denning et al., 2016; Zhou et al., 2017).

The spontaneous beating of iPSC-derived CMs, ranging from 30 to 120 beats per minute (Hoekstra et al., 2012; Barbuti et al., 2016), is a clear sign of immaturity because adult CMs do not spontaneously beat. The spontaneous beating comes from a high level of pacemaker current I_f and a low inward rectifying potassium current I_{K1}, which marks the membrane potential at -20 to -60 mV in iPSC-derived CMs. Adult CMs have a value of -85mV.

iPSC-derived CMs compared to adult CMs are characterized by a less negative resting membrane potential (RMP)/maximal diastolic potential (MDP), a reduced upstroke velocity corresponding to the 10-50 V/s versus 150-350 V/s in adult CMs (Denning et al., 2016) and a less prominent phase 1 (Casini et al., 2017). The difference in the AP is a consequence of the functional differences in the ion channels due to density and gating properties (Casini et al., 2017). The density of I_{KS} (slow delayed rectifier potassium current) is the half in iPSC-derived CMs, with a current density of 0.18 pA7F max (Virág et al., 2001). The I_{Na} (inward sodium current) channel is lower in iPSC-derived CMs in comparison to adult CMs, with a capacitance of 30-70 pF versus 150 pF. The maximal peak amplitude of I_{Na} is larger in iPSC-derived CMs compared with adult CMs (Ma et al., 2011; Portero et al., 2017). *SCN5A*, the encoding gene for sodium channel is expressed at a lower level in iPSC-derived CMs compared to adult CMs (Liang et al., 2013a). Regarding the Ca^{2+} channels, there are two different Ca^{2+} channels: the L-type (I_{CaL}) and the T-type (I_{CaT}). In adult fresh isolated CMs, it is not possible to detect the I_{CaT} (Ono and Iijima, 2010), while in iPSC-derived CMs the presence of the two channels is under debate because some studies detect them (Ivashchenko et al., 2013) and some others not (Ma et al., 2011). I_{CaL} is extensively reported in iPSC-derived CMs (Ma et al., 2011; Veerman et al., 2015) and the current density and the mid/voltage inactivation values are similar to the one in adult CMs (Mewes and Ravens, 1994; Magyar et al., 2000). In general, the voltage dependence of activation in iPSC-derived CMs has more negative potential compared to adult CMs (Casini et al., 2017). Different studies reported that the I_{Kr} (rapid delayed rectifier potassium current) tends to be higher in iPSC-derived CMs, resulting in a consistent AP prolongation and inducing early afterdepolarizations, conducible the I_{Kr} to an important role in the repolarization iPSC-derived CMs (Itzhaki et al., 2011; Ma et al., 2011; Lahti et al., 2012b; Lee et al., 2016) and in the determination of MDP (Doss et al., 2012).

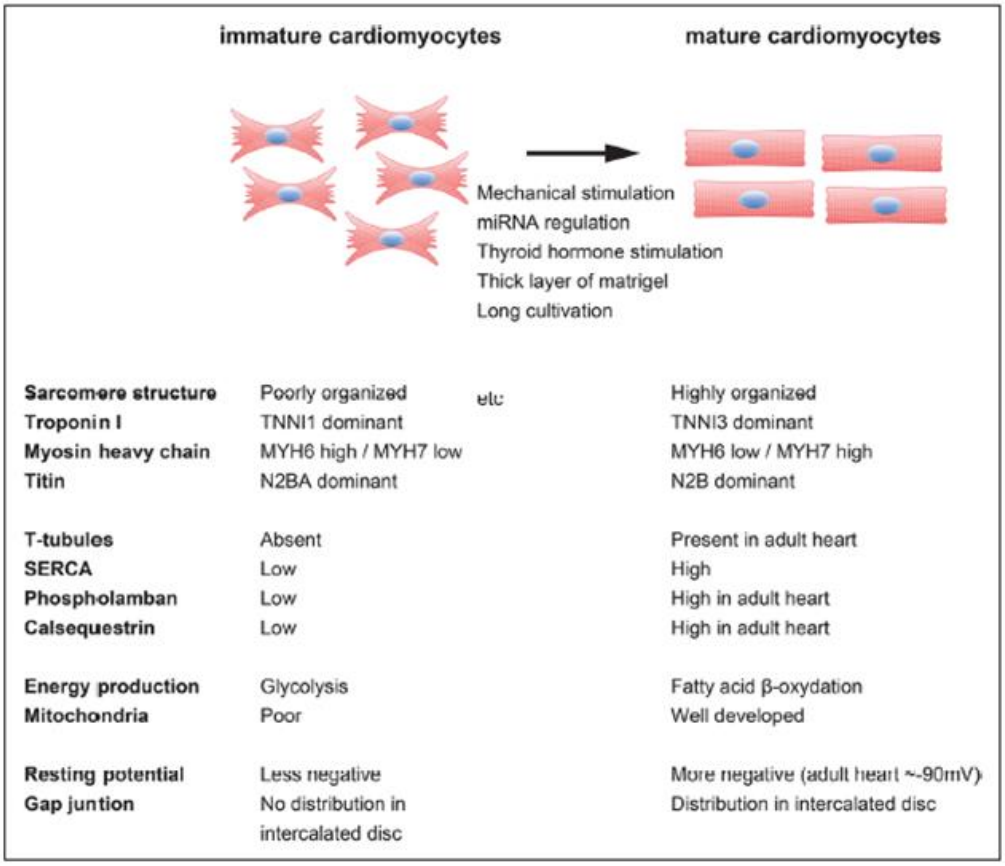

Figure 7: Mechanical, structural, and electrical differences between immature and mature CMs. Reproduced with permission from Yoshida – Circulation Research – American Heart Association Journal -- 2017. *(Yoshida and Yamanaka, 2017)*

4.5 Cardiac Tissue Engineering

The limited heart donor's availability and the immaturity of iPSC-derived CMs in monolayer adherent to plastic, and at the same time their easy availability have highlighted the lack of new innovative strategies for cardiac cell-models and cardiac repair. Based on these premises, a great development of cardiac tissue engineering approaches was observed, aimed at upgrading the iPSC-derived CMs based techniques used to study cardiac pathologies and to perform interventional actions (Hirt et al., 2014).

The first historical allusion to "tissue engineering" came from the painting "Healing of Justinian" by Beato Angelico in 1443. The painting describes the coming of Saints Cosma and Damiano in the proximity of the bed of Justinian. The Saints substituted the Justinian's leg with another one of a dead man, suggesting the idea of a real transplant (Vacanti, 2006). However, we can consider the first allusion to "tissue engineering" even before, already in the book "Genesis" with the creation of Eva from a rib of Adamo. (Vacanti, 2006). In the first scientific language use, back in the 80's, the term "tissue engineering" was still correlated with the use of prosthetic devices in surgical manipulation (Vacanti, 2006). The basis of the modern "tissue engineering" can be found in 1991 with the article "*Functional Organ Replacement: The New Technology of Tissue Engineering*"(Vacanti and Vacanti, 1991), referring to a discipline with the focus on the generation of new tissues, combing the basis of engineering and biological science (Vacanti, 2006). Nowadays, tissue engineering science corresponds to the union of different interdisciplinary fields such as chemistry, bioscience, biotechnology, material science and engineering, which all together giving rise to this new field in science (Fleischer et al., 2017; Rodrigues et al., 2018). The aim of this new discipline is the *in vitro* creation and maintenance of tissue-like constructs to the aim of replacing diseased tissue in different organs and to construct better model of the *in vivo* environment for research application.

The application of tissue engineering for cardiovascular research presented from the early beginning encouraging results. Replacing the scar tissue after a myocardial infarction with surrogates tissue is the final goal of cardiac tissue engineering (Fleischer et al., 2017), but the improvement of the maturity of iPSC-derived CMs, that has been observed with tissue engineering, results also in a significant amelioration of disease models (Hirt et al., 2014).

Many approaches of heart tissue engineering have been developed so far and combined together for creation of an ultimate model both for *in vitro* and *in vivo* applications. In more detail, the main components used for tissue engineering are scaffolds, signaling factors and cells. Scaffolds are used to recreate the native microenvironment and as substrates of tissue development. Signaling molecules control cell phenotypes and functions, comprising metabolism and cell organization. Different cell types can be used for the production of tissue matrixes, for integration of them with the existing tissue or provide metabolic support (Paschos et al., 2015). The new engineering strategies are long-term culture, electrical/mechanical/chemical/biological stimulation, co-culture of different cell' populations, three-dimensional (3D) structures, microfluidics/perfusion system and 3D print (Robertson et al., 2013; Yang et al., 2014; Veerman et al., 2015; Denning et al., 2016).

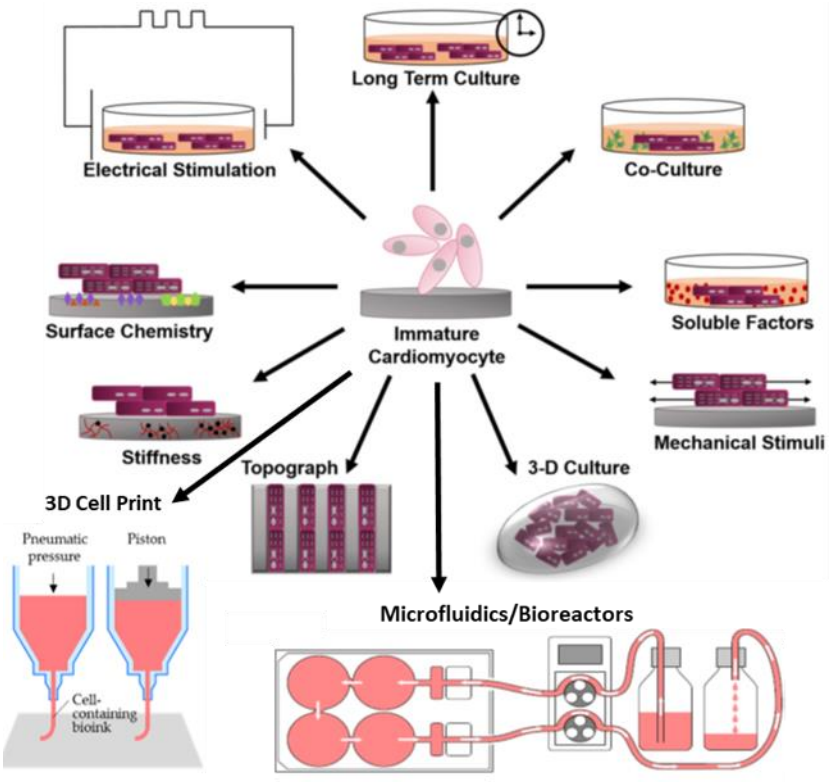

Figure 8: Refiguration of the possible methods of cardiac tissue engineering aimed to ameliorate iPSC-derived CMs models. Reproduced with permission from Besser – Theranostics – Ivyspring -- 2018*. Modified (Besser et al., 2018)*

3D *in vitro* models offer an alternative attractive to the traditional two-dimensional (2D) i*n vitro* models, promoting different advantages and reaching a higher degree of maturation compared to 2D cultures (Hirt et al., 2014). They are a platform for: pilot study on biomimetic, physiological health/diseased functional phenotype (Weinberger et al., 2017; Turnbull et al., 2018), and cell model amelioration through the introduction of mechanical, electrical and biological stimuli, which cells physiologically encounter in the human body (Ma and Vunjak-Novakovic, 2016; Zuppinger, 2019). The replication of a high level of similarities enables a perfect recapitulation of the biology and the geometry of the cells (Ma and Vunjak-Novakovic, 2016). The biomimetic cardiac cell model enables a more detailed analysis for cells dynamics, higher content readout and the elucidation of the diseases, but it is also considered a better tool for the development of a specific drug (Hirt et al., 2014; Ma and Vunjak-Novakovic, 2016). Simple monolayer 2D-models are expected to respond to drugs, toxins and signaling molecules as *in vivo*, but this is not possible because in physiological conditions cells are not adherent to a plastic surface, instead they are embedded in extra cellular matrix (ECM) and subjected to many stimuli (Zuppinger, 2019). The engineered 3D-models, which recapitulate an ECM-like structure, and the correlated stimuli can

provide and predict more detailed results of cardiotoxicity tests and reduce the withdrawal of many drugs (Lasser et al., 2002; Zuppinger, 2019).

4.5.1 Co-culture

The human heart is made of not only by CMs but together with fibroblasts (FBs), vascular smooth cells (VSMCs) endothelial cells (ECs), immune cells and neurons, they compose the whole cell population of the heart (Figure 9) (Wanjare and Huang, 2017; Zamani et al., 2018). Only the 20-30% of cells constitutes the CMs population, the resting 70-80 % is represented by the non-myocytes part of the population (Gilsbach et al., 2014; Bergmann et al., 2015; Weinberger et al., 2017); it is important to consider that the cell population ratio varies in the different region of heart (Zamani et al., 2018). If CMs are the responsible of the transmission of the electrical impulse, the other cells have a principal role in the vascularization, secretion of ECM components and reacting to O_2 debt (Kofron and Mende, 2017). The cooperation of all the cell types grants the cellular organization, differentiation, the best viability and functionalities for heart, modulating the electrical, biochemical and mechanical signals transmission (Kofron and Mende, 2017; Zamani et al., 2018). The communication between cell populations is mediated by cell-cell interactions, paracrine factors and ECM-mediated crosstalk (Zhang et al., 2012b), allowing also to the non-myocytes population to regulates CMs' functions (Kofron and Mende, 2017). As the heart is regulated by all these cell components, it is important to understand the multicellular interactions to elucidate insights for health and diseased conditions of cardiac tissue and for the development of an engineered cardiac tissue (ECT) (Zamani et al., 2018). The importance of a co-culture, otherwise the simultaneous culture of different cell types, is exactly due to the intent to better represent the native myocardium, being composed by many cell types and implementing the ECT model not only from the point of view of the matrixes, but also from the cellular point of view (Liau et al., 2017).

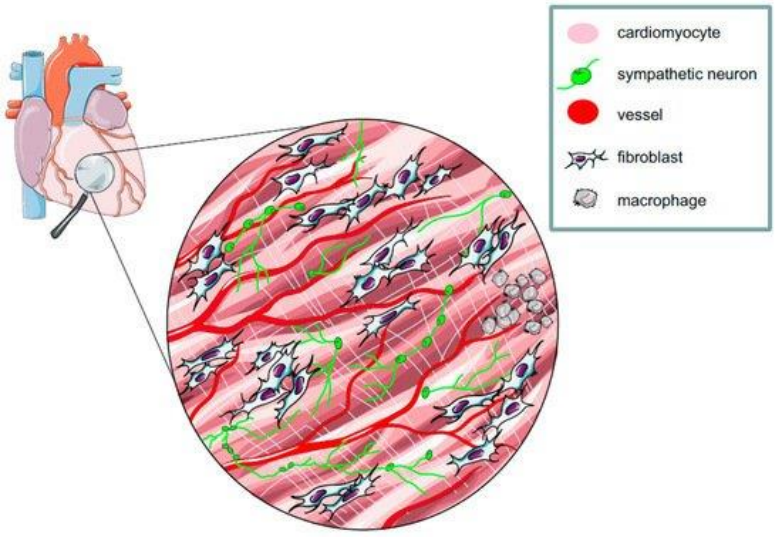

Figure 9: Schematic representation of the multicellular composition of the myocardium. Reproduced with permission from Zaglia – Methods and Protocols – MDPI - 2019. (Zaglia et al., 2019)

The first co-culture has been studied by Lawrence at al. in 1980 for the analysis of cell-cell communication (Lawrence et al., 1978) and from that moment co-culture methods became frequently used (Chan and Haschke, 1982). Successively, with the aim of differentiating stem cell in adult cells (Scheven et al., 1986), they finally acquire the leading role in the development of tissue engineering (Paschos et al., 2015). The cell populations used for the co-cultures can be defined differently: a) target cells are the cells, which compose the ECT and control the main tissue's functionalities; b) assisting cells are the cells which guide the target cells and control their proliferation, differentiation, organization (Paschos et al., 2015). The co-culture used for cell differentiation is one of the main goals of this methodology, where stem cells are usually cultured with terminally differentiated cells (Paschos et al., 2015). The co-culture approach allows for different cell types to be cultured in direct or indirect contact (Paschos et al., 2015). If in direct co-culture, cells are placed in contact and cultured together within the same plate, in indirect co-culture, cells are physically separated within the same microenvironment interacting only through the secretion of paracrine signals and soluble factors (Paschos et al., 2015). With co-culture it is possible to obtain the formation of ECT and to maintain the potency or enhance the differentiation of stem cells through signals' induction (Paschos et al., 2015). In detail, the direct co-culture can exist in 2D with monolayer of different cell types cultured together on the same layer and with the aim to study cell-cell interactions (Guan et al., 2011; Nishiofuku et al., 2011). Secondly, co-cultures can exist in 3D form used principally for the formation of mimetic constructs (Paschos et al., 2015). In the indirect culture there are many strategies for the separation of the two cell populations. For example in 2D, an insert (like a membrane or a separator) can be used to divide the cells (Vats et al., 2006) or in 3D, distinct populations can be maintained through the hydrogel encapsulation. One example is provided by the study of Ou et al. who cultured indirectly CMs in EBs in collagen matrix with cardiac FBs with the aim of cardiomyogenic differentiation stimulation. EBs were separated with well-inserts from FBs, allowing cells to be cultured in a similar microenvironment as the native myocardium. In fact, the direct contact was not necessary for this experiment because the only presence of FBs was sufficient to stimulate the differentiation of EBs, as suggested also by their beating activity and compared to a control culture without FBs (Ou et al., 2011). The cell interactions, which normally take place between cells, can deeply influence the entire system and the interaction types are the following: cell-cell adhesion, cell-ECM adhesion and paracrine signaling which can happen simultaneously with the other interactions or not (Paschos et al., 2015). The adhesion between cells is possible through the adherens, gap and tight junctions (Beeres et al., 2005; Schmidt et al., 2006). The redistribution of Connexin-43 and N-cadherin (gap junctions) has been demonstrated in a co-culture of neonatal CMs and human amniotic fluid-derived stem cells (Guan et al., 2011). The interaction of cell-ECM is very important (Scadden, 2006) because ECM features change strictly the influence on the behavior of cells in culture and, for consequence, of the whole system (Hoben et al., 2008). The remote control of the paracrine signaling is the most used in indirect cell culture and used for the differentiation of stem cells (Paschos et al., 2015). For example, Mummery et al. demonstrated the cardiomyogenic differentiation of human ESCs co-cultured with endoderm-like cells. The new differentiated CMs showed beating and typical electrophysiological characteristics of the cardiac

muscle (Mummery et al., 2003). The presence of CMs in a co-culture has been demonstrated to be essential also for the cardiospheres of progenitors' cardiac cells. Without the co-culture, cardiospheres did not display any beat (Laugwitz et al., 2005).

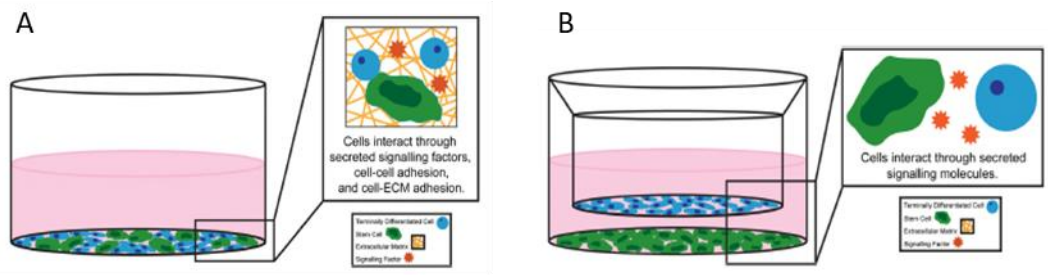

Figure 10: Examples of co-culture systems; image A shows a co-culture of different cell types in direct contact on one layer. On the contrary, image B represents a co-culture system of different cells not in direct contact and on two different layers. The interaction between them occurs through paracrine signaling. Reproduced with permission from Paschos – Journal of Tissue Engineering and Regenerative Medicine– John Wiley & Sons, Ltd.Inc – 2015. *(Paschos et al., 2015)*

4.5.1.1 Co-cultures for Neurocardiology

In the field of neurocardiology, many are the works conducted until now. Takeuchi et al. created a co-culture of superior cervical ganglia (SCG) and ventricular CMs deriving from the same Winstar rat. They cultured the two cell populations separately and on a self-made mini chamber placed on a multi electrode array (MEA) (Takeuchi et al., 2011b; Oiwa et al., 2016). Already after 3 days from CMs seeding, neurites from SCG started to connect with the CMs through microconduits (Figure 11). They detected evoked responses generated by a small number of SCG and a further application of electrical stimulation demonstrated the ability to modulate the beat rate of CMs. The modulation is dependent on the frequency and on the effect of interaction between the frequency and the number of pulses (Takeuchi et al., 2011a). Subsequently, they co-cultured with SCGs pluripotent cell-derived cardiomyocytes P19CMs, confirming the synapse formation and connection with β-3 tubulin, synapsin I, and cTnnI immunostaining. The beating rate of P19CMs is again controlled by the electrical stimulation and pulse frequency (Takeuchi et al., 2012; Takeuchi et al., 2013). This co-culture method evaluated the sympathetic effect on CMs, identifying it as a drug-screening tool for the prediction of cardiotoxicity side effects caused by sympathetic modulation (Sakai et al., 2017).

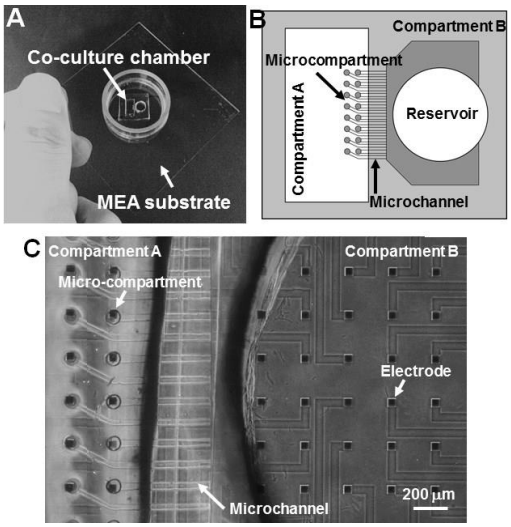

Figure 11: Organization of the two culture chambers connected with microconduit channels. Reproduced with permission from Takeuchi – Annual International Conference IEEE Eng Med Biol Soc – 2013 *(Takeuchi et al., 2013)*

The research group of Paterson co-cultured sympathetic stellate neurons and neonatal ventricular CMs from normal (WKY) and hypertensive (SHR) rats to analyze the cAMP response in CMs. The two populations were cultivated in direct contact. They highlighted the ability of neurons to drive the β-adrenergic phenotype in CMs. In particular, co-culture of SHT-CMs and neurons demonstrated an elevated CMs cAMP response compared to WKY co-cultures, suggesting different sensitivity to nicotine and norepinephrine release. Increasing the concentration of β-adrenergic agonist, SHR-CMs displayed a larger cAMP response compared to WKY-CMs, confirming that the β-adrenergic overactivity resulted in a hypersensitive state. If WKY-neurons were plated onto SHT-CMs, the diseased cAMP response of CMs resulted rescued. On the contrary, if SHT-neurons were plated onto WKY-CMs, the cAMP response of CMs resulted damaged. This work confirmed the dominant role of neurons in driving the β-adrenergic phenotype in CMs (Larsen et al., 2016).

Burton and coworkers published in 2019 (Burton et al., 2019) the co-culture of SNs with a cardiac monolayer analyzed for the first time with macroscopic optical interrogation using a dye-free optical imaging method (Burton et al., 2015) in order to demonstrate the effects of SNs on the behavior of cardiac culture. Ventricular CMs from rat pups were direct co-cultured with cardiac stellate neurons derived from littermates. They demonstrated that conduction velocity in co-cultures was increased and the expression of Connexin 43 (gap junction protein) was higher in co-cultured CMs, in accord with changes in pathways regulating gap junction proteins. Nicotine stimulation of SNs showed an increased beating rate in co-cultures. For the electrophysiological measurement of SNs in co-cultures, they used a high-throughput all-optical approach called OptoDyCe (Klimas et al., 2016), demonstrating that a single neuron could modulate the activity of many connected CMs. SNs were associated with optogenetic tools for the stimulation of CMs and

analyzed with the dye Di-4-ANBDQBS. The cardiac response to SNs stimulation demonstrated a dose-dependent effect, suggesting that culture with a higher concentration of SNs led to a higher cardiac activity. In conclusion they concluded that SNs could have a protective role on the CMs, improving conduction velocity, levels of Connexin 43 and they confirmed the OptoDyCe technique as a method for pharmacological assays and discovery studies (Burton et al., 2019).

Oh et al. created a functional protocol for the development of SNs-derived from induced pluripotent stem cells with and without cell sorting (Oh et al., 2016). The characterization of these SNs showed similarities with the *in vivo* counterpart. Subsequently they co-cultured these SNs with neonatal mouse ventricular myocytes (NMVMs), mouse embryonic stem cell or iPSC–derived CMs. The analyses demonstrated the formation of physical contact and synaptic vesicles between SNs and CMs. The importance of the physical connection was demonstrated by nicotine treatment on mouse embryonic stem cell-derived SNs as well. Nicotine-treated SNs were able to modulate the beating rate of NMVM only when the two cell populations were in contact. The research group also demonstrated the control of neuronal activity, adding optogenetic tools to SNs. In fact, when mouse embryonic stem cell-derived SNs expressing an optogenetic tool were co-cultured with NMVMs and in physical contact, the beating rate of CMs was optogenetically increased, suggesting that the new forming β-adrenergic connection between the two cell populations allowed pharmacological and optogenetic control. After the photostimulation, neurons in co-cultures released more neurotransmitter norepinephrine and they presented an increased level of catecholamine synthesis enzyme, nicotine acetylcholine receptors (nAChRs) and sodium/potassium channel in comparison with monoculture counterpart, assuring that the physical contact between SNs and CMs was crucial for the neuronal maturation. However, no functional and morphological analysis have been conducted on CMs and for consequence, the effect of SNs on CMs was not described (Oh et al., 2016).

Winbo´s group generated a co-culture model produced with sympathetic neurons and cardiomyocytes derived from iPSCs (Winbo et al., 2020). They characterized the newly obtained sympathetic neurons produced with the protocol proposed by Oh's group (Oh et al., 2016) and they confirmed the sympathetic lineage of the cells with different markers and techniques from a molecular and functional point of view. Furthermore, these iPSC-derived SNs were used to create co-cultures with iPSC-derived CMs for a period of 2 weeks. The co-cultures displayed neurites formations starting from iPSC-derived SNs and reaching the iPSC-derived CMs. They observed also the presence of varicosities around the synaptic connections. Functional analyses showed in the iPSC-derived SNs of the co-culture an increased action potential kinetics and upstroke velocity and a decreased decay time compared to the monoculture of neurons. After nicotine stimulation of iPSC-derived SNs, they confirmed the functional connections of the latter with the cardiac population, observing the increase of the beat rate of the iPSC-derived CMs.

5 MATERIALS AND METHODS

5.1 CELL CULTURE

5.1.1 Human iPSC Line

The Gibco Human Episomal iPSC Line (ThermoFisher Scientific - https://www.thermofisher.com/order/catalog/product/A18945#/A18945), (from now on "commercial iPSCs" – c_iPSC, or iPSC), was chosen for the present thesis, in order to avoid any ethical and consensus concerns. This iPSC line was derived from human cord blood-derived CD34+ cells using an integration-free episomal approach and the following factors: Oct4, Sox2, Klf4, Myc, Nanog, Lin28 and SV40 T. Human c_iPSCs were initially cultured on mouse embryonic fibroblasts, as feeder cell layer, and successively were adapted to feeder-free conditions by the supplier. The c_iPSC Line was fully characterized by the supplier. The line was provided with a normal karyotype and the endogenous expression of pluripotent markers was determined via Real Time-PCR (RT-PCR) and immunofluorescence analyses. Additionally, in directed differentiation and teratoma analyses, these human iPSCs retained their differentiation potential for the ectodermal, endodermal, and mesodermal lineages. Finally, vascular, hematopoietic, neural, and cardiac lineages were derived with robust efficiencies.

5.1.1.1 Thawing of iPSCs

One vial of frozen commercial iPSCs (1x10^6 cells/vial) was collected from the liquid nitrogen tank and it was rapidly thawed in a 37° C water bath. Before ice was almost melted, medium was quickly added to dilute the cryoprotectant liquid and the cell suspension was gently pipetted up and down, avoiding the disruption of cell aggregates, to remove all the remaining ice crystals. The cell suspension was then transferred drop by drop in a Falcon tube containing 4 ml of Essential 8 Medium (ThermoFisher Scientific), consisting of Essential 8 Basal Medium and Essential 8 Supplement, with the addition of 1% Penicillin/Streptomycin (Euroclone). While the diluted cell suspension was added dropwise, the tube was gently twisted to the left and right, to avoid osmotic shock to the cells. The cells were centrifuged at 200 xg for 5 minutes. The supernatant was removed, and the cell pellet was resuspended in Essential 8 Medium supplemented with 10 µM Rho-associated protein kinase inhibitor (Y-27632, from now on Y) (Biomed Reagent). Y is a small molecule able to inhibit Rho-associated protein kinase and improve the cells survival after dissociation in single cells during passaging or after thawing. Cells were then plated in colonies in one well of a 6-well plate already coated with 0,083 mg/ml Matrigel™ Growth Factor Reduced Basement Membrane LDEV-Free Matrix (Corning). Cells were kept at 37°C in a saturated humidity atmosphere containing 5% CO_2.

5.1.1.2 Human iPSC colonies maintenance and passaging

Passaging of iPSCs was performed at a maximum of 80-90% confluence. Cells were rinsed once with phosphate-buffered saline (PBS) (Lonza) and subsequently incubated with UltraPure EDTA 0.5 mM pH 8.0 (ThermoFisher Scientific) in PBS (Lonza) for 5 minutes at 37°C. After the incubation time, EDTA was carefully removed, and cells were detached in colonies by an energetically release

of fresh Essential 8 Medium supplemented with 10 mM Y (Biomed Reagent) with a serological pipet. The cell suspension was collected in a tube and cells were plated in a newly prepared 0,083 mg/ml Matrigel-coated plate. Cells were kept at 37°C in a saturated humidity atmosphere containing 5% CO_2, with daily medium change (without Y).

5.1.1.3 Freezing of iPSCs

Cells at a 95% of confluence were detached using EDTA, as previously described in the passaging step (paragraph 5.1.1.2.). After collecting the cell suspension in a tube, cells were centrifuged at 200 xg for 5 minutes. The supernatant was entirely removed, and the pellet was gently resuspended in 1 ml of Essential 8 medium supplemented with 10% of Dimethyl Sulfoxide (DMSO) (Sigma Aldrich). The vial was placed in a freezing container at -80°C for one day and subsequently it was moved and conserved in a liquid nitrogen tank.

5.1.2 Neuroblastoma SH-SY5Y cell culture and passaging

Human neuroblastoma cells (SH-SY5Y, ATCC CRL-2266 – Cell Bank – IRCCS AOU San Martino IST - http://www.iclc.it/details/det_list.php?line_id=HTL95013) were cloned from a bone marrow biopsy derived line called SK-N-S, taken from a four-year old female with neuroblastoma. This cell line is often used as *in vitro* model of neuronal function and differentiation. They are adrenergic in phenotype but express also dopaminergic markers. SH-SY5Y line was cultured in SH-SY5Y basal medium composed of DMEM-F12 supplemented with 10% FBS and 1% penicillin-streptomycin. Confluent SH-SY5Y cells at 70-80% were washed once with PBS and incubated with 2 ml Trypsin-EDTA for 5 minutes at 37°C. The reaction was stopped adding 8 ml of SH-SY5Y basal medium and detaching the cells from the bottom of the petri dish. The cells suspension was collected in a Falcon tube and mixed well. In order to obtain a confluence of the 25%, 2 ml of the cell suspension were seeded in a 100 mm petri dish previously prepared with 5 ml of pre-warmed basal medium. Cells were kept at 37°C in a saturated humidity atmosphere containing 5% CO_2, with medium change twice a week.

5.1.3 Cardiomyogenic differentiation

5.1.3.1 Passaging of iPSCs in single cells and cardiomyogenic differentiation in Monolayer

Cells were rinsed once with PBS (Lonza) and subsequently detached at single cells using UltraPure EDTA 0.5mM pH 8.0 (ThermoFisher Scientific) in PBS (Lonza) for 5 minutes at 37°C. EDTA was removed and cells were detached with Essential 8 Medium, collected in a tube and centrifuged at 200 xg for 5 minutes. Cells were resuspended with fresh Essential 8 Medium supplemented with 10 µM Y (Biomed Reagent) and plated at a density of 5500 cells/cm^2 in a previously prepared Matrigel (Corning) coated plate (0,083 mg/ml).

Cardiomyogenic differentiation was conducted using the PSC Cardiomyocyte Differentiation Kit (Thermo Fisher Scientific). The kit consists of three serum-free and xeno-free media (Medium A, Medium B, and Maintenance Medium) that are able to induce the efficient differentiation of iPSCs to contracting cardiomyocytes in 9-12 days. The protocol of this differentiation kit is based on the modulation of the Wnt signaling pathway described in Burridge et al. In detail, the cardiomyogenic

differentiation protocol was started when iPSCs reached a confluence of 30-40%. Cells were cultured for two days in the Medium A (responsible for the stimulation of Wnt pathway). Then, Medium A was removed and substituted with Medium B (formulated to repress the Wnt pathway) for additional two days. Medium B was subsequently changed with the Maintenance medium, which maintains cells in a differentiated state until cardiomyocytes start beating (Figure 12). Spontaneously contracting cardiomyocytes start to appear after 7-10 days and they can be maintained in culture for different time periods, depending on the downstream experiments that need to be performed.

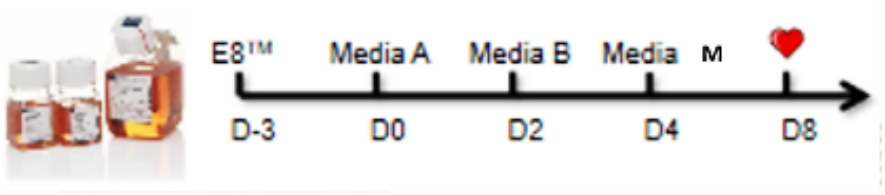

Figure 12: Schematic representation of the cardiomyogenic differentiation protocol

5.1.3.2 Dissociation of the beating cardiomyocytes monolayer

Approximately, at day 18 of the cardiomyogenic differentiation, the beating CMs monolayer was dissociated to obtain a single-cell population of cardiomyocytes for a further enrichment step. The dissociation was performed using an enzymatic mix, the Multi Tissue Dissociation Kit 3 (Miltenyi Biotec), specifically optimized for monolayer cultures of CMs. In detail, CMs were detached by incubating the cells at 37°C for 10 minutes with the Enzyme T (Miltenyi Biotec) diluted in the Buffer X (Miltenyi Biotec). After gently pipetting, CMs were dissociated into single cells and they were transferred to a MACS SmartStrainers (70 µm-filter) (Miltenyi Biotec) placed on a 15 ml falcon tube. The wells were rinsed with cardiomyocytes basal medium composed of RPMI medium w/ L-Glutamine (Euroclone) supplemented with 100 U/mL Penicillin, 0,1mg/mL Streptomycin (P/S) (Euroclone) and B27 supplement 50X (ThermoFisher Scientific). The cells flowed through the filter, which held agglomerates and allows the flow only of single cell per gravity. After gently pipetting, single-cell CMs were centrifuged at 200 xg for 4 minutes. The obtained pellet was resuspended with 1 ml of cardiomyocytes basal medium. Cell count and viability were assessed by using Acridine Orange stain (Logos biosystems) with LUNA FL™ Fluorescence Cell Counter (Logos biosystems).

5.1.3.3 Purification of the cardiomyocytes

In order to obtain a pure population of CMs, after the dissociation into single cells, cardiomyocytes were purified from non-cardiomyocytes cells using the PSC-Derived Cardiomyocyte Isolation Kit (Miltenyi Biotec). In fact, for an optimal *in vitro* modeling of human cardiac diseases, it is crucial to work with a pure and homogenous population of cardiomyocytes to achieve more reliable and reproducible results. The purification yielded to an enrichment of 80-90% of pure cardiomyocytes, which were then replated on Matrigel-coated dishes for further characterization by RT-PCR, Western Blot, immunofluorescence, and electrophysiology analyses. This procedure is based on the depletion of iPSC-derived non-cardiomyocytes by magnetic labeling of these cells and

consistently provides CMs purities of >90%, independently from the differentiation protocol, iPSC line used, time point and efficiency of differentiation (Figure 13 A). In detail, the dissociated cells were resuspended in the freshly prepared Purification Buffer (PBS, 0.5%; BSA; 2 mM EDTA) and with Non-Cardiomyocyte Depletion Cocktail (Miltenyi Biotec) and then incubated at 4°C for 5 minutes. Afterwards cells were centrifuged at 200 xg for 5 minutes, the pellet was resuspended in the Purification Buffer and the Anti-Biotin MicroBeads (Miltenyi Biotec) and incubated at 4°C for 10 minutes. After the incubation time, the cell suspension was ready for the magnetic separation using the LS Column with the appropriate MACS Separator (Miltenyi Biotec)(Figure 13 B)**.** The columns were placed in the magnetic field of the separator and rinsed with Purification Buffer three times. The cell suspension was applied onto the column ($5x10^6$ cells/column) and the flow-through was collected in a tube without the use of a plunger. In this way, only the unlabeled cell fraction, corresponding to the population of single-cell cardiomyocytes, was recovered. On the contrary, the magnetically labeled non-PSC-derived cardiomyocytes remained entrapped in the magnetic column. After the purification, the cells were replated at different densities on Matrigel (0,083 mg/ml)-coated 12-well dishes in cardiomyocytes basal medium supplemented with Y 10 µM. Cells were kept at 37°C in a saturated humidity atmosphere containing 5% CO_2, with medium change every two days.

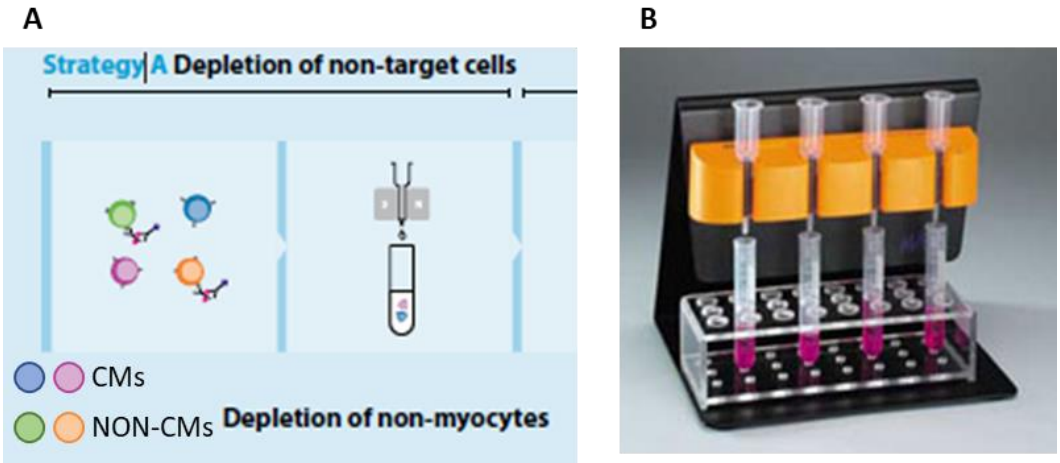

Figure 13: Schematic representation of the enrichment step of PSC-derived CMs. A: Schematic representation of the depletion of PSC-derived non-CMs from the samples. B. CMs flow through the column and are collected in a 15 ml tube. In the second image: the MACS Separator

5.1.4 Sympathetic neuronal differentiation

5.1.4.1 Passaging of iPSCs in single cells and neuronal differentiation in monolayer

Before starting the differentiation protocol, iPSCs were plated as single cells at the density of $7.5x\ 10^4/cm^2$ in a 12 well plate coated with 0,5 mg/ml Matrigel (Corning) in Essential 8 Medium (ThermoFisher Scientific) and 10 µM Y (Biomed Reagent). Matrigel was diluted with KnockOut DMEM (Gibco – ThermoFisher Scientific) to a final concentration of 500 µg/ml. Essential 8 Medium was changed daily without Y until the desired confluence (about 80-90%) was reached. The sympathetic neural differentiation protocol consists of a daily change of medium and factors

to expose the cells with a defined and precise timing to different signaling pathways and molecules able to direct the differentiation towards sympathetic lineage, following the protocol described in Oh et al (Oh et al., 2016). In details, the specification towards sympathetic neurons begins with SMAD pathway inhibitors with the exposure of the cells for the first two days to 500 nM LDN-193189 (LDN, Stemgent) and 10 µM SB431542 (SB, Tocris) in KSR medium. The third day of differentiation the neural crest was induced through the exposure of cells to 3 µM CHIR99021 (CH, Stemgent), 10 µM DAPT (Tocris), 0.2 uM PD173074 (PD, Sigma Aldrich) 500 nM LDN (Stemgent) and 10 µM SB (Tocris) in KRS medium. The fourth day cells are cultured with the same factors as the day before, adding 100 ng/ml recombinant SHH, (R&D System) and 1 µM PMP (Stemgent) in KRS medium for the activation of WNT pathway. At day 5, cells are cultivated with the factors of the previous day, removing LDN in a medium composed of 75% of KRS medium and 25% of NNB medium. From this day on, KSR medium started to be gradually reduced and substituted with NNB medium. For the acceleration of the neural crest specification and the formation of peripheral neurons, at day 6 cells are cultivated with 3 µM CH (Stemgent), 10 µM DAPT (Tocris), 0.2 µM PD173074 (Sigma Aldrich), 100 ng/ml SHH (R&D) and 1 uM PMP (Stemgent) with 75% of KRS medium and 25% of NNB medium. At days 7 and 8 of differentiation cells are cultivated with the same factors as day 6 but in a medium composed of 50% of KRS medium and 50% of NNB medium. At days 9 and 10 cells are cultured only with 100 ng/ml SHH (R&D) and 1 µM PMP (Stemgent) with 25% KRS medium and 75% of NNB medium. From day 11 to day 13 cells are cultivated with the same factors as the previous day with the addition of 10 ng/ml BMP4 (R&D System) in NBB medium. On days 12-13 of differentiation cells were passaged *en bloc* or at single cells ($1{,}5x10^6$ cells/ml for flow cytometry or $5x10^5$ x cm^2 for immunostaining or $1x10^5$ cells/well for MEA) on 24 well plates precoated with 0.06 mg/ml Poly-D-Lysin (Sigma Aldrich) and 10ug/ml Laminin (Sigma Aldrich). At days 14 and 15 of the differentiation, cells were maintained in the NBB medium supplemented with 10 ng/ml recombinant Human BMP4 (R&D).
Further maturation of cells towards sympathetic lineage was reached with the culture of the cells for the next 15 days (from day 16 to day 30) with the following factors: 0.2 mM dibutyryl-cyclic-AMP (cAMP, Enzo Lifesciences), 0.2 mM ascorbic acid (AA Sigma Aldrich), 20 ng/ml recombinant Human BDNF (Peprotech), 10 ng/ml recombinant Human GDNF (Peprotech), 10 ng/ml recombinant Human β-NGF (Peprotech) in NBB medium. SNs in differentiation were maintained in culture with standard conditions (37°C, 5% CO_2, humified atmosphere) up to the desired time point (day 30-40-50).

5.1.5 Co-cultures of iPSC-derived CMs and iPSC-derived SNs

A silicon insert (Culture-Insert 2 Well by Ibidi - #80209-150) composed by two attached and divided rectangular compartments were added with sterile tweezers into the wells of a 24-well plate or µ-Slide 4 well ibiTreat (Ibidi - #80426) or 60 µ-Dish (Ibidi - #80136). One compartment was dedicated to the plating of iPSC-derived CMs and the second to iPSC-derived SNs. In the chamber dedicated to iPSC-derived SNs, the coating of 0,5 mg/ml Matrigel was done by incubating the plate for 5 minutes at 37°C. The same incubation time and temperature were used for iPSC-derived CMs but using 0,083 mg/ml of Matrigel for the coating. Monoculture of iPSC-derived SNs was detached with Accutase for 5 minutes at 37°C and the suspension was collected in a falcon

tube and counted with LUNA FL™ Fluorescence Cell Counter (Logos biosystems). The monoculture of iPSC-derived CMs was detached with the enzyme T resuspended in Buffer X (Miltenyi) for 10 minutes at 37°C. Both cell populations were plated in their basal medium supplemented with Y 10 µM. The day after the plating, individual media were changed without the addition of Y, and kept separately until the removal of the inserts. After two or three days from the plating of the cells, the inserts were slowly removed with sterile tweezers and, in order to coat the gap between the two cell populations, an additional drop of 0,083 mg/ml Matrigel was added on the top of the two cell population and incubated for 30 minutes at 37°C. After the incubation, the cells were maintained with the co-culture medium, which was added in two times up to 1000 µl and changed every three days.

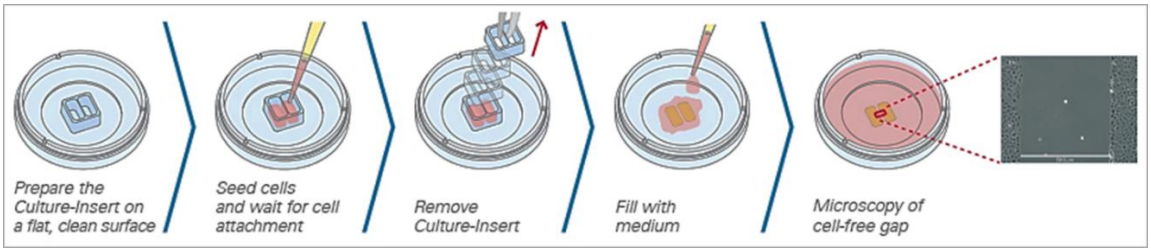

Figure 14: Schematic representation of the plating strategies of the co-cultures with the Ibidi two chambers insert

5.1.6 Medium Recipes

Essential 8

Essential 8 medium	
P/S	1x
Essential 8 supplement	

Cardiomyocyte basal medium

RPMI with L-Glutamine	
P/S	1x
B27 Supplement 50 x	2x

KSR medium

KnockOut DMEM	
KnockOut serum	15 %
L-Glutamine	2mM
P/S	1x
Non-Essential Amino Acids	1x
β-mercaptoethanol	0,01 mM

NBB medium

Neurobasal medium	
N-2 Supplement	0.5x
B-27 supplement	0.5x
P/S	1x

Co-culture medium

1:1NBB medium + Cardiomyocyte basal medium	
Cardiomyocyte basal medium	50%
NBB medium cAMP 0.2mM AA 0.2mM recombinant Human BDNF 20 ng/ml recombinant Human β-NGF 10 ng/ml recombinant Human GDNF 10 ng/ml	50%

SH-SHY basal medium

DMEM/F12 Glutamax	
Fetal Bovine Serum	10x
P/S	1x

5.2 Human iPSC characterization

Although a certificate confirming the validation of the pluripotency of the commercial iPSCs was provided, an in-house analysis consisting of alkaline phosphatase staining and immunofluorescence analysis of pluripotency markers was performed to confirm the preservation of their pluripotency potential during time. Each protocol is described in detail in the next paragraphs.

5.2.1 Alkaline Phosphatase

The pluripotent state of iPSCs is characterized by a high level of alkaline phosphatase expression (Yu et al., 2007) which indicates undifferentiated cells with the potential to self-renew. Alkaline Phosphatase is a hydrolase enzyme responsible for dephosphorylating molecules such as nucleotides, proteins, and alkaloids under alkaline conditions. Briefly, iPSCs were cultured until 60% of confluence and then fixed with 4% paraformaldehyde (PFA) for 20 minutes. Fixed cells were rinsed three times with PBS and stained with a commercial alkaline phosphatase staining kit (Stemgent® Alkaline Phosphatase Staining Kit II) for 15-20 minutes in the dark, according to manufacturer´s instructions. After the incubation time, fixed cells were washed twice with PBS and observed under a brightfield microscope. Undifferentiated iPSCs appeared red and purple, whereas differentiated cells appeared colorless.

5.2.2 Immunofluorescence analysis of the pluripotency markers

Immunofluorescence staining was used to visualize the expression of two key pluripotency markers, OCT4 and SSEA4, in the iPSC line. The commercial PSC 4-Marker Immunocytochemistry Kit (Thermo Scientific) was used following the manufacturer´s indications. The kit contains primary and secondary antibodies and ready-to-use buffers. Briefly, cells were fixed in a dish plate at the confluence of 60% with the Fixative Solution. Next, the Permeabilization solution was added to the cells for 15 minutes and subsequently the Blocking solution was added and incubated for 30 minutes at room temperature. Then, the primary antibodies were directly diluted in the Blocking solution, added to the cells and incubated overnight at 4°C. The following day cells were washed three times with 1X Wash Buffer and secondary antibodies diluted in Blocking Solution were added to the dish plate for one hour at RT. Finally, cells were washed three times with PBS to remove the residual solution with secondary antibodies and nuclei were stained with DAPI. Images were acquired using the Leica SP8-X confocal microscope (Leica Microsystems).

Table 3: List of the antibodies used for immunostaining experiment with the correlated concentrations

Primary Antibody	Animal	Concentration
Anti-OCT4	rabbit	100X
Anti-SSEA4	mouse	100X

5.3 Characterization of iPSC-derived differentiated cells

5.3.1 Flow cytometry

At day 12 and at day 30 of differentiation, c_iPSC-derived sympathetic neurons were tested with flow cytometry. Cells were detached with Accutase and collected in Eppendorf tubes (500.000 cells x condition). After the centrifugation at 200 xg for 5 minutes, supernatant was discarded, and the cells were washed once with sterile FACS buffer (PBS; 0.5% FBS; 2mM EDTA) and then resuspended in 4% PFA and incubated for 15 minutes at room temperature. Cells were washed with sterile FACS buffer and centrifuged at 200 xg for 5 minutes. Subsequently cells were permeabilized for 15 minutes with permeabilization solution (0.1% triton in PBS) and after this step cells were washed with FACS buffer and centrifuged at 200 xg for 5 minutes. Cells were stained with the conjugated antibodies resuspended in permeabilization solution for 30 minutes at room temperature. Following the incubation step, cells were washed with permeabilization solution and centrifuged at 200 xg for 5 minutes. The pellet was resuspended in FACS buffer and filtered with a 50-70 µM cell strainer in FACS tubes. Stained cells were run with the S3e Cell Sorter Biorad and analyzed with FlowJo software.

Table 4: List of the antibodies used for flow cytometry experiment with the correlated concentrations

Primary Antibody	Concentration	Species	Conjugated to	Brand	Cat. Nr
DBH	1ug x $1x10^6$ cells	Ms	FITC	Santacruz	Sc-365710-FITC
IgG_1	1ug x $1x10^6$ cells	Ms	FITC	Santacruz	Sc-28855-FITC
TH	1:100	Rb	PE	Abcam	Ab209921
IgG	1:100	Rb	PE	Abcam	Ab209478

5.3.2 Gene expression analysis

5.3.2.1 RNA extraction

RNA extraction from cells was performed using the Direct-zol™RNA MiniPrep Kit (Zymo Research Corp), following the manufacturer's instruction. Lysates of RNA were prepared starting from cells in culture at the confluence of 90%. Cells were detached as previous described and centrifuged at 200 xg for 5 minutes. The pellet was washed once with PBS by centrifuging the cells at 16,000 xg for 10 minutes. The supernatant was removed, and the remaining pellet was well resuspended in 1 ml of TRIzol® Reagent (Thermo Fisher Scientific). This monophasic solution of phenol and guanidine isothiocyanate is designed to inactivate immediately endogenous ribonuclease (RNase) and to ensure the purification of intact RNA. The cell lysates can be frozen at –80°C or immediately used. The cell suspension was resuspended with an insulin syringe to disrupt all the remaining ice crystals (in case of previous freezing) and plasma membranes, enabling the release all the RNA contained in the sample. The suspension was then diluted in an equal volume of ethanol 100% (VWR) and charged into a Zymo-Spin™ IIC Column (provided by the kit) in a Collection Tube and

centrifuged for 30 seconds. The column was transferred in a new collection tube and washed with RNA Wash Buffer. Then DNase I Reaction mix was added to the column. The Mix contained DNase 1 (6U/µl) and DNA Digestion Buffer. This step eliminated all the DNA components from the samples. Consequently, Direct-zol™ RNA PreWash was added to the column and centrifuged (provided by the kit). The column was then treated with RNA Wash Buffer and centrifuged for 2 minutes to remove all the wash buffer. Finally, DNase/RNase-Free Water was added to the column (not provided by the kit) to elute the RNA of the samples. The column was centrifuged and then discarded. The obtained eluted RNA can be immediately used ore stored at -80°C. RNA was quantified using the Nanodrop instrument (Thermo Scientific).

5.3.2.2 RNA quality check

RNA quality was analyzed with the Experion RNA StdSens Analysis Kit (BioRad). The Gel-stain (GS) solution was prepared adding 600 µl of pre-filtered RNA gel (G) to 65 µl RNA stain. Subsequently, the RNA samples were mixed with RNA ladder 1:1 and denatured at 70° C for 2 minutes. Samples were conserved in ice for 5 minutes. The chip (Experion RNA StdSens - Biorad) was primed with 9 µl of GS in the GS-well in the priming station for 30 seconds. The chip can be loaded with a maximum capacity of 12 samples. The chip was loaded as follows: 9 µl of GS in the second GS-well, 9 µl of filtered gel in the well labeled with G, 5 µl loading buffer into each sample-well and ladder well (L), 1 µl RNA prepared ladder into the well (L) and finally with 1 µl sample in the sample-wells. After checking for the absence of bubbles, the chip was vortexed in the vortex station for 60 seconds and the run was started in the Experion electrophoresis station (BioRad) within 5 minutes. Only samples with an RNA quality indicator (RQI) higher than 9 were used for downstream experiments.

5.3.2.3 Reverse transcription

The reverse transcription is a commonly used technique in molecular biology that consists of the synthesis of complementary DNA (cDNA) starting from purified messenger RNA (mRNA). In this work, we used the SuperScript® VILO™ cDNA Synthesis Kit (Thermo Fisher Scientific), following the manufacturer's instruction. In detail, 1000 ng of total RNA were reverse transcribed for CMs and SNs in a solution containing : 4µl of 5X VILO™ Reaction Mix which includes oligo (dT), random hexamers, $MgCl_2$ and a mix of dNTPs (deoxy-nucleotide-tri-phosphate); 2µl of 10X SuperScript® Enzyme Mix which includes the enzyme SuperScript ™ III Reverse Transcriptase and RNase OUT ™ Recombinant Ribonuclease Inhibitor (RNase inhibitor protein, which protects the target RNA from degradation due to contamination by ribonuclease in the RNA preparation) and RNAse free water up to 20 µl. The retrotranscription reaction was carried out in the thermocycler Mastercycler pro S (Eppendorf) applying the following conditions: 25°C for 10 min, 42°C for 60 min, 85°C for 5 min. The reaction was then kept at 4°C and cDNA was stored for longer periods at -20°C.

5.3.2.4 Real-Time PCR (RT-PCR)

The Real-Time PCR or qPCR (Real-Time Polymerase Chain Reaction or semi- quantitative PCR) is a variant of the classic method of PCR (Polymerase Chain Reaction), a technique used in molecular biology to amplify a single copy or a few copies of a segment of DNA across several orders of

magnitude, generating thousands to millions of copies of a particular DNA sequence (Singh and Roy-Chowdhuri, 2016). The three basic principles of RT-PCR are the same as classic PCR: denaturation, annealing, and extension.

In this work, TaqMan Assay (Applied Biosystem - ThermoFisher Scientific) were used to monitor and quantify the number of amplicons. The amplification reactions were performed in a final volume of 20 µl containing: 10 µl of TaqMan Fast Advanced Master Mix (2X) (Applied Biosystem - ThermoFisher Scientific), 2 µl of cDNA (12.5 ng) as template, 1 µl of TaqMan Assay probe (20X) (Applied Biosystem - ThermoFisher Scientific) and 7 µl of nuclease-free water. The amplification reaction was performed using the CFx96 Real-Time System C1000™ Thermal Cycler (BioRad) and the following program. The initial cycle consisted of 2 minutes at 50°C to activate the UNG. The polymerase activation was achieved at 95°C for 20 seconds. The denaturation step was done at 95°C for 3 seconds followed by the annealing and the extension phase for 30 seconds at 60°C (for a total of 40 cycles).

As normalizer, housekeeping genes, which are genes ubiquitously expressed in any sample, were used. NormFinder and Biorad software were used to identify the optimal normalization gene among the selected candidates. Relative quantitation was performed using the ΔΔCt method. Fold changes in gene expression were estimated as $2^{(-\Delta\Delta Ct)}$ (Livak and Schmittgen, 2001). Specifically, the Ct value of the normalizer was subtracted from the Ct value of the gene of interest. The obtained value is the so called ΔCt. The ΔCt of the sample was then subtracted from the ΔCt value of a reference sample. This latter value is denominated ΔΔCt. The amount of the gene of interest was calculated in relation to the housekeeping gene and the reference sample, using the formula $2^{-\Delta\Delta Ct}$.

Table 5: List of the Taqman Probes used for the experiments

Gene	Fluorophore	Assay ID
PHOX2B	FAM	Hs00243679_m1
TH	FAM	Hs00165941_m1
DBH	FAM	Hs01089840_m1
RPL13	FAM	Hs00366152_m1
UBE2D2	FAM	Hs00744303_s1
GAPDH	FAM	Hs02786624_g1
TNNI3	FAM	Hs00165957_m1
CX43	FAM	Hs00748445_s1
MYH7	FAM	Hs01110632_m1

5.3.3 Western Blot

The Western Blot (WB) is the most common semi-quantitative biochemistry technique used for the detection of specific proteins isolated from different tissues, homogenates or cell extracts (Hnasko and Hnasko, 2015).

5.3.3.1 Protein Extraction from CMs

Cells in culture were washed twice with PBS (Lonza) and incubated with Enzyme T (Miltenyi Biotec) diluted in Buffer X (Miltenyi Biotec), at 37°C for 10 minutes. The enzyme's reaction was stopped with basal medium, and the cells were collected in a tube. CMs were centrifuged at 500 xg for 5 minutes and the obtained pellet was washed once with PBS (Lonza) by centrifuging it at 16,000 xg for 10 minutes. The supernatant was discarded, and the pellet was resuspended in 30 µl of RIPA buffer (Thermo Scientific), a ready-to use commercial detergent for the membrane permeabilization, supplemented with Protease Inhibitors (Complete Tablets, Mini EASYpack, Roche) and Phosphatase Inhibitors (Complete Tablets, Mini EASYpack, Roche). Both inhibitors were used for the inactivation of endogenous proteolytic and phosphorolytic enzymes released from subcellular compartments during cell lysis, to prevent the digestion of the sample by its own enzymes.

5.3.3.2 Protein Extraction from SNs

The culture of SNs was washed twice with PBS (Lonza) and incubated with Accutase (GE healthcare) at 37°C for 5 minutes. The enzyme's reaction was stopped with PBS (Lonza) and the cells were collected in a tube and centrifuged at 500 xg for 5 minutes. The pellet was washed once with PBS (Lonza) by centrifuging it at 16,000 xg for 10 minutes. The remaining pellet was resuspended with 30 µl of RIPA buffer (ThermoFisher Scientific), supplemented with Protease Inhibitors (Complete Tablets, Mini EASYpack, Roche) and Phosphatase Inhibitors (Complete Tablets, Mini EASYpack, Roche).

Both lysates were then sonicated for 10 seconds at the minimum intensity to allow to extract proteins through the lysis of the cellular membrane using ultrasonic waves. The samples can be stored at 80°C for further processing or immediately used.

5.3.3.3 Protein quantification

The quantification of proteins was performed using Pierce™ BCA (Bicinchoninic Acid) protein assay kit (Thermo Scientific) containing a detergent-compatible assay reagent set to measure (A_{562}nm) total protein concentration compared to a protein standard, which is based on a redox reaction. For the preparation of the BCA, the reagent B was mixed with the reagent A in a ratio of 1:50. Reagent A contains bicinchoninic acid, NaOH and sodium tartrate 0.1M, while Reagent B contains 4% of copper sulfate ($CuSO_4$). The BCA Protein Assay was based on the reduction of Cu^{2+} to Cu^{1+} in the protein samples with the colorimetric detection of the cuprous cation (Cu^{1+}) by the BCA. The purple color is given by the binding of two molecules of BCA with a molecule of Cu^{1+}.
A calibration curve was created with known concentrations of bovine serum albumin (BSA) ranging from 0 µg/ml to 2000 µg/ml. 10 µl of each standard or sample (1:10 in RIPA buffer) were added in a 96-well plate and supplemented with 200 µl per well of BCA working solution (10 µl of RIPA buffer and Protease and Phosphatase Inhibitors were used as negative control) and the plate was incubated at 37° C for 15-20 minutes. The absorbance was measured with the spectrometer Victor™ X3 (Perkin Elmer). The protein concentration of each unknown sample was obtained by the interpolation of the optical density (O.D.) of each unknown sample with the calibration curve.

5.3.3.4 Sample Preparation for SDS-PAGE

Sample preparation consisted of a mix composed of 10 µg for SNs and 7 µg for CMs of proteins in a final volume of 20 µl that contains 2 µl NuPAGE® Sample Reducing Agent (10X) (ThermoFisher Scientific) and 5 µl NuPAGE® LDS Sample Buffer (4X) (ThermoFisher Scientific). Samples were denaturate at 95°C for 5 min and then loaded in precast gels for the electrophoresis separation.

5.3.3.5 SDS-PAGE

SDS-PAGE (sodium dodecyl sulfate (SDS) polyacrylamide gel electrophoresis (PAGE)) is a technique widely used in biochemistry and molecular biology to separate proteins according to their molecular weight by migration through a polyacrylamide gel under the application of an electric field. The precast polyacrylamide gel NuPAGE® 4-12% Bis-Tris gels (ThermoFisher Scientific) was mounted in the electrophoretic cell (XCell SureLock® Mini-Cell Electrophoresis Cell - Invitrogen / CRITERION ™ Cell - Biorad). The gel is loaded with 20 µl of each protein samples and 5 ul of marker Precision Plus Protein™ Dual ColorsStandards (by BioRad). The electrophoretic cell was filled with the Running Buffer composed by 475 ml deionized water and 25 ml NuPAGE® MOPS SDS Running Buffer (20X) (Life Technologies). An electric field was applied across the gel, causing the negatively charged proteins to migrate across the gel away from the negative electrode (the cathode) towards the positive electrode (the anode). In details, gel run for 10 minutes at 95 V until samples enter the running gel, then the voltage was increased to 150 V for about 1.5 hours. Depending on their size, each protein moves differently through the gel matrix: smaller proteins travel faster down the gel, while larger ones remain closer to the point of origin.

5.3.3.6 Transfer

For the detection of proteins of interest, it is necessary to transfer and immobilize the proteins from the gel onto polyvinylidene difluoride (PVDF) membrane by “electroblotting” technique. To transfer the proteins, a so-called “sandwich” was prepared. It was composed of (from the negative pole to the positive pole): blotting-pad, filter paper, gel, membrane, filter paper, blotting-pad. Prior the assembly, the PVDF membrane must be activated in 100% methanol because of the hydrophobicity of PVDF and washed once in deionized water. Then, the sandwich was mounted in the transfer cell (Novex Mini Cell - Invitrogen/ Criterion™ Blotter Biorad) containing the transfer buffer composed of 850 ml deionized water; 50 ml NuPAGE® transfer Buffer (20X) (Life Technologies) and 100 ml methanol 100% (Honeywell). The transfer of proteins from the gel to the membrane was obtained using a flow of current from the cathode to the anode thus the negatively charged proteins migrate toward the anode and during this path, they stick on the PVDF membrane. The transfer step was performed at a constant amperage of 100 mA, for 16h at 4°C.

At the end of the transfer step, the Ponceau solution was used to visualize the transferred proteins. Ponceau is a red-colored sodium salt dye, used for the rapid detection of protein bands. Ponceau was incubated at room temperature for 3-5 minutes and then washed away with simple deionized water.

5.3.3.7 Antibodies Incubation

The membrane was blocked either with 5% non-fat milk in TBS-Tween (TBS-T Tris- buffered saline 1%) plus 0,1% Tween 20) or BSA 5% in TBS-T for 1 hour at room temperature in order to avoid the non-specific binding between the membrane and the antibody of interest. The membrane was then incubated overnight at 4°C on agitation with a solution containing the specific primary antibody diluted in the same blocking solution used for the blocking step, but diluted at 2%. The antibodies used in the experiments and their relative working dilutions are listed in Table 6. On the following day, the membrane was washed three times with TBS-T to remove all the residual of antibody and then incubated for 1 hour at room temperature on agitation with the secondary antibody-conjugated to HRP (horseradish peroxidase) diluted 1:1000.

Table 6: List of antibodies used for Western Blot experiments with the correlated concentration

Primary Antibody	Concentration	Species	Blocking	Brand	Cat. Nr.
TH	1:1000	Rb	Milk	Millipore	MAB319
PHOX2B	1:1000	Ms	BSA	SantaCruz	sc-376997
β-actin	1: 5000	Rb	Milk	Cell Signalling	49675
GAPDH	1:5000	Ms	BSA	SantaCruz	Sc-32233
Troponin I	1:1000	Rb	BSA	Abcam	Ab47003
Connexin 43	1:2000	Rb	BSA	Abcam	Ab11370

5.3.3.8 Detection

The detection of the target protein was performed providing the substrate to the enzyme HRP. The substrate for HRP is peroxidase ECL (kit Clarity™ ECL Western Substrate by BioRad). HRP is able to convert ECL into a detectable chemiluminescence signal. In detail, the membrane was incubated for 5 minutes in the dark at RT with ECL and the chemiluminescence signal was detected using the ChemiDoc™ Touch Imaging System (BioRad). The signal of the target protein was quantified by Image Lab 5.2.1 analyzer software (BioRad), normalizing the expression of the target protein in relation to housekeeping proteins stably expressed in our samples.

5.3.4 Immunofluorescence analysis of iPSC-derived CMs, iPSC-derived SNs and co-cultures

Cells were fixed with 4% PFA for 15 minutes and then permeabilized with 0.5% Triton X100 (Sigma Aldrich) in PBS (Lonza) for 10 minutes at RT. Cells were then blocked in 5% Goat serum in PBS for 1 hour at RT and incubated with primary antibodies in blocking solution ON at 4°C. On the next day, samples were washed three times with PBS, and incubated with the proper secondary antibody in blocking solution (2% Goat serum in PBS) for 1 hour at 37°C. Samples were washed

three time with PBS and lastly incubated with DAPI (Invitrogen). The images were acquired using the Leica SP8-X confocal microscope with Leica LAS-X software (Leica Microsystems) with a 63X Oil immerse objective and a resolution of 3504 x 3504 pixel for cardiomyocytes and 2048 x 2048 pixels for sympathetic neurons and co-cultures. Collages of areas of interest were made from 2D projections of confocal stacks. 3D reconstructions were made using Imaris Software (Oxford Instruments). The used antibodies are listed below in Table 7**.**

Table 7: List of antibodies used for Immunostaining experiments with the correlated concentration

Primary Antibody	Concentration	Species	Blocking	Brand	Cat. Nr.
TH	1:200	Rb	Goat Serum	Millipore	MAB319
DBH	1:200	Ms	Goat Serum	Invitrogen	PA5-34664
MAP2	1: 1000	Chk	Goat Serum	Abcam	ab5392
MAP2	1:5000	Chk	Goat Serum	Invitrogen	PA1-10005
TROPONIN I	1:250	Rb	Goat Serum	Abcam	ab47003
ALPHA-ACTININ (sarcomeric)	1:250	Ms	Goat Serum	Sigma-Aldrich	A7732
Synapsin-1	1:250	Rb	Goat Serum	Cell Signalling	D12G5

Secondary Antibody	Concentration	Species	Blocking	Brand	Cat. Nr.
Alexa Fluor 647	1: 1000	Chk	Goat Serum	Invitrogen	A21449
Alexa Fluor 555	1: 1000	Ms	Goat Serum	Invitrogen	A21424
Alexa Fluor 488	1: 1000	Ms	Goat Serum	Invitrogen	A11029
Alexa Fluor 488	1: 1000	Rb	Goat Serum	Invitrogen	A11034
Alexa Fluor 555	1: 1000	Rb	Goat Serum	Invitrogen	A21429

5.3.5 Multi Electrode Array for the monoculture iPSC-derived CMs and iPSC-derived SNs.

iPSC-derived SNs at day 12-13 (replating day) and iPSC-derived CMs at day 17-18(purification day) were detached with the appropriate enzyme (see paragraph above) and plated on a MEA plate (CytoView MEA 24 – White – Axion Biosystem). Before cell transferring, the wells of the MEA plate were coated with 500 µg/ml of Matrigel for SNs or 50 µg/ml fibronectin for CMs, making a drop only in the middle of the well without covering the ground electrodes (8 µl for 24 well plate) and incubated for 30-40 minutes at 37°C. Deionized sterile water was added in the outer rim of the plate to avoid the evaporation of the droplets. The Matrigel was removed by aspiration just before

plating the cells without any washing step and the plate was left for 5 minutes opened under the hood to slightly dry the wells. Fibronectin was aspirated after the incubation period and the plate was dried under the hood with the opened lid. Cells were detached as previously described, collected in a Falcon tube and counted with LUNA FL™ Fluorescence Cell Counter (Logos biosystems). Calculations were made considering to plate, $5x10^5$ iPSC-derived SNs and $7x10^4$ iPSC-derived CMs for each well. The cell suspension was separated in different falcon tubes according to calculations and centrifuged at 200 xg for 5 minutes. The iPSC-derived SNs were resuspended in complete NBB medium and iPSC-derived CMs in cardiomyocyte basal medium, both supplemented with 10 µM Y and plated in the wells. 8 µl of cell suspension containing $1,5x10^5$ iPSC-derived SNs and $7x10^4$ iPSC-derived CMs were plated in one drop in each well of the electrode array and incubated for 1 hours at 37°C. Last, the medium was slowly added to each well in two times up to 500 µl and changed every two days. The plates were read with Maestro Edge system by Axion BioSystem, using the neural module for SNs and the cardiac module for CMs.

5.3.6 Multi Electrode Array for the co-cultures.

In a 6-well MEA plate (CytoView MEA 6 – White – Axion Biosystem), two-chamber silicon inserts (Ibidi) were placed with sterile tweezers into the center of each well. Monoculture of iPSC-derived SNs was plated as previously described for the monoculture (including the coating step). The monoculture of iPSC-derived CMs was plated as previously described, but with a modification in the coating procedure. Instead of fibronectin, the compartment was coated with 0,083 mg/ml Matrigel for 30 minutes at 37°C. The day after the plating, individual media were changed without the addition of Y, and kept separately until the removal of the insert. At the desired timepoint, the insert was slowly removed with sterile tweezers and an additional drop of 0,083 mg/ml Matrigel was added on the top of the two cell populations and incubated for 30 minutes at 37°C. The cells were then kept in the co-culture medium, which was added in two times up to 1000 µl and changed every three days. The plates were read with Maestro Edge system by Axion BioSystem, using the neural module for SNs and the cardiac module for CMs.

5.3.6.1 Acquisition of Multi Electrode Array Data and Analysis

Data were generated using the Axion Maestro Edge MEA system and acquired with Axion's software AxIS Navigator version 3.2.3.1. The instrument provided constant temperature of 37°C and CO_2 concentration of 5%. The plate in use were of two types: the 6 well MEA-plate (CytoView MEA 6 – White – Axion Biosystem) and the 24-MEA plate (CytoView MEA 24 – White – Axion Biosystem). Each well of the 6 well MEA-plate is made with 64 electrodes (grid 8x8) with an electrode diameter of 50µm. Each well of the 24 well MEA-plate is made of 16 electrodes (grid 4x4) with an electrode diameter of 50µm. Before each measurement, each plate was equilibrated in the instrument for 5-10 minutes.

Neurons: MEA recordings with AxIS software used a sampling frequency of 12.5 kHz per well with pass filters of 200Hz-3kHz. Baseline measurements were recorder for 10 minutes, instead paced activity was recorder for 5 minutes with a frequency of 2 Hz. The obtained RAW files were reopened with AxIS software and a threshold was applied for the detection of spike. A threshold

of 5.5 times the standard deviation of the estimated noise on each electrode was set and the RAW file was then converted in an Excel file providing an extensive and detailed data profile of the measurement. The analysis was further performed on the Excel file. The minimum spike rate to consider and electrode active was 5 spike/minute. One burst was detected with a minimum number of 5 spikes with an inter-spike interval of 100 ms. Network burst was detected with a minimum number of 50 spikes with an inter-spike interval of 100 ms and the participation of the 35% of electrodes. The synchrony index was evaluated with a synchrony window of 20 ms. **Cardiomyocytes**: MEA recordings with AxIS software used a sampling frequency of 12.5 kHz acquiring field potential data with a bandwidth of 0.1Hz-2kHz. Field potential activity was recorder for 3 minutes. The obtained RAW files were reopened with AxIS software and a threshold between 100 and 350 uV was applied for the beat detection. The beat period is included between 250 ms and 5 s. The field potential duration (FPD) was calculated with polynomial regression method with a pre detection Holdoff of 50 ms and a post detection Holdoff of 70 ms.

5.3.7 Live time-lapse imaging

Live time-lapse imaging was performed on co-cultures of iPSC-derived CMs and iPSC-derived SNs, using the environmental chamber on the confocal system to maintain temperature, CO_2 and humidity levels. The Leica LAS X software was set to perform 100 stacks overnight, at intervals of 5 minutes, at a resolution of 1024 x 1024 pixels.

6 RESULTS

6.1 Identification of culture conditions and characterization of the commercial iPSC line

A commercial iPSC line (c_iPSCs) was chosen to conduct all the experiments of the present thesis. C_iPSCs were maintained in culture and amplified in colonies as reported in section "6.1.1.2." of "Material and Methods". A growth curve was performed to determine the expansion velocity of the cells (Figure 15C). Starting from a density of the 10% (Figure 15A), the cells reached a density of 40/50% in 4 days of culture (Figure 15B), doubling their amount almost every day (Figure 15C). After thawing, c_iPSCs started growing in small groups of few cells or as single cells with an elongated morphology due to the presence of Y (Wang et al., 2017). After some days in culture, cells acquired a round-shaped morphology, forming tightly packed colonies with well-defined borders and a high ratio nucleus-to-cytoplasm, as expected for iPSCs (https://bibsearch.uibk.ac.at/AC15167706) (Meraviglia et al., 2015). At a confluence from 70 to 90%, cells formed a dense monolayer. As suggested by Liu et al. (Liu et al., 2014), considering the high passage numbers that c_iPSCs acquired before the purchase and the shipment (36 passages in MEF-feeder and 16 passages in feeder-free condition for a total of 52 passages), we established to passage the cells once a week and to use the cells for a maximum of 10 passages to prevent undesired effect of spontaneous differentiation and a reduced level of pluripotency.

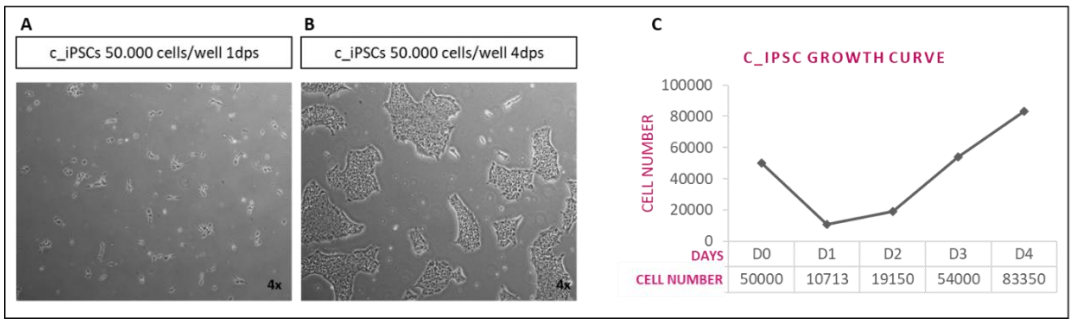

Figure 15: Expansion and growth curve of c_iPSCs. A: C_iPSCs plated at the confluence of 5.000 cells/cm² one day after the split. B: C_iPSCs plated at the confluence of 5.000 cells/cm² four days after the split.
C: Growth curve of c_iPSCs plated at day 0 (D0) at the confluence of 5.000 cells/cm² ls and counted for the next four days.

The pluripotency state of the c_iPSCs was validated by the supplier through the following analyses: karyotype analysis, RT-PCR, immunostaining, direct differentiation, and teratoma formation. Nonetheless, we assessed the pluripotency state of this cell line after 5-7 passages, through alkaline phosphatase staining and immunofluorescence assay for the expression of pluripotency markers. A positive staining is represented in Figure 16 C. All undifferentiated cells are stained in purple-red color, indicating the stemness features of these cells. To corroborate iPSC pluripotent state, the expression and localization of the key typical embryonic stem cell-specific markers SSEA-4 and OCT-4 were confirmed by immunofluorescence staining. (Figure 16 A-B).

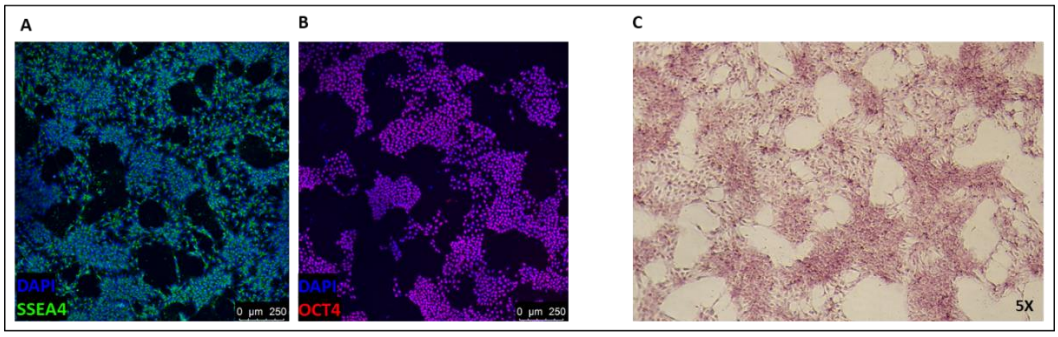

Figure 16: A-B Immunostaining of c_iPSCs with the pluripotency markers SSEA4 and OCT4. Note the typical membrane staining of SSEA4 and nuclear staining of OCT-4. C: Positive alkaline phosphatase staining of c_iPSCs.

6.2 Generation of a highly iPSC-derived CMs pure population using a monolayer differentiation protocol

For the generation of iPSC-derived CMs, c_iPSCs were cultured with a ready-to use cardiomyogenic differentiation kit modulating the WNT pathway (Figure 17A). The differentiation protocol described in my previous master thesis work (https://bibsearch.uibk.ac.at/AC15167706) was adapted to the cell line in use. Considering that the cell density plays a key role for the cardiomyogenic differentiation (https://bibsearch.uibk.ac.at/AC15167706) (https://www.thermofisher.com/order/catalog/product/A2921201#/A2921201), different densities were tested to determine the exact cell number to start each experiment. The appearance of a beating monolayer was considered as a positive outcome of the differentiation. Among all the different evaluated densities, namely 4500 cells/cm^2; 5000 cells/cm^2; 6000 cells/cm^2; 7000 cells/cm^2; 10.000 cells/cm^2, the best conditions resulted 5000 cells/cm^2 and 6000 cells/cm^2. Considering the small range between 5000 cells/cm^2 and 6000 cells/cm^2, the intermediate cells density of 5500 cells/cm^2 was chosen as starting density for the cardiomyogenic differentiation.

As the differentiation protocol produces a heterogenous population of cells (Figure 17 B), including CMs and non-CMs (Hattori et al., 2010; Tohyama et al., 2013), an enrichment step based on the magnetic labeling of non-cardiomyocytes was performed. This step led to an increase of the cardiomyocytes' percentage up to 80-90% (Figure 18 D) (https://bibsearch.uibk.ac.at/AC15167706). The obtained CMs were used for further experiments (Figure 17C).

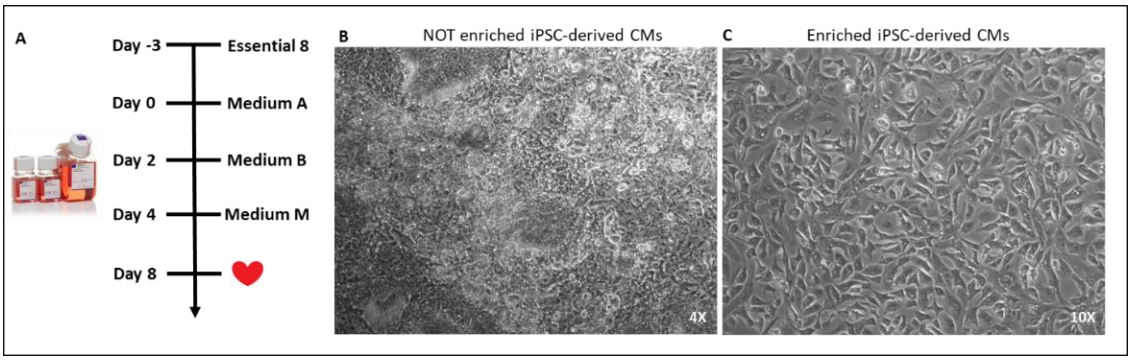

Figure 17: A: Scheme of the cardiomyogenic differentiation protocol.
B: Representative image of iPSC-derived CMs at day 17 of the differentiation protocol before the enrichment step.
C: Representative image iPSC-derived CMs at day 20 of the differentiation protocol after the enrichment step.

6.3 Molecular characterization of iPSC-derived CMs

Pursuing the aim of confirming the identity of the c_iPSC-derived CMs, we performed a molecular characterization of these cells through immunofluorescence staining, Western Blot analyses and gene expression analyses. After ca. 60 days of differentiation, enriched iPSC-derived CMs were stained for specific cardiac markers, namely sarcomeric α-Actinin and cardiac Troponin I (TTNI3) (Figure 18 D), which are the key components of the cardiac sarcomere. iPSC-derived CMs exhibited an organized sarcomeric structure typical of the bands of the cardiac muscle. Western Blot analysis also confirmed the expression of TTNI3 (Figure 18F), although no differences were detected in TTNI3 expression at different timepoints during the differentiation (Figure 18 F). The expression of Connexin 43 (CX43), one of the major components of cardiac gap junctions (Boengler and Schulz, 2017) was also analyzed by Western Blot, confirming its expression although again no significant variation was detected at the different timepoints (Figure 18 G). The expression of the cardiac markers *TTNI3, CX43* and Myosin Heavy Chain 7 (*MYH7*) was then evaluated by RT-PCR (Figure 18 H-L). Of note, *MYH7* is the heavy chain subunit of the myosin, which is mainly expressed in the ventricles (England and Loughna, 2013). The expression trend for each gene in two independent differentiation experiments is reported in Figure 18 M – O, confirming no significant changes over time.

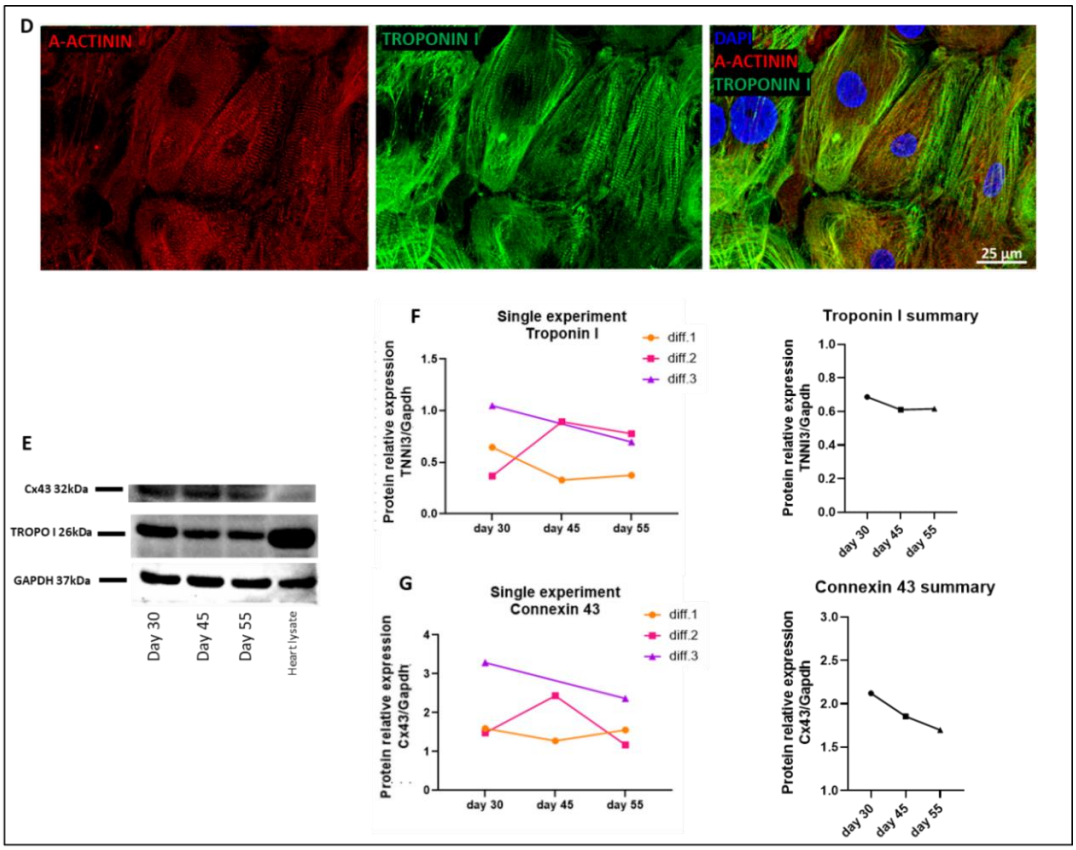
D
A-ACTININ
TROPONIN I
DAPI
A-ACTININ
TROPONIN I
25 µm
E
Cx43 32kDa
TROPO I 26kDa
GAPDH 37kDa
Day 30
Day 45
Day 55
Heart lysate
F
Single experiment
Troponin I
diff.1
diff.2
diff.3
Protein relative expression TNNI3/Gapdh
day 30
day 45
day 55
Troponin I summary
G
Single experiment
Connexin 43
Protein relative expression Cx43/Gapdh
Connexin 43 summary

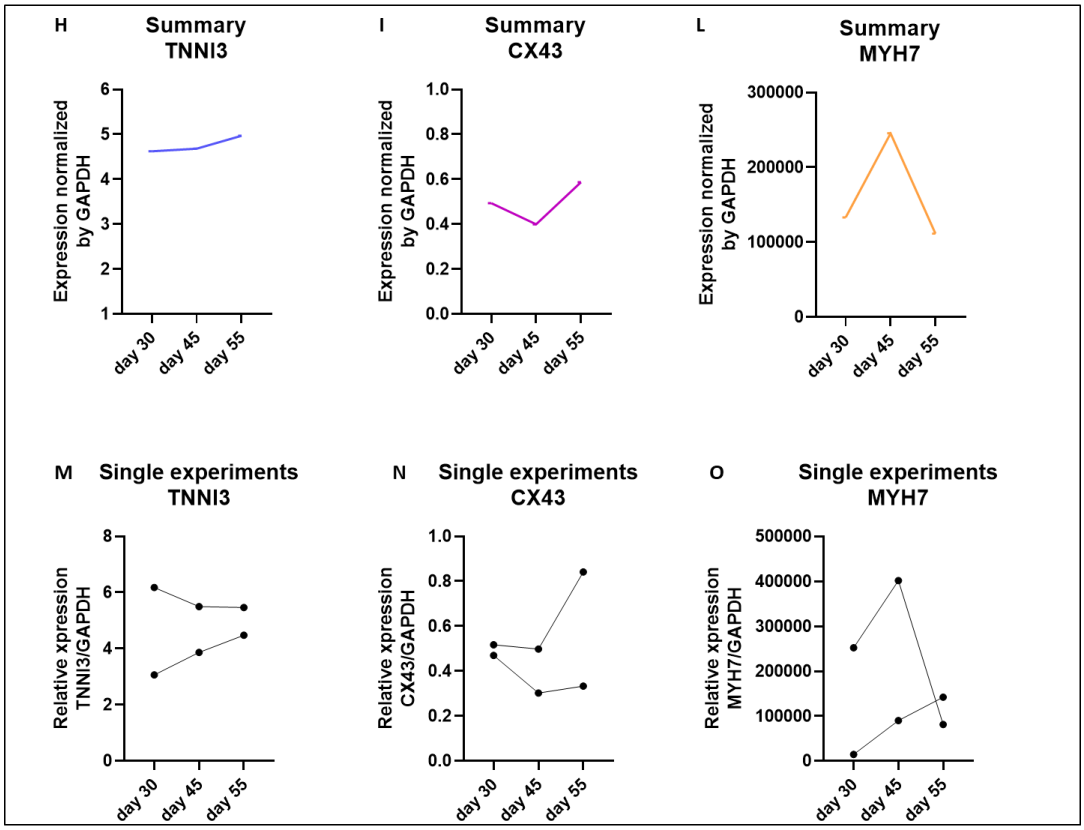
H
Summary
TNNI3
Expression normalized by GAPDH
I
Summary
CX43
L
Summary
MYH7
M
Single experiments
TNNI3
Relative xpression TNNI3/GAPDH
N
Single experiments
CX43
Relative xpression CX43/GAPDH
O
Single experiments
MYH7
Relative xpression MYH7/GAPDH

Figure 18: Characterization of in c_iPSC-derived CMs.
D: Immunostaining of c_iPSC-derived CMs (day 54) with α-actinin (red), troponin-I (green) and DAPI for the nuclei staining. E-G: Western Blot analysis of c_iPSC-derived CMs (n=3) with the cardiac markers. E: Densitometry analysis of the cardiac marker Troponin I on c_iPSC-derived CMs at three different timepoints: days 30, 45 and 55 of differentiation. F: Densitometry analysis of the cardiac marker Connexin 43 on c_iPSC-derived CMs at three different timepoints: days 30, 45 and 55 of differentiation.
H-O: RT-PCR of c_iPSC-derived CMs overtime (N=2 – ctrl sample c_iPSCs). H: mean trend of TNNI3 (N=2 – ctrl sample c_iPSCs) at different timepoints: days 30, 45, and 55. I: mean trend of CX43 (N=2 – ctrl sample c_iPSCs) at different timepoints: days 30, 45, and 55. L: mean trend of MYH7 (N=2 – ctrl sample c_iPSCs) at different timepoints: days 30, 45, and 55.
M:single trend of TNNI3 gene expression of each differentiation experiment at different timepoints: days 30, 45, and 55. N: single trend of CX43 gene expression of each differentiation experiment at different timepoints: days 30, 45, and 55. : single trend of MYH7 gene expression of each differentiation experiment at different timepoints: days 30, 45, and 55.

6.4 Functional characterization of iPSC-derived CMs

Cardiomyocytes are excitable cells; for this reason, it is important to investigate their electrical properties and the ability to form a syncytium as well. The evaluation of the functional activity of c_iPSC-derived CMs has been assessed using a MEA instrument. When c_iPSCs derived CMs were plated in the MEA-plates, a slower recovery of the cells was observed in comparison to cells in standard culture plates. In fact, after the replating, c_iPSC-derived CMs required up to three days to form a strictly connected monolayer. Once the monolayer was formed, the electrical activity of c_iPSC-derived CMs was recorded at days 40, 45 and 50 of the differentiation and the spike amplitude, the beat period and the mean field potential duration were analyzed.

The spike amplitude measures the initial depolarizing phase with influx of Na^+. At day 40 of differentiation, the c_iPSC-derived CMs displayed a mean spike amplitude of 1.25 mV, while at days 45 and 50 of differentiation, a slight increase in the amplitude to 1.95 and 1.86 respectively was observed, indicating a larger depolarization phase (Figure 19 A).

The beat period is defined as the time interval between two spikes. At day 40 of differentiation, the mean beat period of c_iPSC-derived CMs corresponded to 2.07 seconds and it increased at days 45 and 50 of differentiation to 3.2 seconds, indicating an increased interval between spikes (Figure 19 B).

Last, no difference was observed in the mean field potential duration defined as the interval between the start of one depolarizing spike and the next repolarizing phase, at the three timepoints, (day 40 – 287.8 ms; day 45 – 266.86 ms; day 50 – 243.9 ms) (Figure 19C).

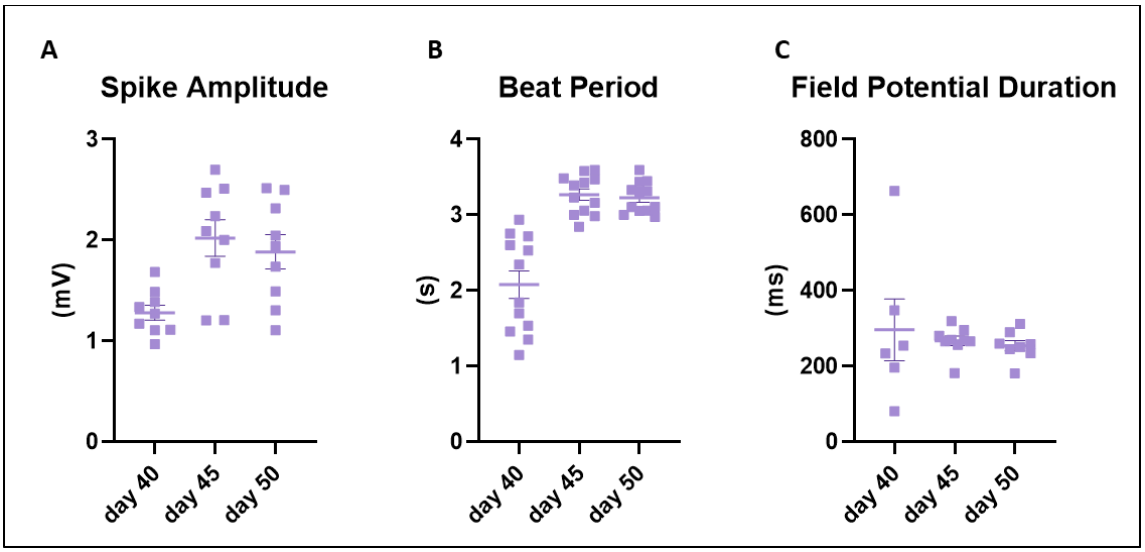

Figure 19: Functional characterization of c_iPSC-derived CMs with Maestro Edge MEA instrument. A: Spike amplitude analysis in c_iPSC-derived CMs at three different timepoints: days 40, 45 and 50 of differentiation (one differentiation – 12 replicates). B: Beat period analysis in c_iPSC-derived CMs at three different timepoints: days 40, 45 and 50 of differentiation (one differentiation – 12 replicates). C: Field potential duration analysis in c_iPSC-derived CMs at three different timepoints: days 40, 45 and 50 of differentiation (one differentiation – 12 replicates).

6.5 Generation of iPSC-derived SNs

For the generation of c_iPSC-derived SNs, the neural differentiation protocol toward the sympathetic linage described in the work of Oh (Oh et al., 2016) was followed (Figure 20 A) During the first week of differentiation the cells continued to proliferate until reaching 100% confluence (Figure 20 B). In the second week of differentiation, c_iPSC-derived neural progenitor cells reduced the proliferation rate and appeared tightly compacted together, with impossibility to distinguish one cell from the other (Figure 20 B). To reduce the density of the cells, at day 12 of the differentiation protocol, a replating step was performed, cutting the monolayer in small blocks. After one week from the replating (3rd week), the blocks started progressively to connect each other, forming an intricate network of axons projecting either from one block to other blocks in the proximity and/or to the same block as well. A very high number of prolongations could originate from one block (Figure 20 B). With a further week in culture (4th week), the cells acquired the typical neuronal morphology, showing an elliptical cell body surrounded by ramifications, ascribable to dendrites, and very long and thin axons (Figure 20 B). C_iPSC-derived SNs were then kept in culture according to the different experimental needs.

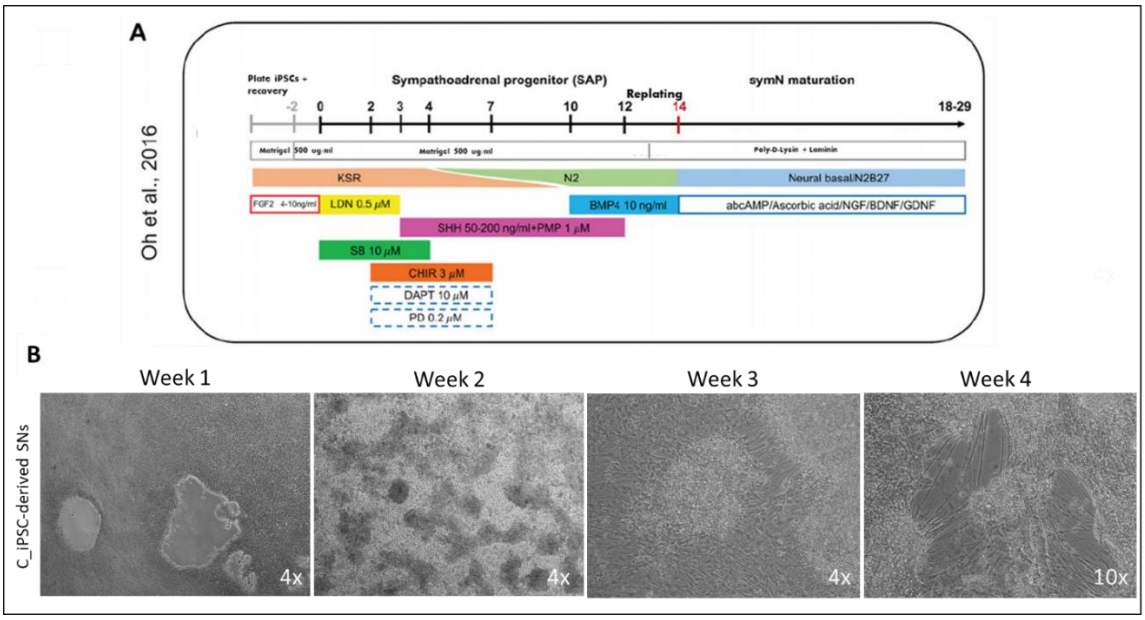

Figure 20: A: scheme of the sympathetic neural differentiation proposed by Oh et al., (Wu and Zeltner, 2019) B: Representative images of c_iPSC-derived SNs at different timing of the sympathetic neural differentiation protocol.

6.6 Molecular characterization of iPSC-derived SNs

In order to understand and highlight their molecular features, we characterized the generated c_iPSC-derived SNs through RT-PCR, immunofluorescence analysis, Western Blot, and FACS analysis (Figure 21). Given the absence of one single specific marker for the univocal characterization of sympathetic neurons, we used a combination of different markers that have been previously used in a wide number of studies (Oh et al., 2016; Kirino et al., 2018; Frith and Tsakiridis, 2019; Saito-Diaz et al., 2019; Takayama et al., 2020; Winbo et al., 2020). The three key markers typically expressed in sympathetic neurons are tyrosine hydroxylase (TH), dopamine beta hydroxylase (DBH), and paired-like homeobox 2b (PHOX2B) (Oh et al., 2016; Kirino et al., 2018; Frith and Tsakiridis, 2019; Saito-Diaz et al., 2019). TH is a precursor enzyme of DBH, which catalyzes the conversion of tyrosine in dopamine in the pathway of the catecholamines. The *DBH* gene encodes the enzyme responsible for the norepinephrine synthesis and it is highly expressed at late stage of differentiation (Saito-Diaz and Zeltner, 2019). PHOX2B is a transcription factor involved in the development of the autonomic nervous system; it is reported to be expressed during the whole differentiation period (Hsieh et al., 2006; Kirino et al., 2018).

As initial investigation of the distinctive characteristic of c_iPSC-derived SNs, gene expression analysis of these genes was performed. To select the most stable and appropriate housekeeping gene for the c_iPSC-derived SNs, three different candidates, namely *CYC1, RPL13, UBE2D2,* were investigated. *RPL13 and UBE2D2* resulted as the most suitable housekeeping genes for our cellular model and were used both as normalizers. In Figure 21 A1-C1 it is reported how the expression of the three genes of interest (*TH, DBH*, and *PHOX2B*) is differently modulated at days 4 – 9 – 12 –

20 – 30 of differentiation. *PHOX2B* expression level increased at early stages of the differentiation, with a peak around day 9 and a decrease immediately after day 12. A stable expression of the gene was then reached after day 20 of differentiation (Figure 21 A2). *TH* expression level increased rapidly during the differentiation, reaching its maximum at day 30 (Figure 21 B2). On the other hand, *DBH* expression, after an initial decrease at days 9 or 12, appeared again relevant at day 20 (Figure 21 C2). Notably, a variation in the peaks of expression of the same gene was detected especially between days 9 and 12 among different experiments (Figure 21 C2). This observation links to the normal variability during the differentiation experiments, given by many different, and sometime unknown, factors such as the change in the operator, the initial cells status or the cell densities (Takayama et al., 2020).

To further confirm the induction of SNs, Western Blot analysis was used to evaluate the protein expression of the same sympathetic neuronal markers previously analyzed. The expression trend of *PHOX2B* and *TH* observed by RT-PCR analysis was confirmed by Western Blot (Figure 21 E), showing the highest expression levels at days 9 and 12 of the differentiation for PHOX2B (Figure 21 F) and a regular increase overtime for TH, reaching the highest level at the later stage of the differentiation (day 30) (Figure 21 G). Unfortunately, Western Blot analysis for DBH was not successful, as it was not possible to find an antibody able to label a protein band at the expected DBH molecular weight. Therefore, DBH expression was investigated on cells at days 12 and 30 of differentiation using flow cytometry (Figure 21 H-L). The day 12 was chosen as first timepoint of detectable expression of DBH, according to the gene expression results. The same experiment was performed at the end of the differentiation protocol, at day 30, in order to confirm the presence of DBH-positive cells. The results established that the differentiation protocol produced DBH-positive cells in a range from 77% to 96% at day 12 (Figure 21 S) and from 60.5% to 17.9% at day 30 (Figure 21 T). Qualitative immunofluorescence staining images of DBH at days 12 and 30 of differentiation are shown in Figure 21 M and N. Cells were stained with only secondary antibody as negative control for the immunofluorescence (Figure 21 O and R). Flow cytometry was also used to confirm the increase of TH-positive cells during time. At day 12, the TH-positive cells corresponded to a range between the 18.8 % and 5.38% (Figure 21 U). The percentage at day 30 increased and corresponded to a range from 41.4% to 11.8% of the cells (Figure 21 V). A representative immunofluorescence staining of TH at the different timepoints is reported in Figure (Figure 21 P-Q).

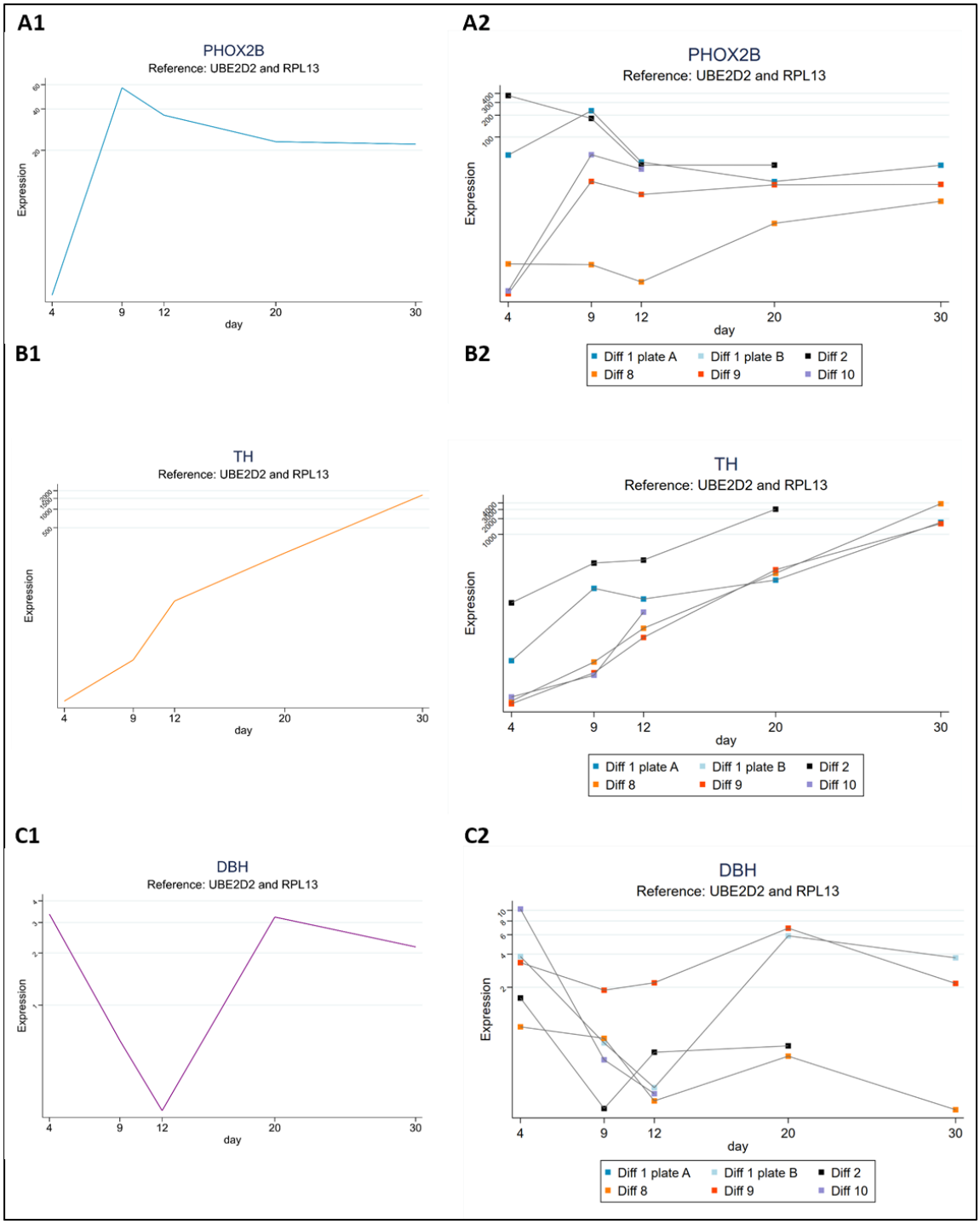
A1
PHOX2B
Reference: UBE2D2 and RPL13
Expression
day
A2
PHOX2B
Reference: UBE2D2 and RPL13
Expression
day
B1
TH
Reference: UBE2D2 and RPL13
Expression
day
B2
TH
Reference: UBE2D2 and RPL13
Expression
day
C1
DBH
Reference: UBE2D2 and RPL13
Expression
day
C2
DBH
Reference: UBE2D2 and RPL13
Expression
day
Diff 1 plate A
Diff 1 plate B
Diff 2
Diff 8
Diff 9
Diff 10

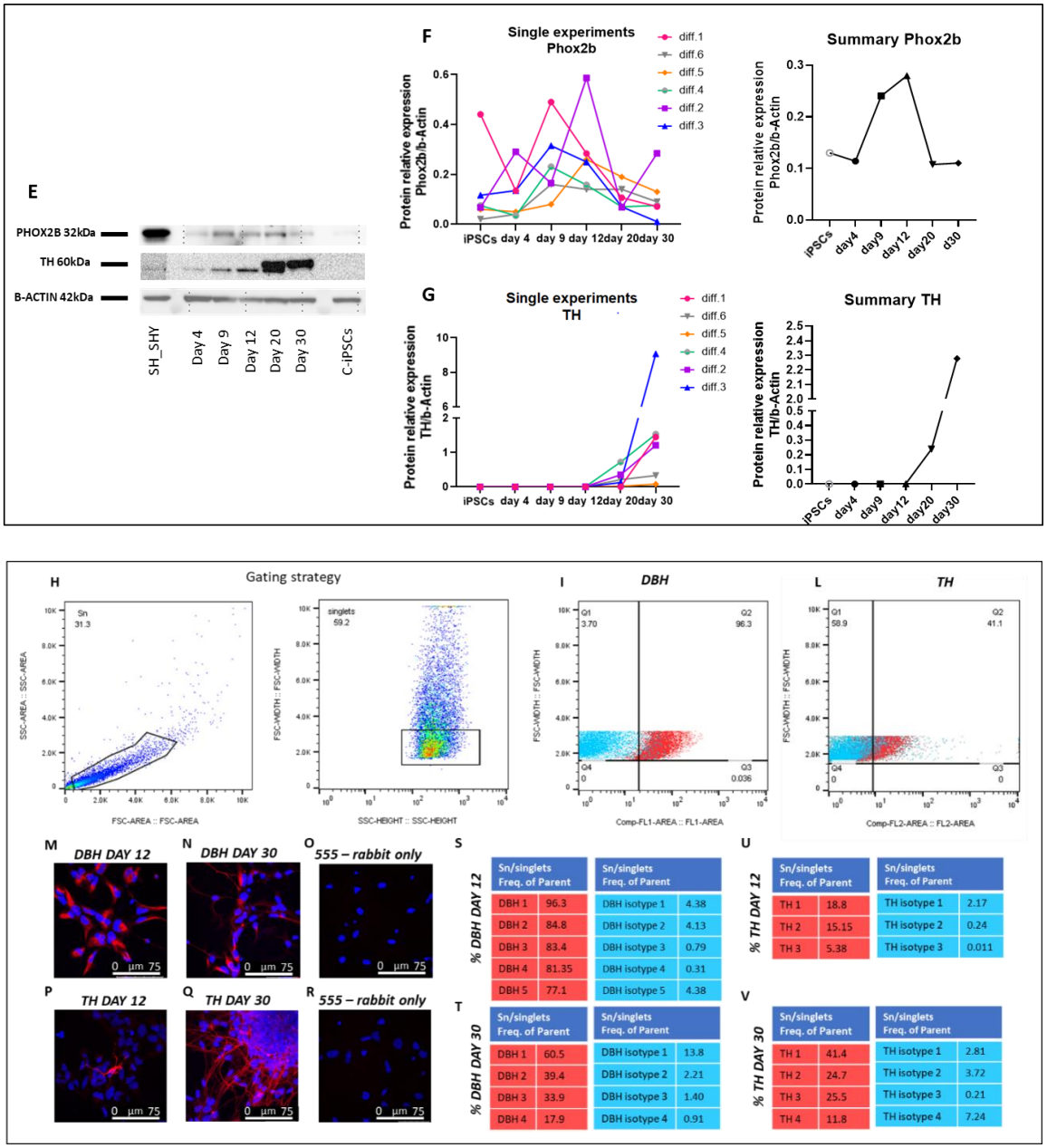

% DBH DAY 12	Sn/singlets Freq. of Parent		Sn/singlets Freq. of Parent	
DBH 1	96.3	DBH isotype 1	4.38	
DBH 2	84.8	DBH isotype 2	4.13	
DBH 3	83.4	DBH isotype 3	0.79	
DBH 4	81.35	DBH isotype 4	0.31	
DBH 5	77.1	DBH isotype 5	4.38	

% TH DAY 12	Sn/singlets Freq. of Parent		Sn/singlets Freq. of Parent	
TH 1	18.8	TH isotype 1	2.17	
TH 2	15.15	TH isotype 2	0.24	
TH 3	5.38	TH isotype 3	0.011	

% DBH DAY 30	Sn/singlets Freq. of Parent		Sn/singlets Freq. of Parent	
DBH 1	60.5	DBH isotype 1	13.8	
DBH 2	39.4	DBH isotype 2	2.21	
DBH 3	33.9	DBH isotype 3	1.40	
DBH 4	17.9	DBH isotype 4	0.91	

% TH DAY 30	Sn/singlets Freq. of Parent		Sn/singlets Freq. of Parent	
TH 1	41.4	TH isotype 1	2.81	
TH 2	24.7	TH isotype 2	3.72	
TH 3	25.5	TH isotype 3	0.21	
TH 4	11.8	TH isotype 4	7.24	

Figure 21: Characterization of c_iPSC-derived SNs.

A-C: RT-PCR of c_iPSC-derived SNs overtime (day 20-30 n=4; day 4-9-12 n=5 – ctrl sample c_iPSCs) A1: mean trend of PHOX2B gene expression of differentiations experiment (n=5). A2: single trend of PHOX2B gene expression of each differentiation experiment at days 4, 9,12, 20, and 30. B1: mean trend of TH gene expression of differentiations experiment (n=5). B2: single trend of TH gene expression of each differentiation experiment at days 4, 9,12, 20, and 30. C1: mean trend of DBH gene expression of differentiations experiment (n=5). C2: single trend of DBH gene expression of each differentiation experiment at days 4, 9,12, 20, and 30. Legend: Diff 1 plate A = differentiation nr.1 conducted on the plate A; Diff 1 plate B = differentiation nr.1 conducted on the plate B; Diff 2= differentiation nr.2; Diff 8= differentiation nr.8; Diff 9= differentiation nr.9; Diff 10= differentiation nr.1.

E-G: Western Blot analysis of c_iPSC-derived SNs (n=6). E: Densitometry analysis of Phox2b on c_iPSC-derived SNs at days 4, 9, 12, 20 and 30. F: Densitometry analysis TH on c_iPSC-derived SNs at days 4, 9, 12, 20 and 30. Legend: Diff 1= differentiation nr.1; Diff 2= differentiation nr.2; Diff 3= differentiation nr.3; Diff 4= differentiation nr.4;

Diff 5= differentiation nr5; Diff 6= differentiation nr.6.
H-V: Flow cytometry analysis of c_iPSCs derived SNs. H: Gating strategy for flow cytometry analysis of I: DBH and L: TH. S: Table of the percentage values of DBH-positive cells at day 12 and T: at day 30. U: Table of the percentage values of TH-positive cells at day 12 and V: at day 30 for each experiment performed.
M-R: Qualitative immunostaining images of c_iPSC-derived SNs marked with DBH and TH. M: DBH immunostaining in c_iPSC-derived SNs at day 12. N: DBH immunostaining in c_iPSC-derived SNs at day 30. O: negative control for immunostaining with secondary antibody only. P: TH immunostaining in c_iPSC-derived SNs at day 12. Q: TH immunostaining in c_iPSC-derived SNs at day 30. R: negative control for immunostaining with secondary antibody only.

6.7 Functional evaluation of iPSC-derived SNs

To evaluate the maturation into post-mitotic sympathetic neurons, immunofluorescence staining was performed on c_iPSC-derived SNs at different later timepoints of the differentiation. Cells at days 30, 40 and 50 of the neuronal differentiation were analyzed and showed the stable expression overtime of the pan-neuronal marker of mature neurons MAP2 (Microtubule-associated protein 2) in the soma and dendrites of most neurons (Figure 22 A). Furthermore, the c_iPSC-derived SNs expressed the typical sympathetic marker TH along the whole axonal projections in a continuous and linear organization but also in a punctate form, resembling small pearls. To investigate these round pearls, a 3D reconstruction of c_iPSC-derived SNs was performed at day 50, pointing out the presence of the round pearls in different areas of the axonal network (Figure 22 B). The pearls represent the varicosities, sites where the neurotransmitters are stored and secreted, ascribable to mature and functional neurons (Zaglia and Mongillo, 2017). These results highlighted and confirmed the maturation of c_iPSC-derived SNs during the differentiation process, making their phenotype very similar to the primary neurons (Zaglia and Mongillo, 2017). To functionally assess the sympathetic neuronal maturation, electrophysiological recordings using the MEA system were performed at different days of differentiation. c_iPSC-derived SNs were plated on special plates suitable for this type of experiments. The center of the plate is constituted by a conductive surface containing gold electrodes for the detection of the electric signals. Due to the well characteristics of the MEA-plates, the coating with PDL/laminin resulted not to be the best coating strategy, causing the continuous detachment of the cells from the surface, making the protocol not reproducible. For this reason, an alternative coating strategy was adopted. The PDL/laminin coating was substituted by 0,5 mg/ml Matrigel, resulting much stronger in comparison to the first one, without affecting the cell viability. On the Matrigel coating, the cells appeared round-shaped for some days and subsequently they started to acquire the typical rhomboid morphology of the neuronal soma. The cell monolayer remained well structured with a dense and compacted structure. Often, in some areas of the monolayer, some holes appeared due to the intense compaction of the cells. In these holes, it was possible to observe the formation of axonal prolongation between the different active cells. c_iPSC-derived SNs electrical activity was recorded every ten days, starting from day 30 of the differentiation, (Figure 22 C-L). The parameters analyzed were the following:

- the number of spikes and the mean firing rate, which indicate the level of activity of the cells,
- the number of bursts, which indicates the frequency of spiking
- the number of network bursts, which indicates the recurrency of synchronized firing.

The days 40 and 50 resulted the most active timepoints. In particular, the neurons were mostly active at day 50 showing 29205.6 spikes (Figure 22 C) with a mean firing rate of 3.04 Hz (Figure 22 E). At this stage, c_iPSC-derived SNs displayed 1081.33 bursts (Figure 22 G) building 101.77 network bursts (Figure 22 I). At day 60 there was a high decrease in the neuronal activity, corresponding to 10046.1 number of spike (Figure 22 C) with a mean firing rate of 1.04 Hz (Figure 22 E). The number of bursts was decreased to 284 (Figure 22 G) with a consequent reduction of the network burst formation to 13.88 (Figure 22 I). The numbers of spikes, bursts and network bursts were further largely decreased at days 70 and 80 (Figure 22 C;G;I), with a little variance in the mean firing rate (Figure 22 E). From days 90 to 150 of the differentiation, all the analyzed parameters remained stable, without showing enormous variations. A general reduction in the firing activity of c_iPSC-derived SNs was detected over time, with a reduced high frequency of the spikes and a consequent decrease in the synchronized firing activity.

When c_iPSC-derived SNs were paced at a frequency of 2 Hz, they were able to follow the stimulation at all timepoints, except from day 50 of differentiation (Figure 22 F). The number of spikes resulted higher in paced cells in comparison to non-paced cells at days 40, 50, and 60 of the differentiation (Figure 22 D). No evident changes were detected in the number of bursts and in the number of network bursts in paced and non-paced cells (Figure 22 H-I).

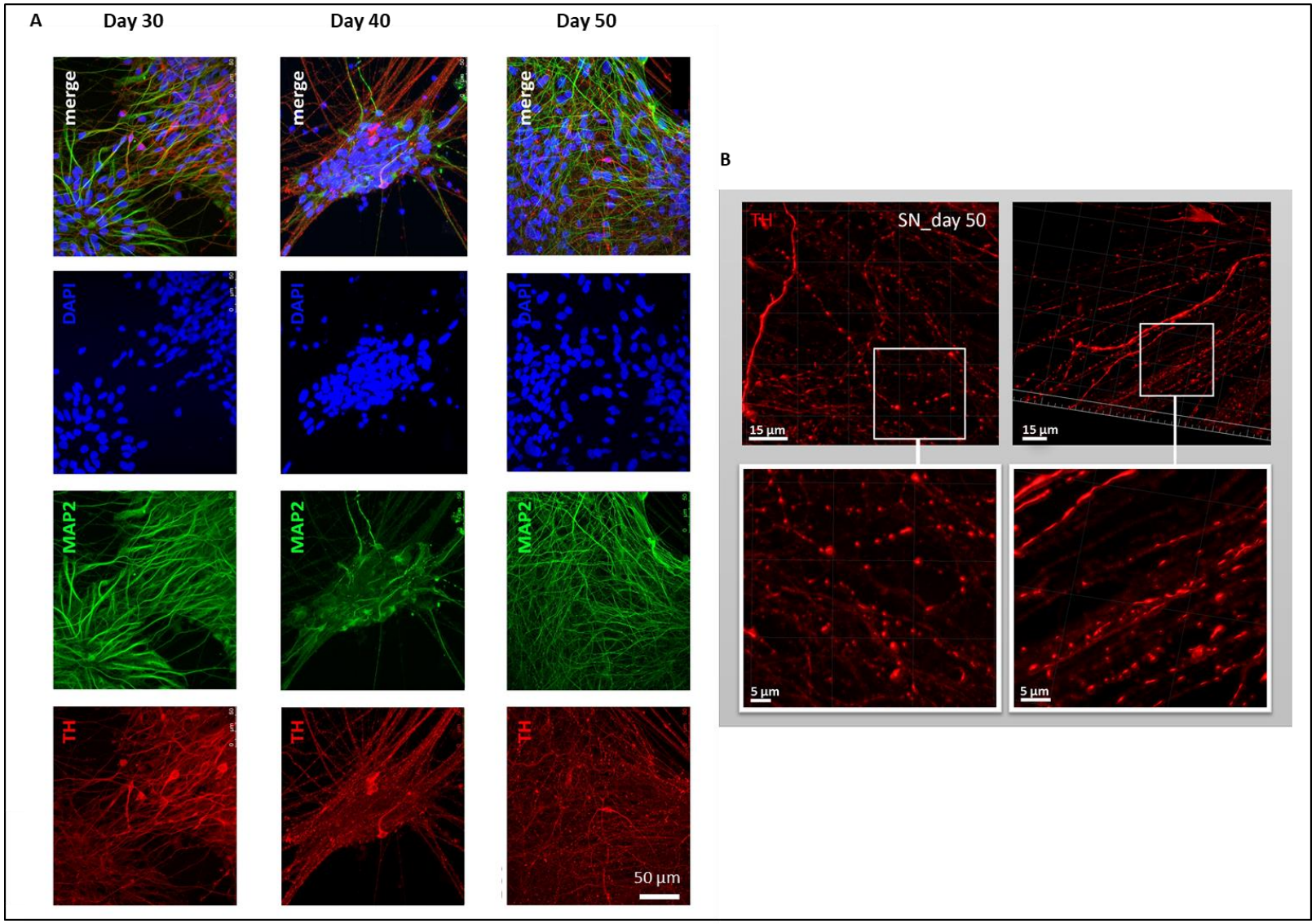
A
Day 30
Day 40
Day 50
merge
DAPI
MAP2
TH
50 µm
B
TH
SN_day 50
15 µm
15 µm
5 µm
5 µm

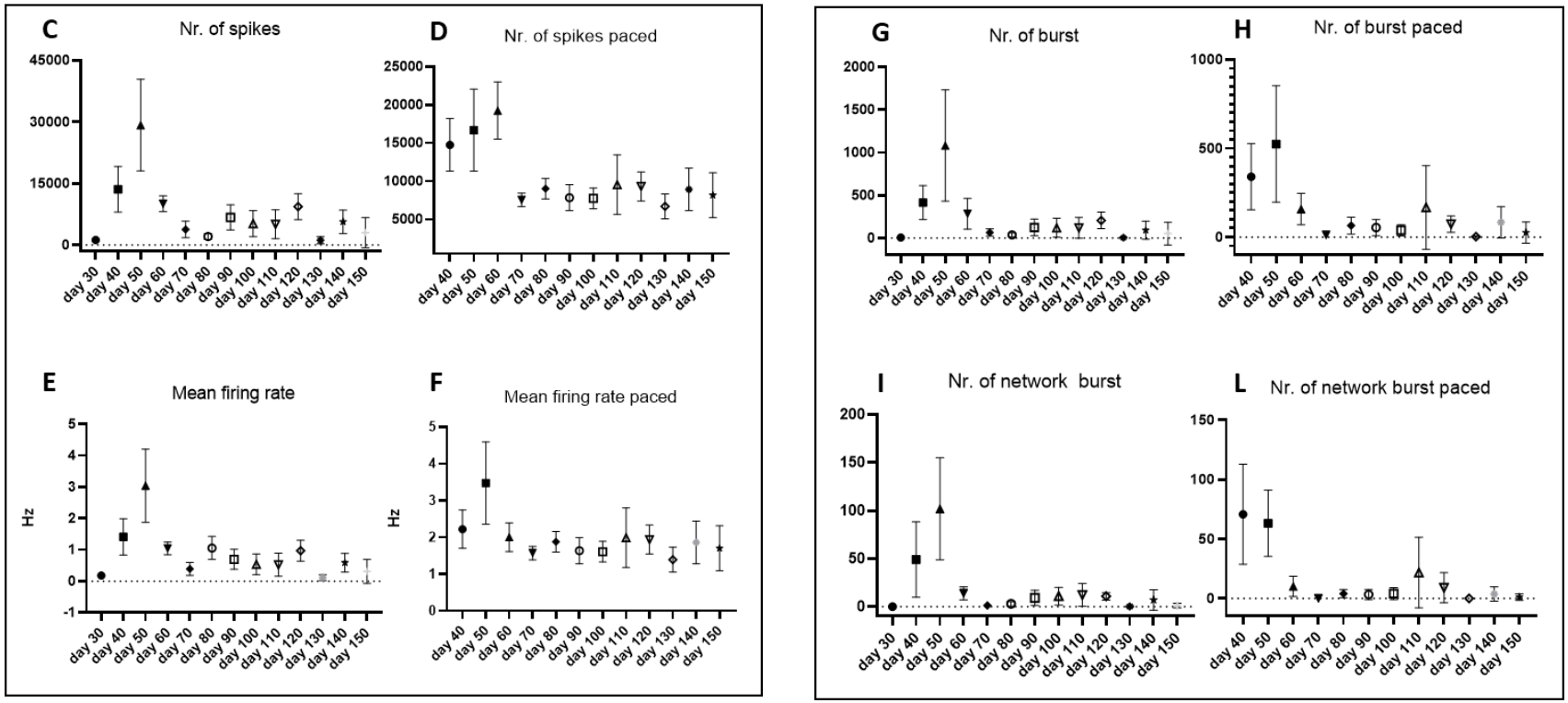

Figure 22: Characterization of the maturity in c_iPSC-derived SNs.

A: Immunostaining images of c_iPSC-derived SNs at different timepoints: days 30, 40, and 50. C_iPSC-derived SNs were marked with TH (red), MAP2 (green) and DAPI (blue).

B: 3D reconstruction of varicosities marked with TH (red) in c_iPSC-derived SNs at day 50.

C-L: Long-term functional profile of c_iPSC-derived SNs obtained with MEA instrument and co-cultured for 150 days (one differentiation – 9 replicates). C: Profile of the spontaneous number of spikes in c_iPSC-derived SNs cultured until day 150. D: Profile of the paced (2Hz) number of spikes in c_iPSC-derived SNs cultured until day 150. E: Profile of the spontaneous mean firing rate in c_iPSC-derived SNs cultured until day 150. F: Profile of the paced (2Hz) mean firing rate in c_iPSC-derived SNs cultured until day 150. G: Profile of the spontaneous number of bursts in c_iPSC-derived SNs cultured until day 150. H: Profile of the paced (2Hz) number of bursts in c_iPSC-derived SNs cultured until day 150. I: Profile of the spontaneous number of network burst in c_iPSC-derived SNs cultured until day 150. L: Profile of the paced (2Hz) number of network burst in c_iPSC-derived SNs cultured until day 150.

6.8 Set-up of the co-culture of c_iPSC-derived SNs with c_iPSC-derived CMs.

The first parameters considered in the optimization of the co-culture of c_iPSC-derived SNs and CMs was the density of both CMs and neurons. To define the proper cell number, four different densities were tested according to the instruction provided by the manufacturer of the inserts (Ibidi) (Figure 23 A). The following cell densities were plated in one chamber of the insert for both cell populations (Figure 23 B-E):

- $2{,}1x10^4$ cells/chamber
- $2{,}8x10^4$ cells/chamber
- $3{,}5x10^4$ cells/chamber
- $4{,}9x10^4$ cells/chamber

The c_iPSC-derived SNs plated at the density of $2.1x10^4$ resulted in too sparse colonies incapable to connect to each other (Figure 23 B). At this density, c_iPSC-derived CMs resulted more packed in comparison to c_iPSC-derived SNs, but still with considerable empty areas. The second tested density was $2.8x10^4$, which resulted better in comparison to the first one, allowing more connections between the SNs (Figure 23 C). However, the two types of cell populations were still not able to form a monolayer. The formation of a monolayer is important for two reasons: firstly, to make the protocol reproducible and secondly, to enable a stable connection with the entire two populations and not only with small areas of them. The last two densities, $3.5x10^4$ cells (Figure 23 D) and $4.9x10^4$cells (Figure 23 E), showed no remarkable differences. In both cases, CMs and neurons formed a monolayer that became always more compact as the days in culture increased. The highest density ($4.9x10^4$ cells/chamber) was chosen in order to obtain in each experiment a dense monolayer of c_iPSC-derived CMs and SNs. However, a certain degree of variability in monolayer formation was observed among different experiments, even if the same density/chamber was used. For this reason, we further increased the cell density of both CMs and neurons to a final number of $7x10^4$ cells/chamber. With this cell density the probability to obtain the formation of a compact monolayer was maximized compared to the densities previously tested.

Of note, a higher cell density allowed also for a better formation of cell networks, enabling the connection between the two cell populations with the consequent migration of axonal projection toward the beating cardiomyocytes. Additionally, only in the co-culture with high cell density it was possible to observe axons sprouting from the neuronal population towards the cardiomyocytes. The connection of the two cell populations was not observed in all the co-cultures with low cell densities.

The second point considered was the choice of the appropriate medium for both CMs and neurons. It has been previously observed (Winbo et al., 2020) that a ratio 1:1 of NBB (neurons) and cardiomyocyte medium could support the culture of both cell populations, allowing neurites to expand and cardiomyocytes to beat. Therefore, we chose this medium composition as the best one for our co-cultures.

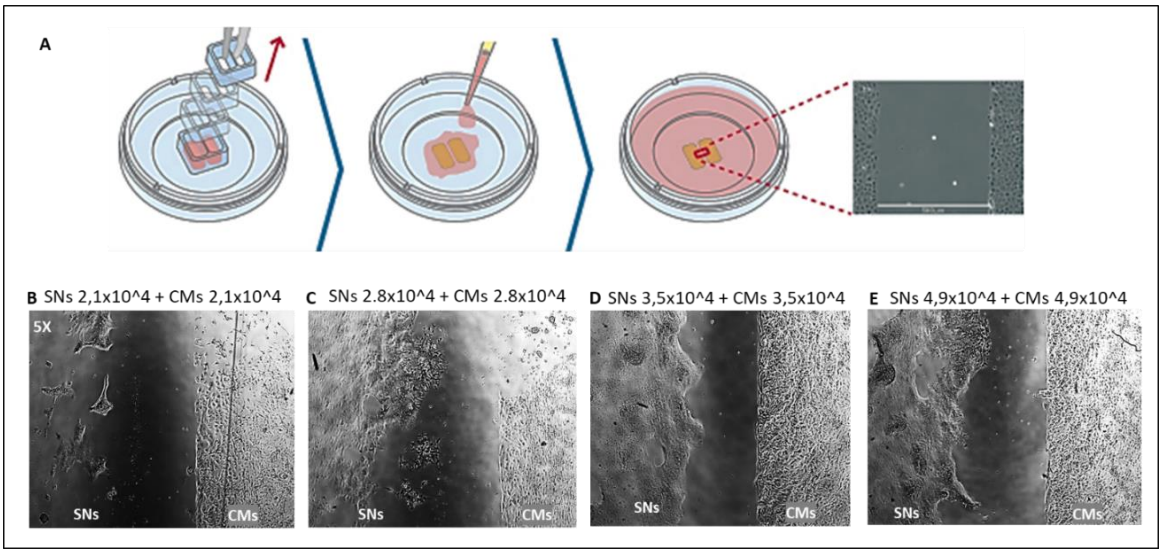

Figure 23: A: Scheme of the workflow followed for the preparation of the co-cultures using the Ibidi two-chambers inserts.B: iPSC-derived SNs (lx) and iPSC-derived CMs (dx) plated at the density of 2,1x104 cells/chamber. Magnification 5X. C: iPSC-derived SNs (lx) and iPSC-derived CMs (dx) plated at the density of 2,8x104 cells/chamber. Magnification 5X. D: iPSC-derived SNs (lx) and iPSC-derived CMs (dx) plated at the density of 3,5x104 cells/chamber. Magnification 5X. E: iPSC-derived SNs (lx) and iPSC-derived CMs (dx) plated at the density of 4,9x104 cells/chamber. Magnification 5X.

The last important aspect that we evaluated in the setting-up of our co-culture model was the coating strategy. In the first attempts, we tried to coat individually the two culture inserts with specific coating for each cell population (PDL/laminin for SNs and Matrigel for CMs). This strategy enabled the attachment of the inserts in the dried well plate and the complete adhesion of the cells in each compartment. Since the gap between the two cell populations was not coated, the connection between the c_iPSC-derived SNs and c_iPSC-derived CMs resulted extremely difficult. Axonal projection started to grow very slowly after the removal of the insert and needed from several days to some weeks to connect to the CMs. The absence of the coating in the gap appeared to be an obstacle for the projections because firstly, they seemed to be blocked by an invisible barrier hindering the progress toward the cardiomyocytes and secondly, because the majority of the connections were established within c_iPSC-derived SNs theirselves, forming extremely thick bundles of axons.
For all these reasons, different tests were conducted to select the appropriate coating for our co-cultures. The tested strategies were the following:

- **A)** Coating of the entire well surface with Matrigel followed by the application of the inserts on the wet surface.
- **B)** Coating of the entire well surface with PDL/laminin followed by the application of the inserts on the dried coating.
- **C)** Application of the inserts in a new dried well surface followed by the coating of the two chambers with PDL/laminin separately. After the removal of the coating a drop of 0.5

mg/ml Matrigel was applied onto the cells and subsequently incubated at 37°C for 30 minutes.

- **D)** Application of the inserts in a new dried well surface followed by the coating of the two chambers with Matrigel separately. After the removal of the coating a drop of 0.5 mg/ml Matrigel was applied onto the cells and subsequently incubated at 37°C for 30 minutes.

The strategy **A** appeared immediately the most unsuccessful because the inserts were not able to properly attach to the well due to the wetness of the surface. This resulted in the spreading of the cells from one chamber to the other and in the impossibility of obtaining a net separation of neurons and cardiomyocytes (Figure 24 A-C).
The strategy **B** (Figure 24 D-F), **C** (Figure 24 G-I), and **D** (Figure 24 L-N) resulted in the attachment of cells and in the formation of connections between them. In comparison to the co-cultures without a coating in the gap, these cells were able to form connections in only 3-5 days after the removal of the inserts and no problem was detected in the extension of axonal projections toward cardiomyocytes. In Figure 24 A; D and G it is evident that c_iPSC-derived SNs migrated in the gap with the whole cell body, starting already from the first days after the insert removal, and formed a compact tissue in which some cell-free areas between the c_iPSC-derived CMs are present. In these empty areas it was possible to observe the axonal formations. Long-term culture of c_iPSC-derived SNs generated a sort of 3D aggregate, characterized by a high number of axons (Figure 24 C;F;I;N). Neurites prolonged toward c_iPSC-derived CMs and entered in the population of cardiomyocytes in the part exposed to the neurons. The portion of CMs exposed to the neurons did not migrate in the gap as in the case of c_iPSC-derived SNs, but we observed that the most exposed cardiac cells changed their orientation towards the neuronal cells (Figure 24 N;H;C). c_iPSC-derived CMs continued to beat during the entire culture period even when they were innervated by c_iPSC-derived SNs. Possible contamination of cells not belonging to cardiac or neural population was observed but it was not further investigated. Considering that there were no considerable differences between the strategies **B**, **C,** and **D**, the strategy **D** was chosen for the experiments of the co-cultures resulting less time-consuming in comparison to the others. Therefore, the definitive coating strategy is represented by the individual plating of the two cells types on a Matrigel coating, and after the removal of the insert, a drop of Matrigel is applied on the top of the two populations to coat the gap as well.

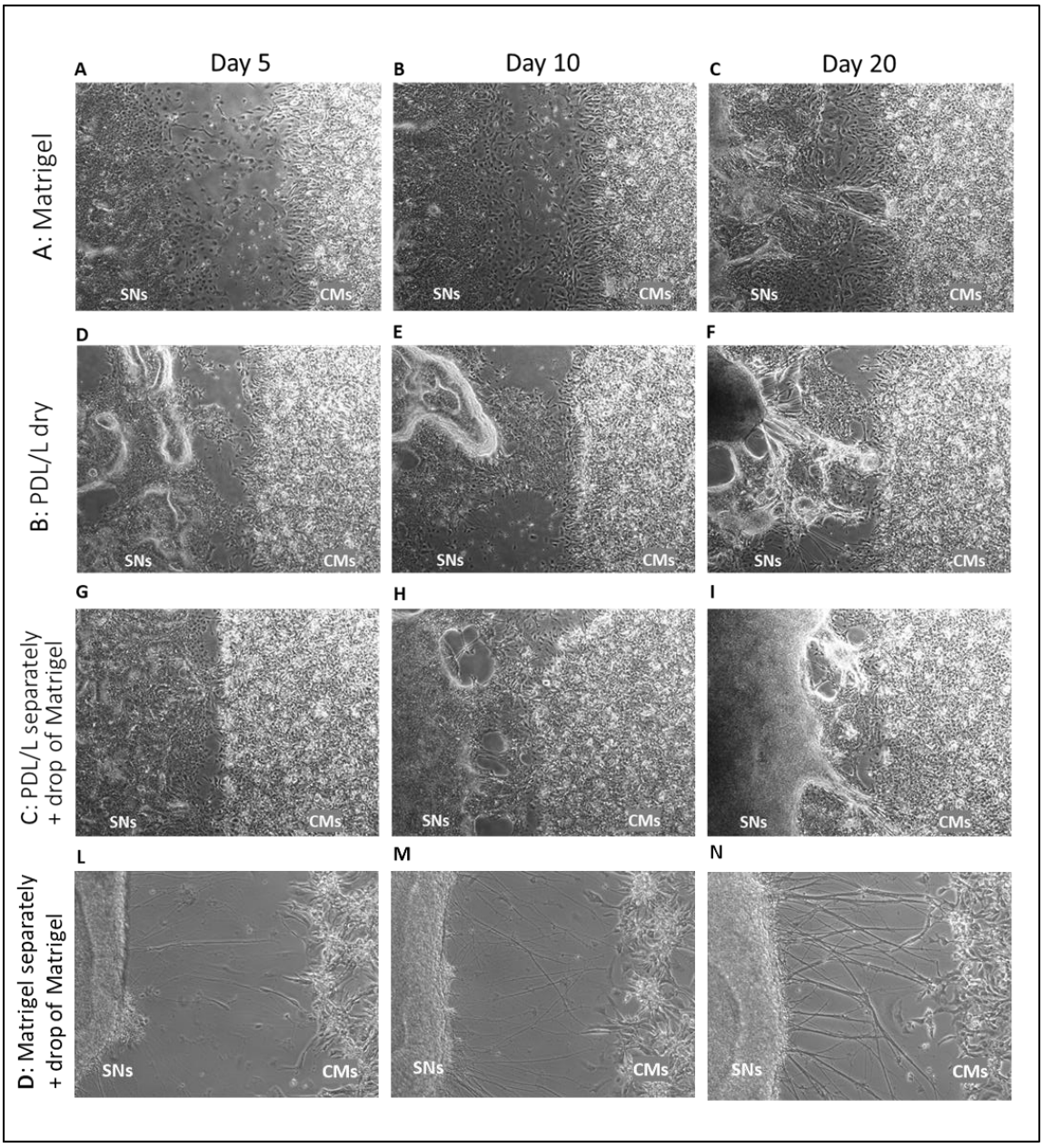

Figure 24: Different coating strategies used for the optimization of the co-culture models.
A-C: Coating of the entire well surface with Matrigel and followed by the application of the insert on the wet surface. Co-culture at A: day 5; B: day 10; C: day20.
D-F: Coating of the entire well surface with PDL/laminin and the following application of the insert on the dried coating. Co-culture at D: day 5; E: day 10; F: day20.
G-I. Application of the insert in a new dried well's surface, followied by the coating of the two chambers with PDL/laminin separately. After the removal of the coating a drop of 0,5 mg/ml Matrigel was applied onto the cells at 37°C for 30 minutes. Co-culture at G: day 5; H: day 10; I: day20.
L-N. Application of the insert in a new dried well's surface, followed by the coating of the two chambers with Matrigel separately. After the removal of the coating a drop of 0,5 mg/ml Matrigel was applied onto the cells at 37°C for 30 minutes. Co-culture at L: day 5; M: day 10; N: day20.

6.9 Characterization of the co-culture model of c_iPSC-derived SNs with c_iPSC-derived CMs.

A preliminary characterization of co-cultures was performed using immunofluorescence staining. Cells were co-stained with cardiac and neuronal markers. For c_iPSC-derived CMs the sarcomeric marker α-actinin was used in each experiment. Instead, for c_iPSC-derived SNs, different markers such MAP2, TH and Synapsin I were analyzed. The Figure 25 A displays a 1540x1320 microns representative area of the co-cultures assembled by a collage of single frame. In fact, it is possible to observe the exact area where the two populations get in touch. The TH-positive neurons formed bundles composed by many single axons together, creating thick bundles. The innervations penetrated in the cardiomyogenic population and one thick bundle could innervate more than one c_iPSC-derived CM (Figure 25 A-white arrows). The intricate network of innervation was denser in the area of cardiac population closer to the neurons. In the center of the cardiac population, the thickness of axon bundles was reduced. In fact, the axon bundles loosened in single axons penetrating and innervating the c_iPSC-derived CMs in depth (Figure 25 A-yellow arrows). With further magnification, it is possible to observe the details of the co-cultures (Figure 25 B-E). The co-staining of c_iPSC-derived SNs with MAP2 and TH highlighted the composition of the nerve bundles (Figure 25 B). The pan-neuronal marker MAP2 is specific for all neurons as cytoskeleton protein, on the contrary not all neuronal types are positive for TH which is specific for a reduced number of neuronal subpopulations, such as sympathetic or dopaminergic neurons. In Figure 25 C, the 3D reconstruction of the co-cultures shows the presence of a high number of TH-positive varicosities in a punctuated form, evidencing the mature-like phenotype of the c_iPSC-derived SNs. Co-cultures were finally stained with Synapsin I, a membrane protein of synaptic vesicles, to observe the pre-synaptic cell contacts. The Figure 25 D displays an accumulation of Synapsin I when axons entered in contact with cardiac cells. In the 3D reconstruction, it is possible to determine the form of Synapsin I, which appeared in puncta-like structures, suggesting the formation of synaptic clusters in the site of neuronal-cardiac contacts (Figure 25 E). Further investigations at the level of post-synaptic sites are required.

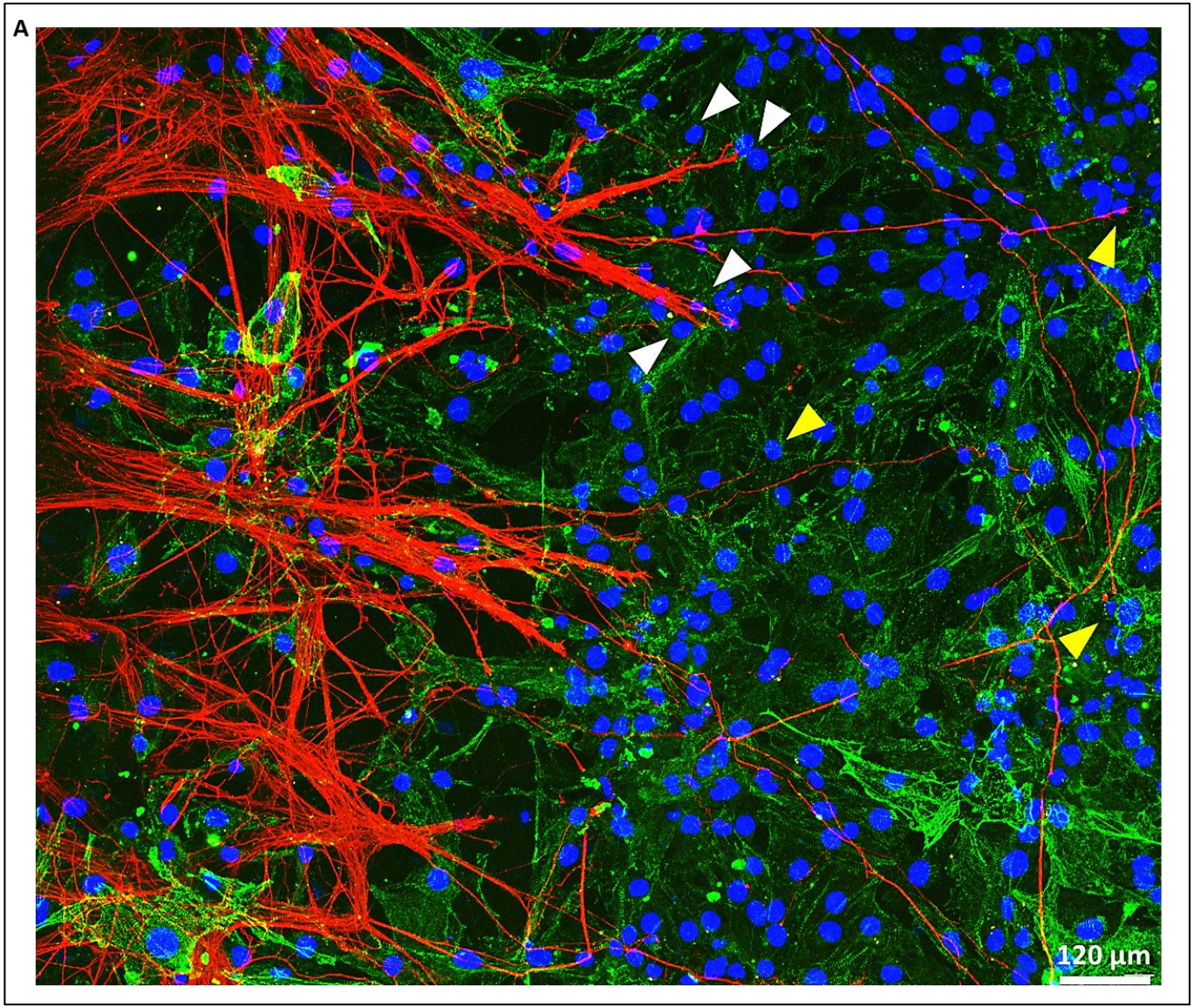
A
120 µm

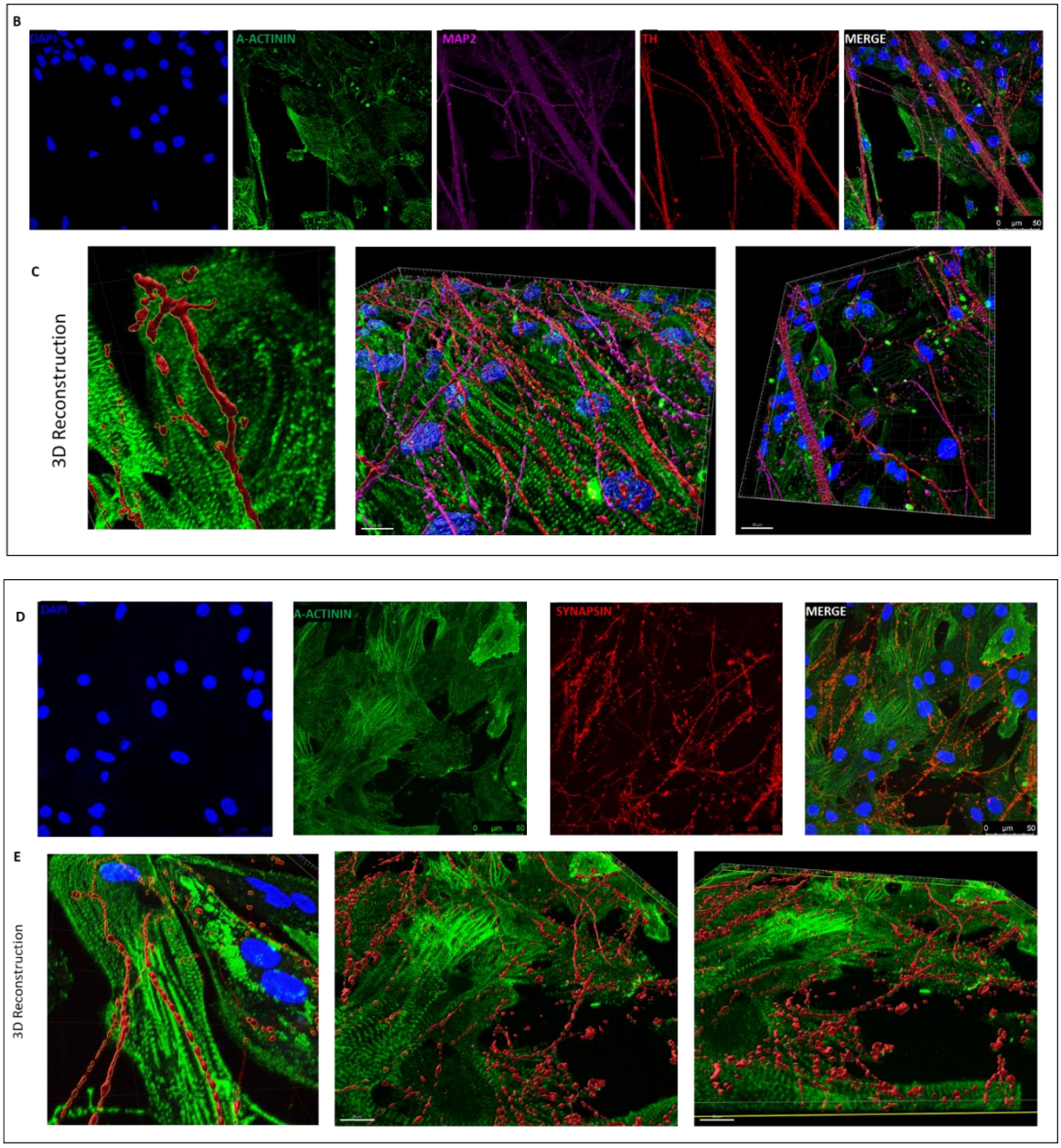

Figure 25: Immunostaining experiment of co-culture models. A: Reconstruction of an area of interest in immunostaining experiment of co-culture models. Different markers for both cell population were used: TH (red) and Troponin-I (green). White arrows indicate the multiple innervations of c_iPSC-derived CMs starting from one nerve. Yellow arrows indicate single innervation of c_iPSC-derived CMs starting from one axon.
B: Immunostaining images of the co-cultures marked with TH (red), MAP2 (magenta), Troponin-I (green) and DAPI (blue).
C: 3D reconstruction of the co-cultures marked with TH (red), MAP2 (magenta), Troponin-I (green) and DAPI (blue).
D: Immunostaining images of the co-cultures marked with Synapsin I (red), Troponin-I (green) and DAPI (blue).
E: 3D reconstruction of the co-cultures marked with Synapsin I (red), Troponin-I (green) and DAPI (blue).

6.10 Functional characterization of the co-culture model of c_iPSC-derived SNs with c_iPSC-derived CMs

To observe the functional effect of c_iPSC-derived SNs on c_iPSC-derived CMs, electrophysiological recordings using the MEA system were performed. Co-cultures were seeded on the MEA plates and measured once a week for two weeks (Figure 26). The day 0 was measured immediately after the removal of the inserts from the well. Considering that at this stage no connections were formed and that the two cell populations have never been connected, the values obtained at this timepoint were considered the reference timepoint for the co-cultures. A preliminary evaluation of the behavior of c_iPSC-derived CMs was assessed analyzing the beat rate (Figure 26). At day 0 of the co-culture, c_iPSC-derived CMs displayed a baseline mean beating rate of 44.26 bpm. When c_iPSC-derived CMs are co-cultured with c_iPSC-derived SNs their beat rate increased. In fact, after two weeks of co-culture, c_iPSC-derived CMs showed an average beat rate of 87.61 bpm. These data suggest an increase in the beat rate of iPSC-derived CMs when connected with iPSC-derived SNs. This increase was not evident when CMs were kept in culture without SNs for the same amount of time on normal plates not equipped with multi-electrodes.

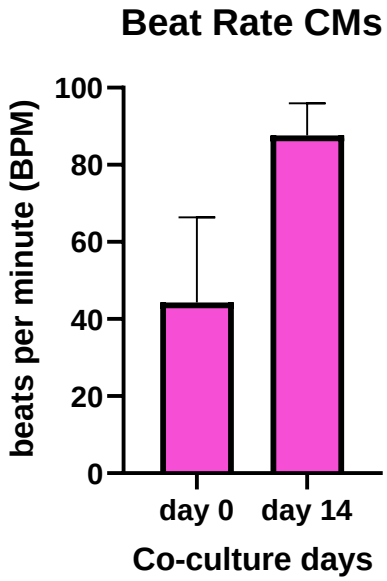

Figure 26: Function analysis of the co-cultures performed using the MEA system. Spontaneous beat rate of c_iPSC-derived CMs in co-cultures with c_iPSC-derived SNs evaluated at day 0 (no connections between the two populations) and day 14 of the co-culture.

7 DISCUSSION

There is a growing evidence that ANS plays an important role in the development of heart diseases, contributing extensively to their onset (Armour, 2008). In particular, it is known that ANS is able to regulate the function of the whole cardiac organ, by modulating the properties of the single cardiomyocytes (Kapa et al., 2010). Many are the cardiovascular disorders that are known to be affected by autonomic dysfunctions such as atrial fibrillation, long QT syndrome, Brugada syndrome, ventricular tachyarrhythmia and arrhythmogenic cardiomyopathy (ACM) (Kapa et al., 2010; Shen and Zipes, 2014b; Jamali et al., 2017; Fedele and Brand, 2020). Two are the most common causes of the above-mentioned disorders, namely the depletion of the connections between ANS and the heart, in terms of reduction of autonomic functions (aging) (Francis Stuart et al., 2018) and connections (heart transplantation) (Awad et al., 2016), and the unbalance of the autonomic activity, such as in atrial fibrillation (Bettoni and Zimmermann, 2002; Amar et al., 2003; Tomita et al., 2003). The different studies conducted on this topic have raised clinical and biological interest in the co-participation of the cardiac and autonomic systems in the pathological mechanisms, leading to the development of the Neurocardiology discipline (Ardell and Armour, 2016). To deeply understand how the cardiac system and the autonomic system interact between each other, it is extremely important to understand and define their interconnection and how this can be modulated (Winbo et al., 2020). However, in the past and for many years, the real anatomy of the cardiac innervation has been poorly understood and subject of debates (Armour et al., 1997). The only possible method for the elucidation of the cardiac ANS was the dissections of human cadavers or mammals (Hanna et al., 2017). Nowadays this technique is considered an extremely invasive method and limited in the number of material collected (Nakao et al., 2020). Moreover, even though some aspects in the functions or in the anatomy of mammals are conserved among species (Hanna et al., 2017), some differences are always present especially in the electrical properties and in the response to drugs (Ohnuki and Takahashi, 2015; Kussauer et al., 2019). These reasons make the necessity clear to have a reliable and predictive neurocardiac model for the recapitulation of the neurocardiac junctions, functions and disorders. Thanks to Yamanaka and his discovery of iPSCs, this became possible (Takahashi and Yamanaka, 2006). In particular, the capability of iPSCs to differentiate in many cell types, has been already largely demonstrated and used for the development of different disease models (Yoshida and Yamanaka, 2017; Kussauer et al., 2019; Liang et al., 2019; Zuppinger, 2019; Chang et al., 2020). Furthermore, the use of iPSCs sustains the principle of the 3R (Refinement, Reduction, Replacement), coined for the first time by Russell and Burch in 1959 (Balls and Straughan, 1996), in support of an ethical animal research and specifically refers to the 3rd "R" – Replacement - as the consequent substitution of animal models with other model systems (Emerson, 2010). In addition, another important advantage coming from the use of iPSCs is the bypass of the ethical problems usually associated with the use of embryonic stem cells and related to the destruction of the embryos (Sommer and Mostoslavsky, 2010). Therefore, iPSCs represent a possible, concrete answer to the necessity of the development of a neurocardiac model in a precise, ethical and reproducible way. These considerations are at the basis of the decision to develop a neurocardiac model with

neurons and cardiomyocytes derived from iPSCs. According to the literature, the present work is one of the few studies (total of = 3 (Oh et al., 2016; Takayama et al., 2020; Winbo et al., 2020)) conducted uniquely with an entirely iPSC-derived model, generating the two different populations from the same line of iPSCs. Furthermore, the starting material used for the study is a commercial line of iPSCs directly bought from the suppliers, thus allowing for easier reproducibility in other research institutions.

The experiments of this work mainly focused in developing and characterizing iPSC-derived SNs following a previously published protocol and in the subsequent set up of a novel co-culture model of iPSC-derived CMs with iPSC-derived SNs. In the past, I was able to establish and optimize a robust technique to obtain an enriched population of iPSC-derived CMs (80-90%) through a magnetic sorting step (https://bibsearch.uibk.ac.at/AC15167706). Indeed, the cardiomyogenic differentiation protocol previously optimized was adapted to the current cell line in terms of cell density and day of enrichment. I successfully obtained iPSC-derived CMs expressing typical cardiac genes such as Troponin I, Connexin 43 and Myosin Heavy Chain 7 and positively stained for the sarcomeric protein α-actinin and Troponin I, organized in alternated striations along the cells. Even though the presence of a sarcomeric structure can be interpreted as a sign of maturity, it is clear that the obtained iPSC-derived CMs displayed an immature morphology, with poorly organized striation. Additionally, the iPSC-derived CMs used in the present thesis are round-shaped, while mature cardiomyocytes are rod-shaped (Mehta et al., 2014). As a matter of fact, the immaturity of iPSC-derived CMs is abundantly reviewed in literature, highlighting that their morphological and functional characteristics are similar to those of embryonic or fetal cardiomyocytes (Mehta et al., 2014) (Tang, 2020). Indeed, presenting unsynchronized Ca^{2+} transients, non-uniform calcium dynamics, high pacemaker current I_f, reduced densities of the hyperpolarizing current I_{K1}, low upstroke velocity and less negative resting membrane potential (Di Baldassarre et al., 2018; Goversen et al., 2018).

Besides the gold-standard method of the whole-patch clamp, nowadays there is another valid method for the evaluation of the electrical properties of cells: the MEA system (Kussauer et al., 2019). Initially developed for neural purposes, now it is employed also in the characterization of iPSC-derived CMs and was used by Kumar and coworkers (Kumar et al., 2019) to provide a detailed characterization of the electrical activity of human induced pluripotent stem cell-derived cardiomyocytes. The iPSC-derived CMs characterized in this work have a slightly different functional profile compared to the one characterized by Kumar et al. Indeed, the cells of Kumar's group displayed an increased beat period over the time in culture, ranging from 1.06 ± 0.04 s in the first week to 1.43 ± 0.03 s (Kumar et al., 2019). On the contrary, the cells analyzed in this work displayed a higher beat period equal to>3 s at 45 and 50 days. Further differences are found in the analysis of the FPD. Kumar and coworkers observed that the FPD of the iPSC-derived CMs increased with prolonged time in culture starting from 241 ms in the first week to 580 ms in the fourth week (Kumar et al., 2019), while the FPD of the iPSC-derived CMs of this thesis was constant for ten days around the value <300 ms, corresponding to a prolonged physiological QT interval of the AP, possibly caused by a different functionality of the hERG channels (Pradhapan et al., 2013).

The differences existing between the functional properties of the cardiomyocytes derived in the present work and those previously characterized in literature are reasonably due to the different cell source, culture conditions (medium, coating, cell density) and differentiation times (Biendarra-Tiegs et al., 2020).

One commonly used strategy to increase the maturity of iPSC-derived CMs *in vitro* has been the prolonged time in culture (Besser et al., 2018). Nevertheless, nowadays there are different methods employed for the maturation of iPSC-derived CMs including their co-culture with other cell types (Robertson et al., 2013; Besser et al., 2018). The second cell population should improve the maturity of the iPSC-derived CMs in terms of morphology, mechanisms and functionalities. iPSC-derived CMs have been already cultured with different cell types, among which endothelial cells (Giacomelli et al., 2017), fibroblasts (Saini et al., 2015) and sympathetic neurons (Oh et al., 2016). However, the principal aim of some neurocardiac co-cultures studies have been aimed to deeply explain the effect of cardiomyocytes on the neural population and not vice versa (Oh et al., 2016). For this reason, the attention in this research was equally posed on iPSC-derived CMs and iPSC-derived SNs.

After an exhaustive literature research, it is evident that the protocols for the generation of iPSC-derived SNs are scarce. In fact, it is possible to identify only four different strategies for the differentiation of iPSC into SNs (Oh et al., 2016; Zeltner et al., 2016; Kirino et al., 2018; Frith and Tsakiridis, 2019). For this research project, the protocol adopted for the derivation of sympathetic neurons is the one proposed by Oh and coworkers (Oh et al., 2016). Particular attention was posed on the initial cell density of iPSCs, which has been demonstrated to deeply influence sympathetic determination (Takayama et al., 2020). The protocol of Oh et al. was however slightly modified for the production of iPSC-derived SNs (Oh et al., 2016). In fact, differently from the original protocol, different media and coating were used. In addition, the sorting procedure was eliminated. This choice was made to make the procedure for the derivation of neurons easier and less time consuming, led to the obtainment of a mixed neuronal population, although reasonably enriched of sympathetic like neurons. In this work, iPSC-derived SNs were successfully maintained in culture for over 3 months. After the production of iPSC-derived SNs, a systematic characterization of the newly obtained cells was performed at different time points. So far, there is a lack of a single marker that identifies uniquely sympathetic neurons (Kirino et al., 2018). However, different markers have been used in combination for the characterization of iPSC-derived SNs (Oh et al., 2016; Kirino et al., 2018; Winbo et al., 2020). One early marker is PHOX2B an essential transcription factor, known to be involved in the development of sympathetic neurons (Pattyn et al., 1999). In fact, previous studies have reported that knockout mice for *Phox2b* and *Mash1* (another important transcription factor involved in autonomic neurons development) presented an impaired ANS (Pattyn et al., 1999; Pattyn et al., 2006). This result goes along with the high degree of conservation of the aminoacidic sequence of *Phox2b* detected among different species (mouse, chimpanzee and rat) (Nagashimada et al., 2012). Moreover, PHOX2B has been observed to be expressed not only at early stages of the differentiation, but also along the entire process until the mature stages (Hsieh et al., 2007; Kirino et al., 2018). Our results confirmed this statement, showing an increased expression of PHOX2B, both at the

transcript and protein level, starting from day 4 of the differentiation, with a decrease around the late stage of differentiation (day 30). The extremely important role of PHOX2B in the autonomic neuronal development is also highlighted by the fact that it regulates the expression of two important enzymes which take part in the pathway of the catecholamines: TH and DBH (Fedele and Brand, 2020). In particular, TH is the enzyme that converts tyrosine into L-DOPA, which is the precursor for dopamine, and DBH is the enzyme that catalyzes the production of norepinephrine, the principal neurotransmitter of the sympathetic neurons and it is well known that it is under the strict control of PHOX2B (Brunet and Pattyn, 2002). DBH has to be considered, together with TH, as a mature marker of the SNs, expressed in the late stage of the differentiation (Saito-Diaz et al., 2019). These two markers seem to be regulated by a synexpression of related genes, (namely the coordinate expression of different genes among processes (Niehrs and Pollet, 1999)) even though TH is a precursor of DBH in the pathway of the catecholamines (Ernsberger et al., 2017). PHOX2B, TH and DBH are used in combination and they represent the most used markers to identify sympathetic neurons. The investigation of the following markers is supported by the RNA-seq analysis conducted by Takayama and coworkers (Takayama et al., 2020), which has identified *PHOX2B* as one of the ANS related gene (together with *ASCL1* and *PHOX2A*) and *TH* as a SN-related gene (together with *GATA2*, *GATA3* and *DDC*). *DBH* was not listed in the top four SN-related genes probably because it is expressed in a later stage of the differentiation. In the same report, a higher expression level of TH in comparison to DBH was observed both in gene and protein analysis. This trend is confirmed by the levels observed by Oh et al. as well (Oh et al., 2016). On the contrary, the flow cytometry results obtained in this thesis revealed a lower percentage of TH-positive cells compared to DBH-positive cells at 12 and at 30 days of differentiation. Nevertheless, the obtained population of TH-positive cells at day 30 of differentiation (11-41%) is almost analog to the one observed in the work of Saito-Diaz and co-workers (TH-positive cells 20-30%) (Saito-Diaz et al., 2019), where the positive cells for DBH were not examined. Immunostaining analysis of TH-positive cells obtained by Takayama et al. was in line with the aforementioned flow cytometry values of TH positive cells, reporting a slight increase up to the 48% of TH-positive cells (Takayama et al., 2020). Of note, the messenger RNA of TH has been reported to be detected earlier in transcripts in comparison to the protein level (Ernsberger et al., 1995; Groves et al., 1995; Tiveron et al., 1996). The discrepancy between the absolute number of TH and DBH positive neurons observed in the present work compared to the previous ones (Oh et al., 2016; Saito-Diaz et al., 2019) could be ascribed to the fact that here the sorting step for PHOX2B positive cells was omitted, thus leading to the production of a mixed neuronal population. (Takayama et al., 2020)

Importantly, few are so far the reports describing the electrophysiological properties of iPSC-derived SNs, which I started analyzing Using a MEA platform.

A key step to be performed before starting with MEA acquisition, is the set-up a of proper protocol for the culture of iPSC-derived SNs on the MEA-plates ensuring the maintenance of a monolayer of cells. This step is important because it has been abundantly demonstrated that the MEA system is extremely sensitive to different variables in the technique, such as the density of cells, monolayer formation and cell detachment, which lead to different results, even using the same

cells (Biffi et al., 2013). Possible variation in all these parameters can lead to different outcomes (Biffi et al., 2013).

Of note, in the present work the obtained iPSC-derived SNs exhibited a low baseline spontaneous activity, which is in line with the observations made by the research group of Takayama (Takayama and Kida, 2016), reporting that iPSC-derived peripheral neurons have shown a sporadic spontaneous electrical activity. More in detail, after the initial increase in the electrical activity of iPSC-derived SNs at day 50, a drastic decrease in the activity, which remained constant over the different months in culture, was observed. The reduction of the activity can be linked to a decrease in the connections between the neurons, attributable to the phenomenon of the pruning, that is the removal of the weak connections with the maintenance of only the stronger ones. Further confirmation about this theory is required.

As previously mentioned, the co-culture studies that have been conducted until now, in most of the cases have employed at least one cell population derived from primary cells (Takeuchi et al., 2011b; Larsen et al., 2016; Oh et al., 2016; Prando et al., 2018; Burton et al., 2019) and only three studies have been conducted with both population derived from iPSCs (Oh et al., 2016; Takayama et al., 2020; Winbo et al., 2020). This implicates the fact that each generated population need to be characterized to confirm the fate before further use. However, after an exhaustive characterization, the cells can be used for further experiments, such as co-culture models. In this work, the *de novo* development of a neurocardiac model was elaborated starting from the basic conditions including cell density and coating procedure. On purpose, it was decided to use inserts with two different culture chambers to maintain the two populations in separated area, allowing further specific investigations or applications on the single cell type. For the choice of the cell density an initial ability in the formation of connections between iPSC-derived SNs and iPSC-derived CMs was evaluated. In our cell model system, a dense monolayer for both populations was able to ensure a stable interconnection and formation of axons prolongations, as previously demonstrated by (Biffi et al., 2013). If the population of iPSC-derived CMs maintained a stable monolayer for the whole culture period and no detachment was observed, as hypothesized by Takayama's group (Takayama et al., 2020), the obtained iPSC-derived SNs would spontaneously organize themselves in interconnected groups of cells, made up of somas and easy ascribable to ganglion-like structures. However, in the present work the formation of ganglion-like structures was not deeply investigated. An additional aspect, that has revealed to be crucial in the formation of an interconnected co-culture is the coating procedure. Here, I noticed that the absence of the coating in the space between the two populations impaired the connection formation between iPSC-derived SNs and iPSC-derived CMs. The introduction of a Matrigel coating in the gap between iPSC-derived SNs and iPSC-derived CMs promoted the formation of a quicker and stable connection, with the axons penetrating the monolayer of iPSC-derived CMs. Notably, it was possible to observe the formation of a thick and intricate network of innervations created by a high number of axons, which migrated from iPSC-derived SNs to iPSC-derived CMs and the more the axon bundles penetrated in the cardiac population, the thinner they became. The infiltration of the axons in cardiomyocytes was demonstrated by the identification of TH positive neurites in

the cardiac population. As other researcher groups confirmed, the neurons formed pearl-like structures identified as the varicosities sites and designated to neurotransmitters release (Prando et al., 2018; Takayama et al., 2020; Winbo et al., 2020). The varicosities are especially observed in the distal part of neurons, far away from the initial plating area, and in particular in the connection sites with cardiomyocytes (Takayama et al., 2020). These findings give an important information regarding the iPSC-derived SNs because they represent a sign of increased maturity and active functional properties (Oh et al., 2016; Prando et al., 2018; Winbo et al., 2020). However, the infiltration of TH positive axons is not sufficient to demonstrate the connection with cardiomyocytes. Investigations with Synapsin I in the co-culture of this work highlighted a considerable degree of synaptogenesis, mainly localized in the sites of cell contact between iPSC-derived SNs to iPSC-derived CMs. As previously reported, this finding demonstrates that in the site were iPSC-derived SNs enter in contact with iPSC-derived CMs, there is the formation of presynaptic vesicles (Shcherbakova et al., 2007). However, further experiments are necessary to characterize the post-synaptic sites.

All these parameters described above are essential prerequisites for the functional investigation of the co-cultures (Oh et al., 2016)

Many studies have demonstrated the modulatory effect of iPSC-derived SNs on the behavior of iPSC-derived CMs from a functional point of view (Takeuchi et al., 2011a; Oh et al., 2016; Takayama et al., 2020; Winbo et al., 2020). Preliminary functional experiments in this work demonstrate that the presence of iPSC-derived SNs is able to modulate the beating activity of iPSC-derived CMs, triggering a higher beating rate during a co-culture period of two weeks. Previous reports (Takeuchi et al., 2011b; Oh et al., 2016; Takayama et al., 2020; Winbo et al., 2020) have demonstrated that the interaction of iPSC-derived SNs with iPSC-derived CMs can lead to a higher maturity of neurons and cardiomyocytes from a functional point of view (Takeuchi et al., 2011a; Oh et al., 2016; Winbo et al., 2020) Of note, it has been observed that the only presence of iPSC-derived SNs in the co-culture without any connection was not sufficient to stimulate the CMs activity, thus confirming the need for a direct contact between the two cell populations (Oh et al., 2016). Some studies (Burton et al., 2015; Oh et al., 2016; Moreno et al., 2019; Takayama et al., 2020) have conducted stimulation experiments in co-cultures using the method of the optogenetic stimulation. However, with the MEA system it is possible to use unmodified cells and to stimulate them with application of different drugs or electric stimuli and record the measurements. On the contrary, for optical stimulation the cell line engineering is required for the insertion of the optogenetic tool. This engineering step can be hard and hamper the entire experimental design.

7.1 Limitation of the study

The present thesis work shows the results of a newly developed project, based on the set up of new protocols not in use in our laboratory. As consequence, the optimization of the different methods required some time and the number of some experiments still need to be increased to make the results more reliable. Some problems were encountered in the DBH detection and quantification. Standing to literature, a high level of DBH was expected, considering it as the principal enzyme of SNs, catalyzing the synthesis of norepinephrine, but as mentioned before,

both in our hands and in a previous report (Oh et al., 2016) *DBH* had a low expression. Of note, in the RNA-seq analysis performed by Takayama's group (Takayama et al., 2020), *DBH* was not even ranked in the top four SNs-related genes. The low level in *DBH* can be linked to the hypothesis that the produced iPSC-derived SNs at day 30 (latest timepoint analyzed in real time) display an immature phenotype. A further analysis of *DBH*, around day 60 or even further, should be performed to solve the doubts. However, other markers should be analyzed for a deeper characterization of iPSC-derived SNs. This further investigation should address SOX10, a transcription factor involved in the development of the peripheral nervous system. It has been previously reported that the expression of SOX10 in SNs is regulated by PHOX2B and the period of time of the segregation of them is detectable at early stages compared to enteric ganglionic progenitors (Nagashimada et al., 2012). This information could confirm the acquisition of the sympathetic lineage already at day 14 (Kirino et al., 2018). Moreover, much more specific experiments can be conducted in relation to the presence of DBH. As some studies reported, an enzyme-linked immunosorbent *assay* can be used to detect the presence of norepinephrine and acetylcholine (Oh et al., 2016; Kirino et al., 2018). However, this method should be validated for the present iPSC-derived SNs line because it has been shown that in some cases the level of the neurotransmitter is too low to be detected (Takayama et al., 2020). It is believed that the immature phenotype of iPSC-derived SNs and the reduced activity of the cells are the cause of the reduced level in the detection of neurotransmitters. As confirmed by Oh's group, the release of neurotransmitters, as well their detection, can be higher in co-cultures, where it is present a target (CMs) for the neurons (SNs) (Oh et al., 2016). Another method for the validation of SNs is to investigate the level of inotropic nicotinic acetylcholine receptors (nAChR) in the post-ganglionic SNs (Winbo et al., 2020). The last indirect confirmation of the obtainment of a population of SNs is the analysis of the produced neurons with markers specific of other neuronal subtypes, in particular of chromaffin cells, because they share the common progenitors as SNs (Takayama et al., 2020).

Another limitation of this study regards the investigation of the interconnection sites of neurons and cardiomyocytes in the neurocardiac model. Here it was reported only the presence of synapsin I positive presynaptic sites, but not the functionalities of them. A method for the detection of active site of endocytosis is shown by Shcherbakova and coworkers, using the internalization of the luminal domain of synaptotagmin (Kraszewski et al., 1995; Shcherbakova et al., 2007). A further amelioration of the characterization of the sites of connection between iPSC-derived SNs and iPSC-derived CMs can be achieved with the investigation and identification of β-adrenoreceptors, which represent the major type of cardiac receptors able to internalize the catecholamine neurotransmitters. They can be investigated either via immunofluorescence or functionally, using different drugs to stimulate (Isoproterenol) or block (Propranolol) the receptors. Furthermore, the stimulation of the neurons in the co-culture with nicotine provides an additional functional demonstration of the adrenergic lineage of the cells. As reported in other works, the nicotine stimulation of neurons causes the release of a high level of norepinephrine, which has an excitatory effect on the cardiomyocytes, increasing their beats (Oh et al., 2016; Takayama et al., 2020; Winbo et al., 2020). Functional experiments of nicotine stimulation of the

neural population could be performed to observe the effect that neurons have on the cardiac cells and in particular in the beat rate of the latter.

In general, an exhaustive and a deeper validation of the co-culture model presented here is required, in particular a more detailed characterization of the neurocardiac model and more insights regarding the behavior and the maturity state of both cell populations is required. The characterization of the dual and reciprocal effect of one population on the other can provide the optimal understanding of the specialized interconnection between ANS and heart.

8 CONCLUSIONS AND FUTURE PERSPECTIVES

The co-culture model developed in the present work is a xeno-free tool with high translational potential that can be applied on several fronts. Particular attention can be posed in its application as a model for the investigation of the pathologies' mechanisms that underly dysfunctions or alterations of CANS. As iPSCs have the capacity to maintain the genotype of the donor's organism and conserve the mutations, the derivation of iPSCs from a diseased donor can recapitulate the diseased phenotype, resulting as an ideal model for the *in vitro* recapitulation of the disease (Liang et al., 2013a; Kussauer et al., 2019). *In vitro* neurocardiac models crossing iPSC-derived SNs with iPSC-derived CMs derived from different donors with different diseases can be used to understand if some pathologies can be rescued. This has been observed in rat co-cultures made of healthy donors for SNs and diseased CMs, where the SNs have been capable to rescue the cardiac diseased phenotype. However, the contrary (healthy CMs with diseased SNs) did not lead to the same results (Larsen et al., 2016). Furthermore, the neurocardiac co-culture can be used for drugs discovery and toxicity test. The discovery of new drugs, including substances related to CANS diseases, can be tested in these co-cultures leading to observation of tailored effects on the pathology itself. Moreover, applying the drugs on the cells derived from specific patients not commonly responding to defined therapies, an *ad hoc* treatment can be developed. This application, known as "personalized medicine," is of particular importance in order to reduce the number of undesired effects and the number of non-responder patients (Doss and Sachinidis, 2019). Many studies have reported the utility of iPSC-derived CMs for the screening of new drugs (Clements and Thomas, 2014; Clements, 2016; Hayes et al., 2019; Kussauer et al., 2019). In particular, with the MEA system, it has been possible to screen a high number of compounds evaluating the hERG channel inhibition, QT prolongation, voltage gated Na^+ and Ca^+ channel and many other ion channels, seem to be all involved in side effects of drugs and their consequent evaluation of toxicity and proarrhythmic effect (Kussauer et al., 2019). A higher degree of structural complexity and a better modeling capability of the human heart could be addressed using a multicellular system, which includes other cell types found in the heart like fibroblasts and parasympathetic neurons.

In conclusion, the development of the above-mentioned co-culture model brings important benefits in the world of the *in vitro* models. Firstly, this neurocardiac model can be used to study the physiological properties of the CANS providing a tool for the understanding of all the mechanisms behind it. Furthermore, the neurocardiac model provides more possibilities to study specific cardiac and neuronal disease where the CANS is involved in. Indeed, deriving iPSCs from patients with specific diseases, offers the chance to recreate a model on which the desired disease can be deeply investigated also from an autonomic point of view, leading to a more complete view on the mechanism behind the disease.

9 BIBLIOGRAPHY

Aasen, T., Raya, A., Barrero, M.J., Garreta, E., Consiglio, A., Gonzalez, F., et al. (2008). Efficient and rapid generation of induced pluripotent stem cells from human keratinocytes. *Nat Biotechnol* 26(11)**,** 1276-1284. doi: 10.1038/nbt.1503.

Abu-Bonsrah, K.D., Zhang, D., Bjorksten, A.R., Dottori, M., and Newgreen, D.F. (2018). Generation of Adrenal Chromaffin-like Cells from Human Pluripotent Stem Cells. *Stem Cell Reports* 10(1)**,** 134-150. doi: 10.1016/j.stemcr.2017.11.003.

Amar, D., Zhang, H., Miodownik, S., and Kadish, A.H. (2003). Competing autonomic mechanisms precede the onset of postoperative atrial fibrillation. *J Am Coll Cardiol* 42(7)**,** 1262-1268. doi: 10.1016/s0735-1097(03)00955-0.

An, M.C., Zhang, N., Scott, G., Montoro, D., Wittkop, T., Mooney, S., et al. (2012). Genetic correction of Huntington's disease phenotypes in induced pluripotent stem cells. *Cell Stem Cell* 11(2)**,** 253-263. doi: 10.1016/j.stem.2012.04.026.

Antz, M., Cappato, R., and Kuck, K.H. (1995). Metoprolol versus sotalol in the treatment of sustained ventricular tachycardia. *J Cardiovasc Pharmacol* 26(4)**,** 627-635. doi: 10.1097/00005344-199510000-00019.

Anversa, P., Capasso, J.M., Ricci, R., Sonnenblick, E.H., and Olivetti, G. (1989). Morphometric analysis of coronary capillaries during physiologic myocardial growth and induced cardiac hypertrophy: a review. *Int J Microcirc Clin Exp* 8(4)**,** 353-363.

Araki, R., Uda, M., Hoki, Y., Sunayama, M., Nakamura, M., Ando, S., et al. (2013). Negligible immunogenicity of terminally differentiated cells derived from induced pluripotent or embryonic stem cells. *Nature* 494(7435)**,** 100-104. doi: 10.1038/nature11807.

Ardell, J.L., and Armour, J.A. (2016). Neurocardiology: Structure-Based Function. *Compr Physiol* 6(4)**,** 1635-1653. doi: 10.1002/cphy.c150046.

Armour, J.A. (2008). Potential clinical relevance of the 'little brain' on the mammalian heart. *Exp Physiol* 93(2)**,** 165-176. doi: 10.1113/expphysiol.2007.041178.

Armour, J.A. (2010). Functional anatomy of intrathoracic neurons innervating the atria and ventricles. *Heart Rhythm* 7(7)**,** 994-996. doi: 10.1016/j.hrthm.2010.02.014.

Armour, J.A., Murphy, D.A., Yuan, B.X., Macdonald, S., and Hopkins, D.A. (1997). Gross and microscopic anatomy of the human intrinsic cardiac nervous system. *Anat Rec* 247(2)**,** 289-298. doi: 10.1002/(sici)1097-0185(199702)247:2<289::Aid-ar15>3.0.Co;2-l.

Asirvatham, S.J., and Kapa, S. (2009). Sleep apnea and atrial fibrillation: the autonomic link. *J Am Coll Cardiol* 54(22)**,** 2084-2086. doi: 10.1016/j.jacc.2009.09.017.

Assmus, B., Honold, J., Schächinger, V., Britten, M.B., Fischer-Rasokat, U., Lehmann, R., et al. (2006). Transcoronary Transplantation of Progenitor Cells after Myocardial Infarction. *New England Journal of Medicine* 355(12)**,** 1222-1232. doi: 10.1056/NEJMoa051779.

Awad, M., Czer, L.S., Hou, M., Golshani, S.S., Goltche, M., De Robertis, M., et al. (2016). Early Denervation and Later Reinnervation of the Heart Following Cardiac Transplantation: A Review. *J Am Heart Assoc* 5(11). doi: 10.1161/jaha.116.004070.

Balls, M., and Straughan, D.W. (1996). The three Rs of Russell & Burch and the testing of biological products. *Dev Biol Stand* 86**,** 11-18.

Barber, M.J., Mueller, T.M., Henry, D.P., Felten, S.Y., and Zipes, D.P. (1983). Transmural myocardial infarction in the dog produces sympathectomy in noninfarcted myocardium. *Circulation* 67(4)**,** 787-796. doi: doi:10.1161/01.CIR.67.4.787.

Barbuti, A., Benzoni, P., Campostrini, G., and Dell'Era, P. (2016). Human derived cardiomyocytes: A decade of knowledge after the discovery of induced pluripotent stem cells. *Dev Dyn* 245(12)**,** 1145-1158. doi: 10.1002/dvdy.24455.

Bauwens, C.L., Peerani, R., Niebruegge, S., Woodhouse, K.A., Kumacheva, E., Husain, M., et al. (2008). Control of human embryonic stem cell colony and aggregate size heterogeneity influences differentiation trajectories. *Stem Cells* 26(9)**,** 2300-2310. doi: 10.1634/stemcells.2008-0183.

Bayliss, W.M., and Starling, E.H. (1892). On some Points in the Innervation of the Mammalian Heart. *J Physiol* 13(5)**,** 407-418.403. doi: 10.1113/jphysiol.1892.sp000416.

Beeres, S.L., Atsma, D.E., van der Laarse, A., Pijnappels, D.A., van Tuyn, J., Fibbe, W.E., et al. (2005). Human adult bone marrow mesenchymal stem cells repair experimental conduction block in rat cardiomyocyte cultures. *J Am Coll Cardiol* 46(10)**,** 1943-1952. doi: 10.1016/j.jacc.2005.07.055.

Beltrao-Braga, P.C., Pignatari, G.C., Maiorka, P.C., Oliveira, N.A., Lizier, N.F., Wenceslau, C.V., et al. (2011). Feeder-free derivation of induced pluripotent stem cells from human immature dental pulp stem cells. *Cell Transplant* 20(11-12)**,** 1707-1719. doi: 10.3727/096368911X566235.

Benzoni, P., Campostrini, G., Landi, S., Bertini, V., Marchina, E., Iascone, M., et al. (2020). Human iPSC modelling of a familial form of atrial fibrillation reveals a gain of function of If and ICaL in patient-derived cardiomyocytes. *Cardiovasc Res* 116(6)**,** 1147-1160. doi: 10.1093/cvr/cvz217.

Bergmann, O., Zdunek, S., Felker, A., Salehpour, M., Alkass, K., Bernard, S., et al. (2015). Dynamics of Cell Generation and Turnover in the Human Heart. *Cell* 161(7)**,** 1566-1575. doi: 10.1016/j.cell.2015.05.026.

Bers, D.M. (2002). Cardiac excitation-contraction coupling. *Nature* 415(6868)**,** 198-205. doi: 10.1038/415198a.

Bers, D.M. (2008). Calcium cycling and signaling in cardiac myocytes. *Annu Rev Physiol* 70**,** 23-49. doi: 10.1146/annurev.physiol.70.113006.100455.

Besser, R.R., Ishahak, M., Mayo, V., Carbonero, D., Claure, I., and Agarwal, A. (2018). Engineered Microenvironments for Maturation of Stem Cell Derived Cardiac Myocytes. *Theranostics* 8(1)**,** 124-140. doi: 10.7150/thno.19441.

Bettoni, M., and Zimmermann, M. (2002). Autonomic tone variations before the onset of paroxysmal atrial fibrillation. *Circulation* 105(23)**,** 2753-2759. doi: 10.1161/01.cir.0000018443.44005.d8.

Bhavsar, P.K., Dhoot, G.K., Cumming, D.V., Butler-Browne, G.S., Yacoub, M.H., and Barton, P.J. (1991). Developmental expression of troponin I isoforms in fetal human heart. *FEBS Lett* 292(1-2)**,** 5-8. doi: 10.1016/0014-5793(91)80820-s.

Biendarra-Tiegs, S.M., Secreto, F.J., and Nelson, T.J. (2020). Addressing Variability and Heterogeneity of Induced Pluripotent Stem Cell-Derived Cardiomyocytes. *Adv Exp Med Biol* 1212**,** 1-29. doi: 10.1007/5584_2019_350.

Biffi, E., Regalia, G., Menegon, A., Ferrigno, G., and Pedrocchi, A. (2013). The influence of neuronal density and maturation on network activity of hippocampal cell cultures: a methodological study. *PLoS One* 8(12)**,** e83899. doi: 10.1371/journal.pone.0083899.

Bilican, B., Serio, A., Barmada, S.J., Nishimura, A.L., Sullivan, G.J., Carrasco, M., et al. (2012). Mutant induced pluripotent stem cell lines recapitulate aspects of TDP-43 proteinopathies and reveal cell-specific vulnerability. *Proc Natl Acad Sci U S A* 109(15)**,** 5803-5808. doi: 10.1073/pnas.1202922109.

Binah, O., Dolnikov, K., Sadan, O., Shilkrut, M., Zeevi-Levin, N., Amit, M., et al. (2007). Functional and developmental properties of human embryonic stem cells-derived cardiomyocytes. *J Electrocardiol* 40(6 Suppl)**,** S192-196. doi: 10.1016/j.jelectrocard.2007.05.035.

Bird, S.D., Doevendans, P.A., van Rooijen, M.A., Brutel de la Riviere, A., Hassink, R.J., Passier, R., et al. (2003). The human adult cardiomyocyte phenotype. *Cardiovasc Res* 58(2)**,** 423-434. doi: 10.1016/s0008-6363(03)00253-0.

Boengler, K., and Schulz, R. (2017). Connexin 43 and Mitochondria in Cardiovascular Health and Disease. *Adv Exp Med Biol* 982**,** 227-246. doi: 10.1007/978-3-319-55330-6_12.

Brennand, K.J., Simone, A., Jou, J., Gelboin-Burkhart, C., Tran, N., Sangar, S., et al. (2011). Modelling schizophrenia using human induced pluripotent stem cells. *Nature* 473(7346)**,** 221-225. doi: 10.1038/nature09915.

Brugada, P., and Brugada, J. (1992). Right bundle branch block, persistent ST segment elevation and sudden cardiac death: a distinct clinical and electrocardiographic syndrome. A multicenter report. *J Am Coll Cardiol* 20(6)**,** 1391-1396. doi: 10.1016/0735-1097(92)90253-j.

Brunet, J.F., and Pattyn, A. (2002). Phox2 genes - from patterning to connectivity. *Curr Opin Genet Dev* 12(4)**,** 435-440. doi: 10.1016/s0959-437x(02)00322-2.

Burney, M.J., Johnston, C., Wong, K.-Y., Teng, S.-W., Beglopoulos, V., Stanton, L.W., et al. (2013). An epigenetic signature of developmental potential in neural stem cells and early neurons. *STEM CELLS* 31(9)**,** 1868-1880. doi: https://doi.org/10.1002/stem.1431.

Burnstock, G. (2008). Non-synaptic transmission at autonomic neuroeffector junctions. *Neurochem Int* 52(1-2)**,** 14-25. doi: 10.1016/j.neuint.2007.03.007.

Burnstock, G. (2009). Autonomic neurotransmission: 60 years since sir Henry Dale. *Annu Rev Pharmacol Toxicol* 49**,** 1-30. doi: 10.1146/annurev.pharmtox.052808.102215.

Burridge, P.W., Anderson, D., Priddle, H., Barbadillo Munoz, M.D., Chamberlain, S., Allegrucci, C., et al. (2007). Improved human embryonic stem cell embryoid body homogeneity and cardiomyocyte differentiation from a novel V-96 plate aggregation system highlights interline variability. *Stem Cells* 25(4)**,** 929-938. doi: 10.1634/stemcells.2006-0598.

Burridge, P.W., Keller, G., Gold, J.D., and Wu, J.C. (2012). Production of de novo cardiomyocytes: human pluripotent stem cell differentiation and direct reprogramming. *Cell Stem Cell* 10(1)**,** 16-28. doi: 10.1016/j.stem.2011.12.013.

Burridge, P.W., Matsa, E., Shukla, P., Lin, Z.C., Churko, J.M., Ebert, A.D., et al. (2014). Chemically defined generation of human cardiomyocytes. *Nat Methods* 11(8)**,** 855-860. doi: 10.1038/nmeth.2999.

Burton, R.A., Klimas, A., Ambrosi, C.M., Tomek, J., Corbett, A., Entcheva, E., et al. (2015). Optical control of excitation waves in cardiac tissue. *Nat Photonics* 9(12)**,** 813-816. doi: 10.1038/nphoton.2015.196.

Burton, R.A.B., Tomek, J., Ambrosi, C.M., Larsen, H.E., Sharkey, A.R., Capel, R.A., et al. (2019). Optical interrogation of sympathetic neuronal effects on macroscopic cardiac monolayer dynamics. *bioRxiv***,** 717991. doi: 10.1101/717991.

Bywater, R.A., Campbell, G., Edwards, F.R., Hirst, G.D., and O'Shea, J.E. (1989). The effects of vagal stimulation and applied acetylcholine on the sinus venosus of the toad. *J Physiol* 415**,** 35-56. doi: 10.1113/jphysiol.1989.sp017710.

Callaghan, N.I., Hadipour-Lakmehsari, S., Lee, S.H., Gramolini, A.O., and Simmons, C.A. (2019). Modeling cardiac complexity: Advancements in myocardial models and analytical techniques for physiological investigation and therapeutic development in vitro. *APL Bioeng* 3(1)**,** 011501. doi: 10.1063/1.5055873.

Camnasio, S., Delli Carri, A., Lombardo, A., Grad, I., Mariotti, C., Castucci, A., et al. (2012). The first reported generation of several induced pluripotent stem cell lines from homozygous and heterozygous Huntington's disease patients demonstrates mutation related enhanced lysosomal activity. *Neurobiol Dis* 46(1)**,** 41-51. doi: 10.1016/j.nbd.2011.12.042.

Campbell, G.D., Edwards, F.R., Hirst, G.D., and O'Shea, J.E. (1989). Effects of vagal stimulation and applied acetylcholine on pacemaker potentials in the guinea-pig heart. *J Physiol* 415**,** 57-68. doi: 10.1113/jphysiol.1989.sp017711.

Cao, J.M., Chen, L.S., KenKnight, B.H., Ohara, T., Lee, M.H., Tsai, J., et al. (2000). Nerve sprouting and sudden cardiac death. *Circ Res* 86(7)**,** 816-821. doi: 10.1161/01.res.86.7.816.

Carr-Wilkinson, J., Prathalingam, N., Pal, D., Moad, M., Lee, N., Sundaresh, A., et al. (2018). Differentiation of Human Embryonic Stem Cells to Sympathetic Neurons: A Potential Model for Understanding Neuroblastoma Pathogenesis. *Stem Cells Int* 2018**,** 4391641. doi: 10.1155/2018/4391641.

Casella, C., and Taglietti, V. (1993). *Principi di fisiologia.* La Goliardica Pavese.

Casini, S., Verkerk, A.O., and Remme, C.A. (2017). Human iPSC-Derived Cardiomyocytes for Investigation of Disease Mechanisms and Therapeutic Strategies in Inherited Arrhythmia Syndromes: Strengths and Limitations. *Cardiovasc Drugs Ther* 31(3)**,** 325-344. doi: 10.1007/s10557-017-6735-0.

Caspi, O., Huber, I., Gepstein, A., Arbel, G., Maizels, L., Boulos, M., et al. (2013). Modeling of Arrhythmogenic Right Ventricular Cardiomyopathy With Human Induced Pluripotent Stem Cells. *Circulation: Cardiovascular Genetics* 6(6)**,** 557-568. doi: 10.1161/CIRCGENETICS.113.000188.

Chambers, S.M., Fasano, C.A., Papapetrou, E.P., Tomishima, M., Sadelain, M., and Studer, L. (2009). Highly efficient neural conversion of human ES and iPS cells by dual inhibition of SMAD signaling. *Nat Biotechnol* 27(3)**,** 275-280. doi: 10.1038/nbt.1529.

Chan, K.Y., and Haschke, R.H. (1982). Isolation and culture of corneal cells and their interactions with dissociated trigeminal neurons. *Exp Eye Res* 35(2)**,** 137-156. doi: 10.1016/s0014-4835(82)80062-6.

Chang, C.-Y., Ting, H.-C., Liu, C.-A., Su, H.-L., Chiou, T.-W., Lin, S.-Z., et al. (2020). Induced Pluripotent Stem Cell (iPSC)-Based Neurodegenerative Disease Models for Phenotype Recapitulation and Drug Screening. *Molecules (Basel, Switzerland)* 25(8)**,** 2000. doi: 10.3390/molecules25082000.

Chen, A.K., Chen, X., Choo, A.B., Reuveny, S., and Oh, S.K. (2011). Critical microcarrier properties affecting the expansion of undifferentiated human embryonic stem cells. *Stem Cell Res* 7(2)**,** 97-111. doi: 10.1016/j.scr.2011.04.007.

Chen, H.S., Kim, C., and Mercola, M. (2009). Electrophysiological challenges of cell-based myocardial repair. *Circulation* 120(24)**,** 2496-2508. doi: 10.1161/CIRCULATIONAHA.107.751412.

Chen, P.-S., and Tan, A.Y. (2007). Autonomic nerve activity and atrial fibrillation. *Heart rhythm* 4(3 Suppl)**,** S61-S64. doi: 10.1016/j.hrthm.2006.12.006.

Chen, P.S., Chen, L.S., Cao, J.M., Sharifi, B., Karagueuzian, H.S., and Fishbein, M.C. (2001). Sympathetic nerve sprouting, electrical remodeling and the mechanisms of sudden cardiac death. *Cardiovasc Res* 50(2)**,** 409-416. doi: 10.1016/s0008-6363(00)00308-4.

Chiang, C.H., Su, Y., Wen, Z., Yoritomo, N., Ross, C.A., Margolis, R.L., et al. (2011). Integration-free induced pluripotent stem cells derived from schizophrenia patients with a DISC1 mutation. *Mol Psychiatry* 16(4)**,** 358-360. doi: 10.1038/mp.2011.13.

Chiou, C.W., Eble, J.N., and Zipes, D.P. (1997). Efferent vagal innervation of the canine atria and sinus and atrioventricular nodes. The third fat pad. *Circulation* 95(11)**,** 2573-2584. doi: 10.1161/01.cir.95.11.2573.

Choate, J.K., Klemm, M., and Hirst, G.D. (1993). Sympathetic and parasympathetic neuromuscular junctions in the guinea-pig sino-atrial node. *J Auton Nerv Syst* 44(1)**,** 1-15. doi: 10.1016/0165-1838(93)90374-4.

Choi, E.K., Shen, M.J., Han, S., Kim, D., Hwang, S., Sayfo, S., et al. (2010). Intrinsic cardiac nerve activity and paroxysmal atrial tachyarrhythmia in ambulatory dogs. *Circulation* 121(24)**,** 2615-2623. doi: 10.1161/circulationaha.109.919829.

Chow, L.T., Chow, S.S., Anderson, R.H., and Gosling, J.A. (1993). Innervation of the human cardiac conduction system at birth. *Br Heart J* 69(5)**,** 430-435. doi: 10.1136/hrt.69.5.430.

Ciani, L., and Salinas, P.C. (2005). WNTs in the vertebrate nervous system: from patterning to neuronal connectivity. *Nat Rev Neurosci* 6(5)**,** 351-362. doi: 10.1038/nrn1665.

Clements, M. (2016). Multielectrode Array (MEA) Assay for Profiling Electrophysiological Drug Effects in Human Stem Cell-Derived Cardiomyocytes. *Current Protocols in Toxicology* 68(1)**,** 22.24.21-22.24.32. doi: https://doi.org/10.1002/cptx.2.

Clements, M., and Thomas, N. (2014). High-throughput multi-parameter profiling of electrophysiological drug effects in human embryonic stem cell derived cardiomyocytes using multi-electrode arrays. *Toxicol Sci* 140(2)**,** 445-461. doi: 10.1093/toxsci/kfu084.

Conlon, K., Collins, T., and Kidd, C. (1996). Modulation of vagal actions on heart rate produced by inhibition of nitric oxide synthase in the anaesthetized ferret. *Exp Physiol* 81(3)**,** 547-550. doi: 10.1113/expphysiol.1996.sp003957.

Corti, S., Faravelli, I., Cardano, M., and Conti, L. (2015). Human pluripotent stem cells as tools for neurodegenerative and neurodevelopmental disease modeling and drug discovery. *Expert Opin Drug Discov* 10(6)**,** 615-629. doi: 10.1517/17460441.2015.1037737.

Coskun, V., and Lombardo, D.M. (2016). Studying the pathophysiologic connection between cardiovascular and nervous systems using stem cells. *Journal of Neuroscience Research* 94(12)**,** 1499-1510. doi: https://doi.org/10.1002/jnr.23924.

Coumel, P., Attuel, P., Lavallée, J., Flammang, D., Leclercq, J.F., and Slama, R. (1978). [The atrial arrhythmia syndrome of vagal origin]. *Arch Mal Coeur Vaiss* 71(6)**,** 645-656.

Crick, S.J., Wharton, J., Sheppard, M.N., Royston, D., Yacoub, M.H., Anderson, R.H., et al. (1994). Innervation of the human cardiac conduction system. A quantitative immunohistochemical and histochemical study. *Circulation* 89(4)**,** 1697-1708. doi: 10.1161/01.cir.89.4.1697.

Csöbönyeiová, M., Polák, Š., and Danišovič, L.u. (2016). Toxicity testing and drug screening using iPSC-derived hepatocytes, cardiomyocytes, and neural cells. *Canadian Journal of Physiology and Pharmacology* 94(7)**,** 687-694. doi: 10.1139/cjpp-2015-0459.

D'Amico, M.A., Ghinassi, B., Izzicupo, P., Di Ruscio, A., and Di Baldassarre, A. (2016). IL-6 Activates PI3K and PKCzeta Signaling and Determines Cardiac Differentiation in Rat Embryonic H9c2 Cells. *J Cell Physiol* 231(3)**,** 576-586. doi: 10.1002/jcp.25101.

Del Alamo, J.C., Lemons, D., Serrano, R., Savchenko, A., Cerignoli, F., Bodmer, R., et al. (2016). High throughput physiological screening of iPSC-derived cardiomyocytes for drug development. *Biochim Biophys Acta* 1863(7 Pt B)**,** 1717-1727. doi: 10.1016/j.bbamcr.2016.03.003.

Denning, C., Borgdorff, V., Crutchley, J., Firth, K.S., George, V., Kalra, S., et al. (2016). Cardiomyocytes from human pluripotent stem cells: From laboratory curiosity to

industrial biomedical platform. *Biochim Biophys Acta* 1863(7 Pt B)**,** 1728-1748. doi: 10.1016/j.bbamcr.2015.10.014.

Devine, M.J., Ryten, M., Vodicka, P., Thomson, A.J., Burdon, T., Houlden, H., et al. (2011). Parkinson's disease induced pluripotent stem cells with triplication of the α-synuclein locus. *Nat Commun* 2**,** 440. doi: 10.1038/ncomms1453.

Di Baldassarre, A., Cimetta, E., Bollini, S., Gaggi, G., and Ghinassi, B. (2018). Human-Induced Pluripotent Stem Cell Technology and Cardiomyocyte Generation: Progress and Clinical Applications. *Cells* 7(6). doi: 10.3390/cells7060048.

Di Bona, A., Vita, V., Costantini, I., and Zaglia, T. (2020). Towards a clearer view of sympathetic innervation of cardiac and skeletal muscles. *Prog Biophys Mol Biol* 154**,** 80-93. doi: 10.1016/j.pbiomolbio.2019.07.003.

Di Pasquale, E., Lodola, F., Miragoli, M., Denegri, M., Avelino-Cruz, J.E., Buonocore, M., et al. (2013a). CaMKII inhibition rectifies arrhythmic phenotype in a patient-specific model of catecholaminergic polymorphic ventricular tachycardia. *Cell Death & Disease* 4(10)**,** e843-e843. doi: 10.1038/cddis.2013.369.

Di Pasquale, E., Lodola, F., Miragoli, M., Denegri, M., Avelino-Cruz, J.E., Buonocore, M., et al. (2013b). CaMKII inhibition rectifies arrhythmic phenotype in a patient-specific model of catecholaminergic polymorphic ventricular tachycardia. *Cell Death Dis* 4**,** e843. doi: 10.1038/cddis.2013.369.

DiFrancesco, D. (2010). The role of the funny current in pacemaker activity. *Circ Res* 106(3)**,** 434-446. doi: 10.1161/circresaha.109.208041.

Doss, M.X., Di Diego, J.M., Goodrow, R.J., Wu, Y., Cordeiro, J.M., Nesterenko, V.V., et al. (2012). Maximum Diastolic Potential of Human Induced Pluripotent Stem Cell-Derived Cardiomyocytes Depends Critically on IKr. *PLOS ONE* 7(7)**,** e40288. doi: 10.1371/journal.pone.0040288.

Doss, M.X., and Sachinidis, A. (2019). Current Challenges of iPSC-Based Disease Modeling and Therapeutic Implications. *Cells* 8(5). doi: 10.3390/cells8050403.

Drew, R.C., and Sinoway, L.I. (2012). "Chapter 36 - Autonomic Control of the Heart," in *Primer on the Autonomic Nervous System (Third Edition),* eds. D. Robertson, I. Biaggioni, G. Burnstock, P.A. Low & J.F.R. Paton. (San Diego: Academic Press), 177-180.

Duraes Campos, I., Pinto, V., Sousa, N., and Pereira, V.H. (2018). A brain within the heart: A review on the intracardiac nervous system. *J Mol Cell Cardiol* 119**,** 1-9. doi: 10.1016/j.yjmcc.2018.04.005.

Egashira, T., Yuasa, S., Suzuki, T., Aizawa, Y., Yamakawa, H., Matsuhashi, T., et al. (2012). Disease characterization using LQTS-specific induced pluripotent stem cells. *Cardiovascular Research* 95(4)**,** 419-429. doi: 10.1093/cvr/cvs206.

Egawa, N., Kitaoka, S., Tsukita, K., Naitoh, M., Takahashi, K., Yamamoto, T., et al. (2012). Drug screening for ALS using patient-specific induced pluripotent stem cells. *Sci Transl Med* 4(145)**,** 145ra104. doi: 10.1126/scitranslmed.3004052.

Ehinger, B., Falck, B., and Sporrong, B. (1970). Possible axo-axonal synapses between peripheral adrenergic and cholinergic nerve terminals. *Z Zellforsch Mikrosk Anat* 107(4)**,** 508-521. doi: 10.1007/bf00335438.

Elliott, D.A., Braam, S.R., Koutsis, K., Ng, E.S., Jenny, R., Lagerqvist, E.L., et al. (2011). NKX2-5(eGFP/w) hESCs for isolation of human cardiac progenitors and cardiomyocytes. *Nat Methods* 8(12)**,** 1037-1040. doi: 10.1038/nmeth.1740.

Emerson, M. (2010). Refinement, reduction and replacement approaches to in vivo cardiovascular research. *Br J Pharmacol* 161(4)**,** 749-754. doi: 10.1111/j.1476-5381.2010.00959.x.

England, J., and Loughna, S. (2013). Heavy and light roles: myosin in the morphogenesis of the heart. *Cell Mol Life Sci* 70(7)**,** 1221-1239. doi: 10.1007/s00018-012-1131-1.

Ernsberger, U. (2001). The development of postganglionic sympathetic neurons: coordinating neuronal differentiation and diversification. *Auton Neurosci* 94(1-2)**,** 1-13. doi: 10.1016/S1566-0702(01)00336-8.

Ernsberger, U., Kramer, M., Tsarovina, K., Deller, T., and Rohrer, H. (2017). Coordinate expression of pan-neuronal and functional signature genes in sympathetic neurons. *Cell Tissue Res* 370(2)**,** 227-241. doi: 10.1007/s00441-017-2688-7.

Ernsberger, U., Patzke, H., Tissier-Seta, J.P., Reh, T., Goridis, C., and Rohrer, H. (1995). The expression of tyrosine hydroxylase and the transcription factors cPhox-2 and Cash-1: evidence for distinct inductive steps in the differentiation of chick sympathetic precursor cells. *Mech Dev* 52(1)**,** 125-136. doi: 10.1016/0925-4773(95)00396-i.

Ernsberger, U., and Rohrer, H. (2018). Sympathetic tales: subdivisons of the autonomic nervous system and the impact of developmental studies. *Neural Dev* 13(1)**,** 20. doi: 10.1186/s13064-018-0117-6.

Estes, E.H., Jr., and Izlar, H.L., Jr. (1961). Recurrent ventricular tachycardia. A case successfully treated by bilateral cardiac sympathectomy. *Am J Med* 31**,** 493-497. doi: 10.1016/0002-9343(61)90132-2.

Fasano, C.A., Chambers, S.M., Lee, G., Tomishima, M.J., and Studer, L. (2010). Efficient derivation of functional floor plate tissue from human embryonic stem cells. *Cell Stem Cell* 6(4)**,** 336-347. doi: 10.1016/j.stem.2010.03.001.

Fatima, A., Xu, G., Shao, K., Papadopoulos, S., Lehmann, M., Arnaiz-Cot, J.J., et al. (2011). In vitro modeling of ryanodine receptor 2 dysfunction using human induced pluripotent stem cells. *Cell Physiol Biochem* 28(4)**,** 579-592. doi: 10.1159/000335753.

Fedele, L., and Brand, T. (2020). The Intrinsic Cardiac Nervous System and Its Role in Cardiac Pacemaking and Conduction. *J Cardiovasc Dev Dis* 7(4). doi: 10.3390/jcdd7040054.

Fei, T., Xia, K., Li, Z., Zhou, B., Zhu, S., Chen, H., et al. (2010). Genome-wide mapping of SMAD target genes reveals the role of BMP signaling in embryonic stem cell fate determination. *Genome Res* 20(1)**,** 36-44. doi: 10.1101/gr.092114.109.

Finlay, M., Harmer, S.C., and Tinker, A. (2017). The control of cardiac ventricular excitability by autonomic pathways. *Pharmacol Ther* 174**,** 97-111. doi: 10.1016/j.pharmthera.2017.02.023.

Fleischer, S., Feiner, R., and Dvir, T. (2017). Cardiac tissue engineering: from matrix design to the engineering of bionic hearts. *Regen Med* 12(3)**,** 275-284. doi: 10.2217/rme-2016-0150.

Fonoudi, H., Ansari, H., Abbasalizadeh, S., Larijani, M.R., Kiani, S., Hashemizadeh, S., et al. (2015). A Universal and Robust Integrated Platform for the Scalable Production of Human Cardiomyocytes From Pluripotent Stem Cells. *Stem Cells Transl Med* 4(12)**,** 1482-1494. doi: 10.5966/sctm.2014-0275.

Francis Stuart, S.D., Wang, L., Woodard, W.R., Ng, G.A., Habecker, B.A., and Ripplinger, C.M. (2018). Age-related changes in cardiac electrophysiology and calcium handling in response to sympathetic nerve stimulation. *The Journal of Physiology* 596(17)**,** 3977-3991. doi: https://doi.org/10.1113/JP276396.

Freeman, K., Tao, W., Sun, H., Soonpaa, M.H., and Rubart, M. (2014). In situ three-dimensional reconstruction of mouse heart sympathetic innervation by two-photon excitation

fluorescence imaging. *J Neurosci Methods* 221**,** 48-61. doi: 10.1016/j.jneumeth.2013.09.005.

Frith, T.J., Granata, I., Wind, M., Stout, E., Thompson, O., Neumann, K., et al. (2018). Human axial progenitors generate trunk neural crest cells in vitro. *Elife* 7. doi: 10.7554/eLife.35786.

Frith, T.J.R., and Tsakiridis, A. (2019). Efficient Generation of Trunk Neural Crest and Sympathetic Neurons from Human Pluripotent Stem Cells Via a Neuromesodermal Axial Progenitor Intermediate. *Curr Protoc Stem Cell Biol* 49(1)**,** e81. doi: 10.1002/cpsc.81.

Fu, J.D., Li, J., Tweedie, D., Yu, H.M., Chen, L., Wang, R., et al. (2006). Crucial role of the sarcoplasmic reticulum in the developmental regulation of Ca2+ transients and contraction in cardiomyocytes derived from embryonic stem cells. *Faseb j* 20(1)**,** 181-183. doi: 10.1096/fj.05-4501fje.

Fuccillo, M., Joyner, A.L., and Fishell, G. (2006). Morphogen to mitogen: the multiple roles of hedgehog signalling in vertebrate neural development. *Nat Rev Neurosci* 7(10)**,** 772-783. doi: 10.1038/nrn1990.

Fujiwara, M., Yan, P., Otsuji, T.G., Narazaki, G., Uosaki, H., Fukushima, H., et al. (2011). Induction and enhancement of cardiac cell differentiation from mouse and human induced pluripotent stem cells with cyclosporin-A. *PLoS One* 6(2)**,** e16734. doi: 10.1371/journal.pone.0016734.

Fusaki, N., Ban, H., Nishiyama, A., Saeki, K., and Hasegawa, M. (2009). Efficient induction of transgene-free human pluripotent stem cells using a vector based on Sendai virus, an RNA virus that does not integrate into the host genome. *Proc Jpn Acad Ser B Phys Biol Sci* 85(8)**,** 348-362. doi: 10.2183/pjab.85.348.

Gerdes, A.M., Kellerman, S.E., Moore, J.A., Muffly, K.E., Clark, L.C., Reaves, P.Y., et al. (1992). Structural remodeling of cardiac myocytes in patients with ischemic cardiomyopathy. *Circulation* 86(2)**,** 426-430. doi: 10.1161/01.cir.86.2.426.

Ghaleb, A.M., Aggarwal, G., Bialkowska, A.B., Nandan, M.O., and Yang, V.W. (2008). Notch inhibits expression of the Kruppel-like factor 4 tumor suppressor in the intestinal epithelium. *Mol Cancer Res* 6(12)**,** 1920-1927. doi: 10.1158/1541-7786.MCR-08-0224.

Ghias, M., Scherlag, B.J., Lu, Z., Niu, G., Moers, A., Jackman, W.M., et al. (2009). The role of ganglionated plexi in apnea-related atrial fibrillation. *J Am Coll Cardiol* 54(22)**,** 2075-2083. doi: 10.1016/j.jacc.2009.09.014.

Giacomelli, E., Bellin, M., Sala, L., van Meer, B.J., Tertoolen, L.G., Orlova, V.V., et al. (2017). Three-dimensional cardiac microtissues composed of cardiomyocytes and endothelial cells co-differentiated from human pluripotent stem cells. *Development* 144(6)**,** 1008-1017. doi: 10.1242/dev.143438.

Gilsbach, R., Preissl, S., Gruning, B.A., Schnick, T., Burger, L., Benes, V., et al. (2014). Dynamic DNA methylation orchestrates cardiomyocyte development, maturation and disease. *Nat Commun* 5**,** 5288. doi: 10.1038/ncomms6288.

Giorgetti, A., Montserrat, N., Aasen, T., Gonzalez, F., Rodríguez-Pizà, I., Vassena, R., et al. (2009). Generation of induced pluripotent stem cells from human cord blood using OCT4 and SOX2. *Cell Stem Cell* 5(4)**,** 353-357. doi: 10.1016/j.stem.2009.09.008.

Gnecchi, M., He, H., Noiseux, N., Liang, O.D., Zhang, L., Morello, F., et al. (2006). Evidence supporting paracrine hypothesis for Akt-modified mesenchymal stem cell-mediated cardiac protection and functional improvement. *FASEB J* 20(6)**,** 661-669. doi: 10.1096/fj.05-5211com.

Goversen, B., van der Heyden, M.A.G., van Veen, T.A.B., and de Boer, T.P. (2018). The immature electrophysiological phenotype of iPSC-CMs still hampers in vitro drug screening: Special focus on IK1. *Pharmacology & Therapeutics* 183**,** 127-136. doi: https://doi.org/10.1016/j.pharmthera.2017.10.001.

Grandi, E., and Dobrev, D. (2020). Atrial fibrillation in a dish: insights into atrial arrhythmogenesis from induced pluripotent stem cell-derived cardiomyocytes. *Cardiovasc Res* 116(6)**,** 1089-1091. doi: 10.1093/cvr/cvz342.

Groves, A.K., George, K.M., Tissier-Seta, J.P., Engel, J.D., Brunet, J.F., and Anderson, D.J. (1995). Differential regulation of transcription factor gene expression and phenotypic markers in developing sympathetic neurons. *Development* 121(3)**,** 887-901.

Guan, X., Delo, D.M., Atala, A., and Soker, S. (2011). In vitro cardiomyogenic potential of human amniotic fluid stem cells. *J Tissue Eng Regen Med* 5(3)**,** 220-228. doi: 10.1002/term.308.

Guha, P., Morgan, J.W., Mostoslavsky, G., Rodrigues, N.P., and Boyd, A.S. (2013). Lack of immune response to differentiated cells derived from syngeneic induced pluripotent stem cells. *Cell Stem Cell* 12(4)**,** 407-412. doi: 10.1016/j.stem.2013.01.006.

Guo, Y., Niu, C., Breslin, P., Tang, M., Zhang, S., Wei, W., et al. (2009). c-Myc-mediated control of cell fate in megakaryocyte-erythrocyte progenitors. *Blood* 114(10)**,** 2097-2106. doi: 10.1182/blood-2009-01-197947.

Hackland, J.O.S., Frith, T.J.R., Thompson, O., Marin Navarro, A., Garcia-Castro, M.I., Unger, C., et al. (2017). Top-Down Inhibition of BMP Signaling Enables Robust Induction of hPSCs Into Neural Crest in Fully Defined, Xeno-free Conditions. *Stem Cell Reports* 9(4)**,** 1043-1052. doi: 10.1016/j.stemcr.2017.08.008.

Hailstones, D., Barton, P., Chan-Thomas, P., Sasse, S., Sutherland, C., Hardeman, E., et al. (1992). Differential regulation of the atrial isoforms of the myosin light chains during striated muscle development. *J Biol Chem* 267(32)**,** 23295-23300.

Haïssaguerre, M., Jaïs, P., Shah, D.C., Takahashi, A., Hocini, M., Quiniou, G., et al. (1998). Spontaneous initiation of atrial fibrillation by ectopic beats originating in the pulmonary veins. *N Engl J Med* 339(10)**,** 659-666. doi: 10.1056/nejm199809033391003.

Haïssaguerre, M., Shah, D.C., Jaïs, P., Hocini, M., Yamane, T., Deisenhofer, I., et al. (2000). Electrophysiological breakthroughs from the left atrium to the pulmonary veins. *Circulation* 102(20)**,** 2463-2465. doi: 10.1161/01.cir.102.20.2463.

Hamill, R.W., and Shapiro, R.E. (2004). "5 - Peripheral Autonomic Nervous System," in *Primer on the Autonomic Nervous System (Second Edition),* eds. D. Robertson, I. Biaggioni, G. Burnstock & P.A. Low. (San Diego: Academic Press), 20-28.

Han, S., Kobayashi, K., Joung, B., Piccirillo, G., Maruyama, M., Vinters, H.V., et al. (2012). Electroanatomic remodeling of the left stellate ganglion after myocardial infarction. *J Am Coll Cardiol* 59(10)**,** 954-961. doi: 10.1016/j.jacc.2011.11.030.

Hanna, P., Rajendran, P.S., Ajijola, O.A., Vaseghi, M., Andrew Armour, J., Ardell, J.L., et al. (2017). Cardiac neuroanatomy - Imaging nerves to define functional control. *Auton Neurosci* 207**,** 48-58. doi: 10.1016/j.autneu.2017.07.008.

Hartzell, H.C. (1980). Distribution of muscarinic acetylcholine receptors and presynaptic nerve terminals in amphibian heart. *J Cell Biol* 86(1)**,** 6-20. doi: 10.1083/jcb.86.1.6.

Hasan, W. (2013). Autonomic cardiac innervation: development and adult plasticity. *Organogenesis* 9(3)**,** 176-193. doi: 10.4161/org.24892.

Hattori, F., Chen, H., Yamashita, H., Tohyama, S., Satoh, Y.S., Yuasa, S., et al. (2010). Nongenetic method for purifying stem cell-derived cardiomyocytes. *Nat Methods* 7(1)**,** 61-66. doi: 10.1038/nmeth.1403.

Hayes, H.B., Nicolini, A.M., Arrowood, C.A., Chvatal, S.A., Wolfson, D.W., Cho, H.C., et al. (2019). Novel method for action potential measurements from intact cardiac monolayers with multiwell microelectrode array technology. *Scientific Reports* 9(1)**,** 11893. doi: 10.1038/s41598-019-48174-5.

Henrique, D., Abranches, E., Verrier, L., and Storey, K.G. (2015). Neuromesodermal progenitors and the making of the spinal cord. *Development* 142(17)**,** 2864-2875. doi: 10.1242/dev.119768.

Herring, N., Cranley, J., Lokale, M.N., Li, D., Shanks, J., Alston, E.N., et al. (2012). The cardiac sympathetic co-transmitter galanin reduces acetylcholine release and vagal bradycardia: implications for neural control of cardiac excitability. *J Mol Cell Cardiol* 52(3)**,** 667-676. doi: 10.1016/j.yjmcc.2011.11.016.

Herring, N., Lokale, M.N., Danson, E.J., Heaton, D.A., and Paterson, D.J. (2008). Neuropeptide Y reduces acetylcholine release and vagal bradycardia via a Y2 receptor-mediated, protein kinase C-dependent pathway. *J Mol Cell Cardiol* 44(3)**,** 477-485. doi: 10.1016/j.yjmcc.2007.10.001.

Herrmann, M., Anders, S., Straub, R.H., and Jenei-Lanzl, Z. (2018). TNF inhibits catecholamine production from induced sympathetic neuron-like cells in rheumatoid arthritis and osteoarthritis in vitro. *Sci Rep* 8(1)**,** 9645. doi: 10.1038/s41598-018-27927-8.

Hirsch, E., Hilfiker-Kleiner, D., Balligand, J.-L., Tarone, G., De Windt, L., Bauersachs, J., et al. (2013). Interaction of the heart and its close and distant neighbours: report of the Meeting of the ESC Working Groups Myocardial Function and Cellular Biology. *Cardiovascular Research* 99(4)**,** 595-599. doi: 10.1093/cvr/cvt179.

Hirst, G.D., Choate, J.K., Cousins, H.M., Edwards, F.R., and Klemm, M.F. (1996). Transmission by post-ganglionic axons of the autonomic nervous system: the importance of the specialized neuroeffector junction. *Neuroscience* 73(1)**,** 7-23. doi: 10.1016/0306-4522(96)00031-0.

Hirt, M.N., Hansen, A., and Eschenhagen, T. (2014). Cardiac tissue engineering: state of the art. *Circ Res* 114(2)**,** 354-367. doi: 10.1161/CIRCRESAHA.114.300522.

Hnasko, T.S., and Hnasko, R.M. (2015). "The Western Blot," in *ELISA: Methods and Protocols,* ed. R. Hnasko. (New York, NY: Springer New York), 87-96.

Hoben, G.M., Koay, E.J., and Athanasiou, K.A. (2008). Fibrochondrogenesis in two embryonic stem cell lines: effects of differentiation timelines. *Stem Cells* 26(2)**,** 422-430. doi: 10.1634/stemcells.2007-0641.

Hoekstra, M., Mummery, C.L., Wilde, A.A., Bezzina, C.R., and Verkerk, A.O. (2012). Induced pluripotent stem cell derived cardiomyocytes as models for cardiac arrhythmias. *Front Physiol* 3**,** 346. doi: 10.3389/fphys.2012.00346.

Hopkins, D.A., and Armour, J.A. (1984). Localization of sympathetic postganglionic and parasympathetic preganglionic neurons which innervate different regions of the dog heart. *J Comp Neurol* 229(2)**,** 186-198. doi: 10.1002/cne.902290205.

Hou, Y., Scherlag, B.J., Lin, J., Zhang, Y., Lu, Z., Truong, K., et al. (2007). Ganglionated plexi modulate extrinsic cardiac autonomic nerve input: effects on sinus rate, atrioventricular conduction, refractoriness, and inducibility of atrial fibrillation. *J Am Coll Cardiol* 50(1)**,** 61-68. doi: 10.1016/j.jacc.2007.02.066.

Hsieh, P.C., Davis, M.E., Lisowski, L.K., and Lee, R.T. (2006). Endothelial-cardiomyocyte interactions in cardiac development and repair. *Annu Rev Physiol* 68**,** 51-66. doi: 10.1146/annurev.physiol.68.040104.124629.

Hsieh, P.C., Segers, V.F., Davis, M.E., MacGillivray, C., Gannon, J., Molkentin, J.D., et al. (2007). Evidence from a genetic fate-mapping study that stem cells refresh adult mammalian cardiomyocytes after injury. *Nat Med* 13(8)**,** 970-974. doi: 10.1038/nm1618.

Huang, M., Miller, M.L., McHenry, L.K., Zheng, T., Zhen, Q., Ilkhanizadeh, S., et al. (2016). Generating trunk neural crest from human pluripotent stem cells. *Sci Rep* 6**,** 19727. doi: 10.1038/srep19727.

Huffaker, R., Lamp, S.T., Weiss, J.N., and Kogan, B. (2004). Intracellular calcium cycling, early afterdepolarizations, and reentry in simulated long QT syndrome. *Heart Rhythm* 1(4)**,** 441-448. doi: 10.1016/j.hrthm.2004.06.005.

Ieda, M., Kanazawa, H., Kimura, K., Hattori, F., Ieda, Y., Taniguchi, M., et al. (2007). Sema3a maintains normal heart rhythm through sympathetic innervation patterning. *Nat Med* 13(5)**,** 604-612. doi: 10.1038/nm1570.

Imaizumi, Y., Okada, Y., Akamatsu, W., Koike, M., Kuzumaki, N., Hayakawa, H., et al. (2012). Mitochondrial dysfunction associated with increased oxidative stress and α-synuclein accumulation in PARK2 iPSC-derived neurons and postmortem brain tissue. *Mol Brain* 5**,** 35. doi: 10.1186/1756-6606-5-35.

Imaizumi, Y., and Okano, H. (2014). Modeling human neurological disorders with induced pluripotent stem cells. *J Neurochem* 129(3)**,** 388-399. doi: 10.1111/jnc.12625.

Israel, M.A., Yuan, S.H., Bardy, C., Reyna, S.M., Mu, Y., Herrera, C., et al. (2012). Probing sporadic and familial Alzheimer's disease using induced pluripotent stem cells. *Nature* 482(7384)**,** 216-220. doi: 10.1038/nature10821.

Itskovitz-Eldor, J., Schuldiner, M., Karsenti, D., Eden, A., Yanuka, O., Amit, M., et al. (2000). Differentiation of human embryonic stem cells into embryoid bodies compromising the three embryonic germ layers. *Mol Med* 6(2)**,** 88-95.

Itzhaki, I., Maizels, L., Huber, I., Gepstein, A., Arbel, G., Caspi, O., et al. (2012). Modeling of Catecholaminergic Polymorphic Ventricular Tachycardia With Patient-Specific Human-Induced Pluripotent Stem Cells. *Journal of the American College of Cardiology* 60(11)**,** 990-1000. doi: https://doi.org/10.1016/j.jacc.2012.02.066.

Itzhaki, I., Maizels, L., Huber, I., Zwi-Dantsis, L., Caspi, O., Winterstern, A., et al. (2011). Modelling the long QT syndrome with induced pluripotent stem cells. *Nature* 471(7337)**,** 225-229. doi: 10.1038/nature09747.

Itzhaki, I., Schiller, J., Beyar, R., Satin, J., and Gepstein, L. (2006). Calcium handling in embryonic stem cell-derived cardiac myocytes: of mice and men. *Ann N Y Acad Sci* 1080**,** 207-215. doi: 10.1196/annals.1380.017.

Ivashchenko, C.Y., Pipes, G.C., Lozinskaya, I.M., Lin, Z., Xiaoping, X., Needle, S., et al. (2013). Human-induced pluripotent stem cell-derived cardiomyocytes exhibit temporal changes in phenotype. *Am J Physiol Heart Circ Physiol* 305(6)**,** H913-922. doi: 10.1152/ajpheart.00819.2012.

Izumo, S., Nadal-Ginard, B., and Mahdavi, V. (1988). Protooncogene induction and reprogramming of cardiac gene expression produced by pressure overload. *Proceedings of the National Academy of Sciences of the United States of America* 85(2)**,** 339-343. doi: 10.1073/pnas.85.2.339.

Jais, P., Haissaguerre, M., Shah, D.C., Chouairi, S., Gencel, L., Hocini, M., et al. (1997). A focal source of atrial fibrillation treated by discrete radiofrequency ablation. *Circulation* 95(3)**,** 572-576. doi: 10.1161/01.cir.95.3.572.

Jamali, H.K., Waqar, F., and Gerson, M.C. (2017). Cardiac autonomic innervation. *J Nucl Cardiol* 24(5)**,** 1558-1570. doi: 10.1007/s12350-016-0725-7.

Janes, R.D., Brandys, J.C., Hopkins, D.A., Johnstone, D.E., Murphy, D.A., and Armour, J.A. (1986). Anatomy of human extrinsic cardiac nerves and ganglia. *Am J Cardiol* 57(4)**,** 299-309. doi: 10.1016/0002-9149(86)90908-2.

Jeon, I., Lee, N., Li, J.Y., Park, I.H., Park, K.S., Moon, J., et al. (2012). Neuronal properties, in vivo effects, and pathology of a Huntington's disease patient-derived induced pluripotent stem cells. *Stem Cells* 30(9)**,** 2054-2062. doi: 10.1002/stem.1135.

Jiang, H., Ren, Y., Yuen, E.Y., Zhong, P., Ghaedi, M., Hu, Z., et al. (2012). Parkin controls dopamine utilization in human midbrain dopaminergic neurons derived from induced pluripotent stem cells. *Nat Commun* 3**,** 668. doi: 10.1038/ncomms1669.

Jing, D., Parikh, A., and Tzanakakis, E.S. (2010). Cardiac cell generation from encapsulated embryonic stem cells in static and scalable culture systems. *Cell Transplant* 19(11)**,** 1397-1412. doi: 10.3727/096368910x513955.

Julian, D.G., and Sheridan, D.J. (1978). Neural regulation of the heart: by W. C. Randall (ed.), viii + 440 pages, 113 illustrations, 3 tables, Oxford University Press, Oxford, New York, Toronto, 1977, £ 13.50. *Journal of the Neurological Sciences* 38(1)**,** 127. doi: https://doi.org/10.1016/0022-510X(78)90258-7.

Jung, C.B., Moretti, A., Mederos y Schnitzler, M., Iop, L., Storch, U., Bellin, M., et al. (2012). Dantrolene rescues arrhythmogenic RYR2 defect in a patient-specific stem cell model of catecholaminergic polymorphic ventricular tachycardia. *EMBO Molecular Medicine* 4(3)**,** 180-191. doi: https://doi.org/10.1002/emmm.201100194.

Juopperi, T.A., Kim, W.R., Chiang, C.H., Yu, H., Margolis, R.L., Ross, C.A., et al. (2012). Astrocytes generated from patient induced pluripotent stem cells recapitulate features of Huntington's disease patient cells. *Mol Brain* 5**,** 17. doi: 10.1186/1756-6606-5-17.

Kapa, S., Venkatachalam, K.L., and Asirvatham, S.J. (2010). The autonomic nervous system in cardiac electrophysiology: an elegant interaction and emerging concepts. *Cardiol Rev* 18(6)**,** 275-284. doi: 10.1097/CRD.0b013e3181ebb152.

Karagiannis, P., Takahashi, K., Saito, M., Yoshida, Y., Okita, K., Watanabe, A., et al. (2019). Induced Pluripotent Stem Cells and Their Use in Human Models of Disease and Development. *Physiol Rev* 99(1)**,** 79-114. doi: 10.1152/physrev.00039.2017.

Karakikes, I., Ameen, M., Termglinchan, V., and Wu, J.C. (2015). Human induced pluripotent stem cell-derived cardiomyocytes: insights into molecular, cellular, and functional phenotypes. *Circ Res* 117(1)**,** 80-88. doi: 10.1161/CIRCRESAHA.117.305365.

Karakikes, I., Senyei, G.D., Hansen, J., Kong, C.W., Azeloglu, E.U., Stillitano, F., et al. (2014). Small molecule-mediated directed differentiation of human embryonic stem cells toward ventricular cardiomyocytes. *Stem Cells Transl Med* 3(1)**,** 18-31. doi: 10.5966/sctm.2013-0110.

Kasanuki, H., Ohnishi, S., Ohtuka, M., Matsuda, N., Nirei, T., Isogai, R., et al. (1997). Idiopathic ventricular fibrillation induced with vagal activity in patients without obvious heart disease. *Circulation* 95(9)**,** 2277-2285. doi: 10.1161/01.cir.95.9.2277.

Katritsis, D.G., Giazitzoglou, E., Zografos, T., Pokushalov, E., Po, S.S., and Camm, A.J. (2011). Rapid pulmonary vein isolation combined with autonomic ganglia modification: a randomized study. *Heart Rhythm* 8(5)**,** 672-678. doi: 10.1016/j.hrthm.2010.12.047.

Kawashima, T. (2005). The autonomic nervous system of the human heart with special reference to its origin, course, and peripheral distribution. *Anat Embryol (Berl)* 209(6)**,** 425-438. doi: 10.1007/s00429-005-0462-1.

Kempf, H., Olmer, R., Kropp, C., Rückert, M., Jara-Avaca, M., Robles-Diaz, D., et al. (2014a). Controlling expansion and cardiomyogenic differentiation of human pluripotent stem

cells in scalable suspension culture. *Stem cell reports* 3(6)**,** 1132-1146. doi: 10.1016/j.stemcr.2014.09.017.

Kempf, H., Olmer, R., Kropp, C., Rückert, M., Jara-Avaca, M., Robles-Diaz, D., et al. (2014b). Controlling expansion and cardiomyogenic differentiation of human pluripotent stem cells in scalable suspension culture. *Stem Cell Reports* 3(6)**,** 1132-1146. doi: 10.1016/j.stemcr.2014.09.017.

Khan, J.M., Lyon, A.R., and Harding, S.E. (2013). The case for induced pluripotent stem cell-derived cardiomyocytes in pharmacological screening. *Br J Pharmacol* 169(2)**,** 304-317. doi: 10.1111/j.1476-5381.2012.02118.x.

Khemani, P., and Mehdirad, A.A. (2020). Cardiovascular Disorders Mediated by Autonomic Nervous System Dysfunction. *Cardiol Rev* 28(2)**,** 65-72. doi: 10.1097/CRD.0000000000000280.

Kidder, B.L., Yang, J., and Palmer, S. (2008). Stat3 and c-Myc genome-wide promoter occupancy in embryonic stem cells. *PLoS One* 3(12)**,** e3932. doi: 10.1371/journal.pone.0003932.

Kikuchi, S. (1976). The structure and innervation of the sinu-atrial node of the mole heart. *Cell Tissue Res* 172(3)**,** 345-356. doi: 10.1007/BF00399517.

Kim, C., Wong, J., Wen, J., Wang, S., Wang, C., Spiering, S., et al. (2013). Studying arrhythmogenic right ventricular dysplasia with patient-specific iPSCs. *Nature* 494(7435)**,** 105-110. doi: 10.1038/nature11799.

Kim, D., Kim, C.H., Moon, J.I., Chung, Y.G., Chang, M.Y., Han, B.S., et al. (2009). Generation of human induced pluripotent stem cells by direct delivery of reprogramming proteins. *Cell Stem Cell* 4(6)**,** 472-476. doi: 10.1016/j.stem.2009.05.005.

Kim, H., Kim, S.-H.L., Choi, Y.-H., Ahn, Y.-H., and Hwang, N.S. (2018). "Biomaterials for Stem Cell Therapy for Cardiac Disease," in *Biomimetic Medical Materials: From Nanotechnology to 3D Bioprinting,* ed. I. Noh. (Singapore: Springer Singapore), 181-193.

Kim, H.D., Kim, D.J., Lee, I.J., Rah, B.J., Sawa, Y., and Schaper, J. (1992). Human fetal heart development after mid-term: morphometry and ultrastructural study. *J Mol Cell Cardiol* 24(9)**,** 949-965. doi: 10.1016/0022-2828(92)91862-y.

Kim, K., Doi, A., Wen, B., Ng, K., Zhao, R., Cahan, P., et al. (2010). Epigenetic memory in induced pluripotent stem cells. *Nature* 467(7313)**,** 285-290. doi: 10.1038/nature09342.

Kimura, K., Ieda, M., and Fukuda, K. (2012). Development, maturation, and transdifferentiation of cardiac sympathetic nerves. *Circ Res* 110(2)**,** 325-336. doi: 10.1161/circresaha.111.257253.

Kirino, K., Nakahata, T., Taguchi, T., and Saito, M.K. (2018). Efficient derivation of sympathetic neurons from human pluripotent stem cells with a defined condition. *Sci Rep* 8(1)**,** 12865. doi: 10.1038/s41598-018-31256-1.

Klemm, M., Hirst, G.D., and Campbell, G. (1992). Structure of autonomic neuromuscular junctions in the sinus venosus of the toad. *J Auton Nerv Syst* 39(2)**,** 139-150. doi: 10.1016/0165-1838(92)90054-k.

Klimas, A., Ambrosi, C.M., Yu, J., Williams, J.C., Bien, H., and Entcheva, E. (2016). OptoDyCE as an automated system for high-throughput all-optical dynamic cardiac electrophysiology. *Nat Commun* 7**,** 11542. doi: 10.1038/ncomms11542.

Kofron, C.M., and Mende, U. (2017). In vitro models of the cardiac microenvironment to study myocyte and non-myocyte crosstalk: bioinspired approaches beyond the polystyrene dish. *J Physiol* 595(12)**,** 3891-3905. doi: 10.1113/JP273100.

Kola, I., and Landis, J. (2004). Can the pharmaceutical industry reduce attrition rates? *Nat Rev Drug Discov* 3(8)**,** 711-715. doi: 10.1038/nrd1470.

Kondo, T., Asai, M., Tsukita, K., Kutoku, Y., Ohsawa, Y., Sunada, Y., et al. (2013). Modeling Alzheimer's disease with iPSCs reveals stress phenotypes associated with intracellular Abeta and differential drug responsiveness. *Cell Stem Cell* 12(4)**,** 487-496. doi: 10.1016/j.stem.2013.01.009.

Kraszewski, K., Mundigl, O., Daniell, L., Verderio, C., Matteoli, M., and De Camilli, P. (1995). Synaptic vesicle dynamics in living cultured hippocampal neurons visualized with CY3-conjugated antibodies directed against the lumenal domain of synaptotagmin. *J Neurosci* 15(6)**,** 4328-4342.

Kuder, T., and Nowak, E. (2015). Autonomic cardiac nerves: literature review. *Folia Morphol (Warsz)* 74(1)**,** 1-8. doi: 10.5603/fm.2015.0003.

Kujala, K., Paavola, J., Lahti, A., Larsson, K., Pekkanen-Mattila, M., Viitasalo, M., et al. (2012). Cell Model of Catecholaminergic Polymorphic Ventricular Tachycardia Reveals Early and Delayed Afterdepolarizations. *PLOS ONE* 7(9)**,** e44660. doi: 10.1371/journal.pone.0044660.

Kumar, N., Dougherty, J.A., Manring, H.R., Elmadbouh, I., Mergaye, M., Czirok, A., et al. (2019). Assessment of temporal functional changes and miRNA profiling of human iPSC-derived cardiomyocytes. *Scientific Reports* 9(1)**,** 13188. doi: 10.1038/s41598-019-49653-5.

Kussauer, S., David, R., and Lemcke, H. (2019). hiPSCs Derived Cardiac Cells for Drug and Toxicity Screening and Disease Modeling: What Micro- Electrode-Array Analyses Can Tell Us. *Cells* 8(11). doi: 10.3390/cells8111331.

Lachman, N., Syed, F.F., Habib, A., Kapa, S., Bisco, S.E., Venkatachalam, K.L., et al. (2011). Correlative anatomy for the electrophysiologist, part II: cardiac ganglia, phrenic nerve, coronary venous system. *J Cardiovasc Electrophysiol* 22(1)**,** 104-110. doi: 10.1111/j.1540-8167.2010.01882.x.

Laflamme, M.A., Chen, K.Y., Naumova, A.V., Muskheli, V., Fugate, J.A., Dupras, S.K., et al. (2007). Cardiomyocytes derived from human embryonic stem cells in pro-survival factors enhance function of infarcted rat hearts. *Nat Biotechnol* 25(9)**,** 1015-1024. doi: 10.1038/nbt1327.

Laflamme, M.A., and Murry, C.E. (2011). Heart regeneration. *Nature* 473(7347)**,** 326-335. doi: 10.1038/nature10147.

Lahmers, S., Wu, Y., Call, D.R., Labeit, S., and Granzier, H. (2004). Developmental control of titin isoform expression and passive stiffness in fetal and neonatal myocardium. *Circ Res* 94(4)**,** 505-513. doi: 10.1161/01.Res.0000115522.52554.86.

Lahti, A.L., Kujala, V.J., Chapman, H., Koivisto, A.-P., Pekkanen-Mattila, M., Kerkelä, E., et al. (2012a). Model for long QT syndrome type 2 using human iPS cells demonstrates arrhythmogenic characteristics in cell culture. *Disease Models & Mechanisms* 5(2)**,** 220-230. doi: 10.1242/dmm.008409.

Lahti, A.L., Kujala, V.J., Chapman, H., Koivisto, A.P., Pekkanen-Mattila, M., Kerkelä, E., et al. (2012b). Model for long QT syndrome type 2 using human iPS cells demonstrates arrhythmogenic characteristics in cell culture. *Dis Model Mech* 5(2)**,** 220-230. doi: 10.1242/dmm.008409.

Lan, F., Lee, Andrew S., Liang, P., Sanchez-Freire, V., Nguyen, Patricia K., Wang, L., et al. (2013). Abnormal Calcium Handling Properties Underlie Familial Hypertrophic Cardiomyopathy Pathology in Patient-Specific Induced Pluripotent Stem Cells. *Cell Stem Cell* 12(1)**,** 101-113. doi: https://doi.org/10.1016/j.stem.2012.10.010.

Larsen, H.E., Lefkimmiatis, K., and Paterson, D.J. (2016). Sympathetic neurons are a powerful driver of myocyte function in cardiovascular disease. *Sci Rep* 6**,** 38898. doi: 10.1038/srep38898.

Lasser, K.E., Allen, P.D., Woolhandler, S.J., Himmelstein, D.U., Wolfe, S.M., and Bor, D.H. (2002). Timing of new black box warnings and withdrawals for prescription medications. *Jama* 287(17)**,** 2215-2220. doi: 10.1001/jama.287.17.2215.

Laugwitz, K.L., Moretti, A., Lam, J., Gruber, P., Chen, Y., Woodard, S., et al. (2005). Postnatal isl1+ cardioblasts enter fully differentiated cardiomyocyte lineages. *Nature* 433(7026)**,** 647-653. doi: 10.1038/nature03215.

Laustriat, D., Gide, J., and Peschanski, M. (2010). Human pluripotent stem cells in drug discovery and predictive toxicology. *Biochem Soc Trans* 38(4)**,** 1051-1057. doi: 10.1042/bst0381051.

Lavery, C.E., Mittleman, M.A., Cohen, M.C., Muller, J.E., and Verrier, R.L. (1997). Nonuniform nighttime distribution of acute cardiac events: a possible effect of sleep states. *Circulation* 96(10)**,** 3321-3327. doi: 10.1161/01.cir.96.10.3321.

Lawrence, T.S., Beers, W.H., and Gilula, N.B. (1978). Transmission of hormonal stimulation by cell-to-cell communication. *Nature* 272(5653)**,** 501-506. doi: 10.1038/272501a0.

Lee, G., Chambers, S.M., Tomishima, M.J., and Studer, L. (2010). Derivation of neural crest cells from human pluripotent stem cells. *Nat Protoc* 5(4)**,** 688-701. doi: 10.1038/nprot.2010.35.

Lee, G., Kim, H., Elkabetz, Y., Al Shamy, G., Panagiotakos, G., Barberi, T., et al. (2007). Isolation and directed differentiation of neural crest stem cells derived from human embryonic stem cells. *Nat Biotechnol* 25(12)**,** 1468-1475. doi: 10.1038/nbt1365.

Lee, G., Papapetrou, E.P., Kim, H., Chambers, S.M., Tomishima, M.J., Fasano, C.A., et al. (2009). Modelling pathogenesis and treatment of familial dysautonomia using patient-specific iPSCs. *Nature* 461(7262)**,** 402-406. doi: 10.1038/nature08320.

Lee, G., Ramirez, C.N., Kim, H., Zeltner, N., Liu, B., Radu, C., et al. (2012). Large-scale screening using familial dysautonomia induced pluripotent stem cells identifies compounds that rescue IKBKAP expression. *Nat Biotechnol* 30(12)**,** 1244-1248. doi: 10.1038/nbt.2435.

Lee, S., Lee, H.A., Choi, S.W., Kim, S.J., and Kim, K.S. (2016). Evaluation of nefazodone-induced cardiotoxicity in human induced pluripotent stem cell-derived cardiomyocytes. *Toxicol Appl Pharmacol* 296**,** 42-53. doi: 10.1016/j.taap.2016.01.015.

Levy, M.N. (1990). Autonomic interactions in cardiac control. *Ann N Y Acad Sci* 601**,** 209-221. doi: 10.1111/j.1749-6632.1990.tb37302.x.

Li, X.J., Du, Z.W., Zarnowska, E.D., Pankratz, M., Hansen, L.O., Pearce, R.A., et al. (2005). Specification of motoneurons from human embryonic stem cells. *Nat Biotechnol* 23(2)**,** 215-221. doi: 10.1038/nbt1063.

Lian, Q., Chow, Y., Esteban, M.A., Pei, D., and Tse, H.F. (2010). Future perspective of induced pluripotent stem cells for diagnosis, drug screening and treatment of human diseases. *Thromb Haemost* 104(1)**,** 39-44. doi: 10.1160/th10-05-0269.

Lian, X., Bao, X., Zilberter, M., Westman, M., Fisahn, A., Hsiao, C., et al. (2015). Chemically defined, albumin-free human cardiomyocyte generation. *Nat Methods* 12(7)**,** 595-596. doi: 10.1038/nmeth.3448.

Lian, X., Zhang, J., Azarin, S.M., Zhu, K., Hazeltine, L.B., Bao, X., et al. (2013). Directed cardiomyocyte differentiation from human pluripotent stem cells by modulating Wnt/beta-catenin signaling under fully defined conditions. *Nat Protoc* 8(1)**,** 162-175. doi: 10.1038/nprot.2012.150.

Liang, P., Lan, F., Lee, A.S., Gong, T., Sanchez-Freire, V., Wang, Y., et al. (2013a). Drug screening using a library of human induced pluripotent stem cell-derived cardiomyocytes reveals disease-specific patterns of cardiotoxicity. *Circulation* 127(16)**,** 1677-1691. doi: 10.1161/CIRCULATIONAHA.113.001883.

Liang, P., Lan, F., Lee, A.S., Gong, T., Sanchez-Freire, V., Wang, Y., et al. (2013b). Drug Screening Using a Library of Human Induced Pluripotent Stem Cell–Derived Cardiomyocytes Reveals Disease-Specific Patterns of Cardiotoxicity. *Circulation* 127(16)**,** 1677-1691. doi: 10.1161/CIRCULATIONAHA.113.001883.

Liang, W., Gasparyan, L., AlQarawi, W., and Davis, D.R. (2019). Disease modeling of cardiac arrhythmias using human induced pluripotent stem cells. *Expert Opinion on Biological Therapy* 19(4)**,** 313-333. doi: 10.1080/14712598.2019.1575359.

Liau, B., Jackman, C.P., Li, Y., and Bursac, N. (2017). Developmental stage-dependent effects of cardiac fibroblasts on function of stem cell-derived engineered cardiac tissues. *Sci Rep* 7**,** 42290. doi: 10.1038/srep42290.

Lieu, D.K., Liu, J., Siu, C.W., McNerney, G.P., Tse, H.F., Abu-Khalil, A., et al. (2009). Absence of transverse tubules contributes to non-uniform Ca(2+) wavefronts in mouse and human embryonic stem cell-derived cardiomyocytes. *Stem Cells Dev* 18(10)**,** 1493-1500. doi: 10.1089/scd.2009.0052.

Liu, A., and Niswander, L.A. (2005). Bone morphogenetic protein signalling and vertebrate nervous system development. *Nat Rev Neurosci* 6(12)**,** 945-954. doi: 10.1038/nrn1805.

Liu, G.H., Qu, J., Suzuki, K., Nivet, E., Li, M., Montserrat, N., et al. (2012). Progressive degeneration of human neural stem cells caused by pathogenic LRRK2. *Nature* 491(7425)**,** 603-607. doi: 10.1038/nature11557.

Liu, P., Kaplan, A., Yuan, B., Hanna, J.H., Lupski, J.R., and Reiner, O. (2014). Passage Number is a Major Contributor to Genomic Structural Variations in Mouse iPSCs. *STEM CELLS* 32(10)**,** 2657-2667. doi: https://doi.org/10.1002/stem.1779.

Liu, Y., Scherlag, B.J., Fan, Y., Varma, V., Male, S., Chaudhry, M.A., et al. (2013). Inducibility of atrial fibrillation after GP ablations and "autonomic blockade": evidence for the pathophysiological role of the nonadrenergic and noncholinergic neurotransmitters. *J Cardiovasc Electrophysiol* 24(2)**,** 188-195. doi: 10.1111/j.1540-8167.2012.02449.x.

Livak, K., and Schmittgen, T. (2001). Analysis of relative gene expression data using real-time quantitative PCR and the 2(-Delta Delta C(T)) Method. Methods 2001;25:402-8). *Methods* 25**,** 402-408.

Lodola, F., Morone, D., Denegri, M., Bongianino, R., Nakahama, H., Rutigliano, L., et al. (2016). Adeno-associated virus-mediated CASQ2 delivery rescues phenotypic alterations in a patient-specific model of recessive catecholaminergic polymorphic ventricular tachycardia. *Cell Death & Disease* 7(10)**,** e2393-e2393. doi: 10.1038/cddis.2016.304.

Loffelholz, K., and Pappano, A.J. (1985). The parasympathetic neuroeffector junction of the heart. *Pharmacol Rev* 37(1)**,** 1-24.

Loh, Y.H., Agarwal, S., Park, I.H., Urbach, A., Huo, H., Heffner, G.C., et al. (2009). Generation of induced pluripotent stem cells from human blood. *Blood* 113(22)**,** 5476-5479. doi: 10.1182/blood-2009-02-204800.

Lopaschuk, G.D., and Jaswal, J.S. (2010). Energy metabolic phenotype of the cardiomyocyte during development, differentiation, and postnatal maturation. *J Cardiovasc Pharmacol* 56(2)**,** 130-140. doi: 10.1097/FJC.0b013e3181e74a14.

Lundy, S.D., Zhu, W.Z., Regnier, M., and Laflamme, M.A. (2013). Structural and functional maturation of cardiomyocytes derived from human pluripotent stem cells. *Stem Cells Dev* 22(14)**,** 1991-2002. doi: 10.1089/scd.2012.0490.

Ma, D., Wei, H., Lu, J., Ho, S., Zhang, G., Sun, X., et al. (2013a). Generation of patient-specific induced pluripotent stem cell-derived cardiomyocytes as a cellular model of arrhythmogenic right ventricular cardiomyopathy. *Eur Heart J* 34(15)**,** 1122-1133. doi: 10.1093/eurheartj/ehs226.

Ma, D., Wei, H., Zhao, Y., Lu, J., Li, G., Sahib, N.B., et al. (2013b). Modeling type 3 long QT syndrome with cardiomyocytes derived from patient-specific induced pluripotent stem cells. *Int J Cardiol* 168(6)**,** 5277-5286. doi: 10.1016/j.ijcard.2013.08.015.

Ma, D., Wei, H., Zhao, Y., Lu, J., Li, G., Sahib, N.B.E., et al. (2013c). Modeling type 3 long QT syndrome with cardiomyocytes derived from patient-specific induced pluripotent stem cells. *International Journal of Cardiology* 168(6)**,** 5277-5286. doi: https://doi.org/10.1016/j.ijcard.2013.08.015.

Ma, J., Guo, L., Fiene, S.J., Anson, B.D., Thomson, J.A., Kamp, T.J., et al. (2011). High purity human-induced pluripotent stem cell-derived cardiomyocytes: electrophysiological properties of action potentials and ionic currents. *Am J Physiol Heart Circ Physiol* 301(5)**,** H2006-2017. doi: 10.1152/ajpheart.00694.2011.

Ma, S.P., and Vunjak-Novakovic, G. (2016). Tissue-Engineering for the Study of Cardiac Biomechanics. *J Biomech Eng* 138(2)**,** 021010. doi: 10.1115/1.4032355.

Macarthur, C.C., Fontes, A., Ravinder, N., Kuninger, D., Kaur, J., Bailey, M., et al. (2012). Generation of human-induced pluripotent stem cells by a nonintegrating RNA Sendai virus vector in feeder-free or xeno-free conditions. *Stem Cells Int* 2012**,** 564612. doi: 10.1155/2012/564612.

MacDonald, J.S., and Robertson, R.T. (2009). Toxicity testing in the 21st century: a view from the pharmaceutical industry. *Toxicol Sci* 110(1)**,** 40-46. doi: 10.1093/toxsci/kfp088.

Machiraju, P., and Greenway, S.C. (2019). Current methods for the maturation of induced pluripotent stem cell-derived cardiomyocytes. *World J Stem Cells* 11(1)**,** 33-43. doi: 10.4252/wjsc.v11.i1.33.

Maden, M. (2007). Retinoic acid in the development, regeneration and maintenance of the nervous system. *Nat Rev Neurosci* 8(10)**,** 755-765. doi: 10.1038/nrn2212.

Magyar, J., Iost, N., Körtvély, A., Bányász, T., Virág, L., Szigligeti, P., et al. (2000). Effects of endothelin-1 on calcium and potassium currents in undiseased human ventricular myocytes. *Pflugers Arch* 441(1)**,** 144-149. doi: 10.1007/s004240000400.

Manabe, N., Foldes, F.F., Töröcsik, A., Nagashima, H., Goldiner, P.L., and Vizi, E.S. (1991). Presynaptic interaction between vagal and sympathetic innervation in the heart: modulation of acetylcholine and noradrenaline release. *J Auton Nerv Syst* 32(3)**,** 233-242. doi: 10.1016/0165-1838(91)90117-l.

Mandenius, C.F., Steel, D., Noor, F., Meyer, T., Heinzle, E., Asp, J., et al. (2011). Cardiotoxicity testing using pluripotent stem cell-derived human cardiomyocytes and state-of-the-art bioanalytics: a review. *J Appl Toxicol* 31(3)**,** 191-205. doi: 10.1002/jat.1663.

Mardanpour, P., Nayernia, K., Khodayari, S., Khodayari, H., Molcanyi, M., and Hescheler, J. (2019). Application of Stem Cell Technologies to Regenerate Injured Myocardium and Improve Cardiac Function. *Cell Physiol Biochem* 53(1)**,** 101-120. doi: 10.33594/000000124.

Martinez-Fernandez, A., Nelson, T.J., Ikeda, Y., and Terzic, A. (2010). c-MYC independent nuclear reprogramming favors cardiogenic potential of induced pluripotent stem cells. *J Cardiovasc Transl Res* 3(1)**,** 13-23. doi: 10.1007/s12265-009-9150-5.

Mason, I. (2007). Initiation to end point: the multiple roles of fibroblast growth factors in neural development. *Nat Rev Neurosci* 8(8)**,** 583-596. doi: 10.1038/nrn2189.

Masui, S., Nakatake, Y., Toyooka, Y., Shimosato, D., Yagi, R., Takahashi, K., et al. (2007). Pluripotency governed by Sox2 via regulation of Oct3/4 expression in mouse embryonic stem cells. *Nat Cell Biol* 9(6)**,** 625-635. doi: 10.1038/ncb1589.

Matsa, E., Dixon, J.E., Medway, C., Georgiou, O., Patel, M.J., Morgan, K., et al. (2014). Allele-specific RNA interference rescues the long-QT syndrome phenotype in human-induced pluripotency stem cell cardiomyocytes. *Eur Heart J* 35(16)**,** 1078-1087. doi: 10.1093/eurheartj/eht067.

Matsa, E., Rajamohan, D., Dick, E., Young, L., Mellor, I., Staniforth, A., et al. (2011). Drug evaluation in cardiomyocytes derived from human induced pluripotent stem cells carrying a long QT syndrome type 2 mutation. *European Heart Journal* 32(8)**,** 952-962. doi: 10.1093/eurheartj/ehr073.

Matsuo, K., Kurita, T., Inagaki, M., Kakishita, M., Aihara, N., Shimizu, W., et al. (1999). The circadian pattern of the development of ventricular fibrillation in patients with Brugada syndrome. *Eur Heart J* 20(6)**,** 465-470. doi: 10.1053/euhj.1998.1332.

Maury, Y., Côme, J., Piskorowski, R.A., Salah-Mohellibi, N., Chevaleyre, V., Peschanski, M., et al. (2015). Combinatorial analysis of developmental cues efficiently converts human pluripotent stem cells into multiple neuronal subtypes. *Nat Biotechnol* 33(1)**,** 89-96. doi: 10.1038/nbt.3049.

Mehta, A., Verma, V., Nandihalli, M., Ramachandra, C.J.A., Sequiera, G.L., Sudibyo, Y., et al. (2014). A Systemic Evaluation of Cardiac Differentiation from mRNA Reprogrammed Human Induced Pluripotent Stem Cells. *PLOS ONE* 9(7)**,** e103485. doi: 10.1371/journal.pone.0103485.

Menendez, L., Kulik, M.J., Page, A.T., Park, S.S., Lauderdale, J.D., Cunningham, M.L., et al. (2013). Directed differentiation of human pluripotent cells to neural crest stem cells. *Nat Protoc* 8(1)**,** 203-212. doi: 10.1038/nprot.2012.156.

Menendez, L., Yatskievych, T.A., Antin, P.B., and Dalton, S. (2011). Wnt signaling and a Smad pathway blockade direct the differentiation of human pluripotent stem cells to multipotent neural crest cells. *Proc Natl Acad Sci U S A* 108(48)**,** 19240-19245. doi: 10.1073/pnas.1113746108.

Meraviglia, V., Zanon, A., Lavdas, A.A., Schwienbacher, C., Silipigni, R., Di Segni, M., et al. (2015). Generation of Induced Pluripotent Stem Cells from Frozen Buffy Coats using Non-integrating Episomal Plasmids. *J Vis Exp* (100)**,** e52885. doi: 10.3791/52885.

Mertens, J., Marchetto, M.C., Bardy, C., and Gage, F.H. (2016). Evaluating cell reprogramming, differentiation and conversion technologies in neuroscience. *Nat Rev Neurosci* 17(7)**,** 424-437. doi: 10.1038/nrn.2016.46.

Metzger, J.M., Michele, D.E., Rust, E.M., Borton, A.R., and Westfall, M.V. (2003). Sarcomere thin filament regulatory isoforms. Evidence of a dominant effect of slow skeletal troponin I on cardiac contraction. *J Biol Chem* 278(15)**,** 13118-13123. doi: 10.1074/jbc.M212601200.

Mewes, T., and Ravens, U. (1994). L-type calcium currents of human myocytes from ventricle of non-failing and failing hearts and from atrium. *J Mol Cell Cardiol* 26(10)**,** 1307-1320. doi: 10.1006/jmcc.1994.1149.

Mica, Y., Lee, G., Chambers, S.M., Tomishima, M.J., and Studer, L. (2013). Modeling neural crest induction, melanocyte specification, and disease-related pigmentation defects in hESCs and patient-specific iPSCs. *Cell Rep* 3(4)**,** 1140-1152. doi: 10.1016/j.celrep.2013.03.025.

Mitne-Neto, M., Machado-Costa, M., Marchetto, M.C., Bengtson, M.H., Joazeiro, C.A., Tsuda, H., et al. (2011). Downregulation of VAPB expression in motor neurons derived from induced pluripotent stem cells of ALS8 patients. *Hum Mol Genet* 20(18)**,** 3642-3652. doi: 10.1093/hmg/ddr284.

Miyoshi, N., Ishii, H., Nagano, H., Haraguchi, N., Dewi, D.L., Kano, Y., et al. (2011). Reprogramming of mouse and human cells to pluripotency using mature microRNAs. *Cell Stem Cell* 8(6)**,** 633-638. doi: 10.1016/j.stem.2011.05.001.

Mohr, J.C., Zhang, J., Azarin, S.M., Soerens, A.G., de Pablo, J.J., Thomson, J.A., et al. (2010). The microwell control of embryoid body size in order to regulate cardiac differentiation of human embryonic stem cells. *Biomaterials* 31(7)**,** 1885-1893. doi: 10.1016/j.biomaterials.2009.11.033.

Moreno, A., Endicott, K., Skancke, M., Dwyer, M.K., Brennan, J., Efimov, I.R., et al. (2019). Sudden Heart Rate Reduction Upon Optogenetic Release of Acetylcholine From Cardiac Parasympathetic Neurons in Perfused Hearts. *Front Physiol* 10**,** 16. doi: 10.3389/fphys.2019.00016.

Moretti, A., Bellin, M., Welling, A., Jung, C.B., Lam, J.T., Bott-Flügel, L., et al. (2010a). Patient-Specific Induced Pluripotent Stem-Cell Models for Long-QT Syndrome. *New England Journal of Medicine* 363(15)**,** 1397-1409. doi: 10.1056/NEJMoa0908679.

Moretti, A., Bellin, M., Welling, A., Jung, C.B., Lam, J.T., Bott-Flugel, L., et al. (2010b). Patient-specific induced pluripotent stem-cell models for long-QT syndrome. *N Engl J Med* 363(15)**,** 1397-1409. doi: 10.1056/NEJMoa0908679.

Moss, A.J., Schwartz, P.J., Crampton, R.S., Tzivoni, D., Locati, E.H., MacCluer, J., et al. (1991). The long QT syndrome. Prospective longitudinal study of 328 families. *Circulation* 84(3)**,** 1136-1144. doi: 10.1161/01.cir.84.3.1136.

Mummery, C., Ward-van Oostwaard, D., Doevendans, P., Spijker, R., van den Brink, S., Hassink, R., et al. (2003). Differentiation of human embryonic stem cells to cardiomyocytes: role of coculture with visceral endoderm-like cells. *Circulation* 107(21)**,** 2733-2740. doi: 10.1161/01.CIR.0000068356.38592.68.

Mummery, C.L., Zhang, J., Ng, E.S., Elliott, D.A., Elefanty, A.G., and Kamp, T.J. (2012). Differentiation of human embryonic stem cells and induced pluripotent stem cells to cardiomyocytes: a methods overview. *Circ Res* 111(3)**,** 344-358. doi: 10.1161/CIRCRESAHA.110.227512.

Nagashimada, M., Ohta, H., Li, C., Nakao, K., Uesaka, T., Brunet, J.F., et al. (2012). Autonomic neurocristopathy-associated mutations in PHOX2B dysregulate Sox10 expression. *J Clin Invest* 122(9)**,** 3145-3158. doi: 10.1172/JCI63401.

Nakao, S., Ihara, D., Hasegawa, K., and Kawamura, T. (2020). Applications for Induced Pluripotent Stem Cells in Disease Modelling and Drug Development for Heart Diseases. *Eur Cardiol* 15**,** 1-10. doi: 10.15420/ecr.2019.03.

Nguyen, H.N., Byers, B., Cord, B., Shcheglovitov, A., Byrne, J., Gujar, P., et al. (2011). LRRK2 mutant iPSC-derived DA neurons demonstrate increased susceptibility to oxidative stress. *Cell Stem Cell* 8(3)**,** 267-280. doi: 10.1016/j.stem.2011.01.013.

Niebruegge, S., Bauwens, C.L., Peerani, R., Thavandiran, N., Masse, S., Sevaptisidis, E., et al. (2009). Generation of human embryonic stem cell-derived mesoderm and cardiac cells

using size-specified aggregates in an oxygen-controlled bioreactor. *Biotechnol Bioeng* 102(2)**,** 493-507. doi: 10.1002/bit.22065.

Niehrs, C., and Pollet, N. (1999). Synexpression groups in eukaryotes. *Nature* 402(6761)**,** 483-487. doi: 10.1038/990025.

Nishimura, K., Sano, M., Ohtaka, M., Furuta, B., Umemura, Y., Nakajima, Y., et al. (2011). Development of defective and persistent Sendai virus vector: a unique gene delivery/expression system ideal for cell reprogramming. *J Biol Chem* 286(6)**,** 4760-4771. doi: 10.1074/jbc.M110.183780.

Nishiofuku, M., Yoshikawa, M., Ouji, Y., Saito, K., Moriya, K., Ishizaka, S., et al. (2011). Modulated differentiation of embryonic stem cells into hepatocyte-like cells by coculture with hepatic stellate cells. *J Biosci Bioeng* 111(1)**,** 71-77. doi: 10.1016/j.jbiosc.2010.08.005.

O'Connell, T.D., Ishizaka, S., Nakamura, A., Swigart, P.M., Rodrigo, M.C., Simpson, G.L., et al. (2003). The alpha(1A/C)- and alpha(1B)-adrenergic receptors are required for physiological cardiac hypertrophy in the double-knockout mouse. *J Clin Invest* 111(11)**,** 1783-1791. doi: 10.1172/jci16100.

Oh, Y., Cho, G.S., Li, Z., Hong, I., Zhu, R., Kim, M.J., et al. (2016). Functional Coupling with Cardiac Muscle Promotes Maturation of hPSC-Derived Sympathetic Neurons. *Cell Stem Cell* 19(1)**,** 95-106. doi: 10.1016/j.stem.2016.05.002.

Ohnuki, M., and Takahashi, K. (2015). Present and future challenges of induced pluripotent stem cells. *Philos Trans R Soc Lond B Biol Sci* 370(1680)**,** 20140367. doi: 10.1098/rstb.2014.0367.

Oiwa, K., Shimba, K., Numata, T., Takeuchi, A., Kotani, K., and Jimbo, Y. (2016). A device for co-culturing autonomic neurons and cardiomyocytes using micro-fabrication techniques. *Integr Biol (Camb)* 8(3)**,** 341-348. doi: 10.1039/c5ib00273g.

Okita, K., Ichisaka, T., and Yamanaka, S. (2007). Generation of germline-competent induced pluripotent stem cells. *Nature* 448(7151)**,** 313-317. doi: 10.1038/nature05934.

Okita, K., Matsumura, Y., Sato, Y., Okada, A., Morizane, A., Okamoto, S., et al. (2011). A more efficient method to generate integration-free human iPS cells. *Nat Methods* 8(5)**,** 409-412. doi: 10.1038/nmeth.1591.

Ono, K., and Iijima, T. (2010). Cardiac T-type Ca(2+) channels in the heart. *J Mol Cell Cardiol* 48(1)**,** 65-70. doi: 10.1016/j.yjmcc.2009.08.021.

Opitz, C.A., Leake, M.C., Makarenko, I., Benes, V., and Linke, W.A. (2004). Developmentally regulated switching of titin size alters myofibrillar stiffness in the perinatal heart. *Circ Res* 94(7)**,** 967-975. doi: 10.1161/01.Res.0000124301.48193.E1.

Opthof, T., Misier, A.R., Coronel, R., Vermeulen, J.T., Verberne, H.J., Frank, R.G., et al. (1991). Dispersion of refractoriness in canine ventricular myocardium. Effects of sympathetic stimulation. *Circ Res* 68(5)**,** 1204-1215. doi: 10.1161/01.res.68.5.1204.

Osório, J. (2016). Landscape and mechanisms of transcription factor cooperativity. *Nature Reviews Genetics* 17(1)**,** 5-5. doi: 10.1038/nrg.2015.11.

Ou, D.B., He, Y., Chen, R., Teng, J.W., Wang, H.T., Zeng, D., et al. (2011). Three-dimensional co-culture facilitates the differentiation of embryonic stem cells into mature cardiomyocytes. *J Cell Biochem* 112(12)**,** 3555-3562. doi: 10.1002/jcb.23283.

Paige, S.L., Osugi, T., Afanasiev, O.K., Pabon, L., Reinecke, H., and Murry, C.E. (2010). Endogenous Wnt/beta-catenin signaling is required for cardiac differentiation in human embryonic stem cells. *PLoS One* 5(6)**,** e11134. doi: 10.1371/journal.pone.0011134.

Parikh, S.S., Blackwell, D.J., Gomez-Hurtado, N., Frisk, M., Wang, L., Kim, K., et al. (2017). Thyroid and Glucocorticoid Hormones Promote Functional T-Tubule Development in Human-

Induced Pluripotent Stem Cell-Derived Cardiomyocytes. *Circ Res* 121(12)**,** 1323-1330. doi: 10.1161/circresaha.117.311920.

Park, I.H., Arora, N., Huo, H., Maherali, N., Ahfeldt, T., Shimamura, A., et al. (2008). Disease-specific induced pluripotent stem cells. *Cell* 134(5)**,** 877-886. doi: 10.1016/j.cell.2008.07.041.

Paschos, N.K., Brown, W.E., Eswaramoorthy, R., Hu, J.C., and Athanasiou, K.A. (2015). Advances in tissue engineering through stem cell-based co-culture. *J Tissue Eng Regen Med* 9(5)**,** 488-503. doi: 10.1002/term.1870.

Passier, R., Oostwaard, D.W., Snapper, J., Kloots, J., Hassink, R.J., Kuijk, E., et al. (2005). Increased cardiomyocyte differentiation from human embryonic stem cells in serum-free cultures. *Stem Cells* 23(6)**,** 772-780. doi: 10.1634/stemcells.2004-0184.

Patterson, E., Lazzara, R., Szabo, B., Liu, H., Tang, D., Li, Y.H., et al. (2006). Sodium-calcium exchange initiated by the Ca2+ transient: an arrhythmia trigger within pulmonary veins. *J Am Coll Cardiol* 47(6)**,** 1196-1206. doi: 10.1016/j.jacc.2005.12.023.

Pattyn, A., Guillemot, F., and Brunet, J.F. (2006). Delays in neuronal differentiation in Mash1/Ascl1 mutants. *Dev Biol* 295(1)**,** 67-75. doi: 10.1016/j.ydbio.2006.03.008.

Pattyn, A., Morin, X., Cremer, H., Goridis, C., and Brunet, J.F. (1999). The homeobox gene Phox2b is essential for the development of autonomic neural crest derivatives. *Nature* 399(6734)**,** 366-370. doi: 10.1038/20700.

Paulsen Bda, S., de Moraes Maciel, R., Galina, A., Souza da Silveira, M., dos Santos Souza, C., Drummond, H., et al. (2012). Altered oxygen metabolism associated to neurogenesis of induced pluripotent stem cells derived from a schizophrenic patient. *Cell Transplant* 21(7)**,** 1547-1559. doi: 10.3727/096368911x600957.

Pauza, D.H., Skripka, V., Pauziene, N., and Stropus, R. (2000). Morphology, distribution, and variability of the epicardiac neural ganglionated subplexuses in the human heart. *Anat Rec* 259(4)**,** 353-382. doi: 10.1002/1097-0185(20000801)259:4<353::Aid-ar10>3.0.Co;2-r.

Pedrosa, E., Sandler, V., Shah, A., Carroll, R., Chang, C., Rockowitz, S., et al. (2011). Development of patient-specific neurons in schizophrenia using induced pluripotent stem cells. *J Neurogenet* 25(3)**,** 88-103. doi: 10.3109/01677063.2011.597908.

Peters, N.S., Severs, N.J., Rothery, S.M., Lincoln, C., Yacoub, M.H., and Green, C.R. (1994). Spatiotemporal relation between gap junctions and fascia adherens junctions during postnatal development of human ventricular myocardium. *Circulation* 90(2)**,** 713-725. doi: 10.1161/01.cir.90.2.713.

Piccolino, M., and Bresadola, M. *Shocking frogs : Galvani, Volta, and the electric origins of neuroscience.*

Platt, M., Mandapati, R., and Scherlag, B. (2004). Limiting the number and extent of radiofrequency applications to terminate atrial fibrillation and subsequently prevent its inducibility. *Heart Rhythm* 1**,** S11.

Polo, J.M., Liu, S., Figueroa, M.E., Kulalert, W., Eminli, S., Tan, K.Y., et al. (2010). Cell type of origin influences the molecular and functional properties of mouse induced pluripotent stem cells. *Nat Biotechnol* 28(8)**,** 848-855. doi: 10.1038/nbt.1667.

Pons-Espinal, M., de Luca, E., Marzi, M.J., Beckervordersandforth, R., Armirotti, A., Nicassio, F., et al. (2017). Synergic Functions of miRNAs Determine Neuronal Fate of Adult Neural Stem Cells. *Stem Cell Reports* 8(4)**,** 1046-1061. doi: https://doi.org/10.1016/j.stemcr.2017.02.012.

Portero, V., Casini, S., Hoekstra, M., Verkerk, A.O., Mengarelli, I., Belardinelli, L., et al. (2017). Anti-arrhythmic potential of the late sodium current inhibitor GS-458967 in murine Scn5a-1798insD+/- and human SCN5A-1795insD+/- iPSC-derived cardiomyocytes. *Cardiovasc Res* 113(7)**,** 829-838. doi: 10.1093/cvr/cvx077.

Pradhapan, P., Kuusela, J., Viik, J., Aalto-Setälä, K., and Hyttinen, J. (2013). Cardiomyocyte MEA Data Analysis (CardioMDA) – A Novel Field Potential Data Analysis Software for Pluripotent Stem Cell Derived Cardiomyocytes. *PLOS ONE* 8(9)**,** e73637. doi: 10.1371/journal.pone.0073637.

Prando, V., Da Broi, F., Franzoso, M., Plazzo, A.P., Pianca, N., Francolini, M., et al. (2018). Dynamics of neuroeffector coupling at cardiac sympathetic synapses. *J Physiol* 596(11)**,** 2055-2075. doi: 10.1113/jp275693.

Protas, L., Qu, J., and Robinson, R.B. (2003). Neuropeptide y: neurotransmitter or trophic factor in the heart? *News Physiol Sci* 18**,** 181-185. doi: 10.1152/nips.01437.2003.

Rakovic, A., Shurkewitsch, K., Seibler, P., Grünewald, A., Zanon, A., Hagenah, J., et al. (2013). Phosphatase and tensin homolog (PTEN)-induced putative kinase 1 (PINK1)-dependent ubiquitination of endogenous Parkin attenuates mitophagy: study in human primary fibroblasts and induced pluripotent stem cell-derived neurons. *J Biol Chem* 288(4)**,** 2223-2237. doi: 10.1074/jbc.M112.391680.

Randall, W.C., and Ardell, J.L. (1985). Selective parasympathectomy of automatic and conductile tissues of the canine heart. *American Journal of Physiology-Heart and Circulatory Physiology* 248(1)**,** H61-H68. doi: 10.1152/ajpheart.1985.248.1.H61.

Randall, W.C., Milosavljevic, M., Wurster, R.D., Geis, G.S., and Ardell, J.L. (1986). Selective vagal innervation of the heart. *Ann Clin Lab Sci* 16(3)**,** 198-208.

Reinhardt, P., Schmid, B., Burbulla, L.F., Schöndorf, D.C., Wagner, L., Glatza, M., et al. (2013). Genetic correction of a LRRK2 mutation in human iPSCs links parkinsonian neurodegeneration to ERK-dependent changes in gene expression. *Cell Stem Cell* 12(3)**,** 354-367. doi: 10.1016/j.stem.2013.01.008.

Ren, C., Wang, F., Li, G., Jiao, Q., Bai, J., Yu, D., et al. (2008). Nerve sprouting suppresses myocardial I(to) and I(K1) channels and increases severity to ventricular fibrillation in rat. *Auton Neurosci* 144(1-2)**,** 22-29. doi: 10.1016/j.autneu.2008.08.004.

Robertson, C., Tran, D.D., and George, S.C. (2013). Concise review: maturation phases of human pluripotent stem cell-derived cardiomyocytes. *Stem Cells* 31(5)**,** 829-837. doi: 10.1002/stem.1331.

Robertson, D., and Biaggioni, I. (2012). *Primer on the autonomic nervous system.* Amsterdam ; Boston: Elsevier/AP.

Rochais, F., Vandecasteele, G., Lefebvre, F., Lugnier, C., Lum, H., Mazet, J.L., et al. (2004). Negative feedback exerted by cAMP-dependent protein kinase and cAMP phosphodiesterase on subsarcolemmal cAMP signals in intact cardiac myocytes: an in vivo study using adenovirus-mediated expression of CNG channels. *J Biol Chem* 279(50)**,** 52095-52105. doi: 10.1074/jbc.M405697200.

Rodrigues, I.C.P., Kaasi, A., Maciel Filho, R., Jardini, A.L., and Gabriel, L.P. (2018). Cardiac tissue engineering: current state-of-the-art materials, cells and tissue formation. *Einstein (Sao Paulo)* 16(3)**,** eRB4538. doi: 10.1590/S1679-45082018RB4538.

Rump, L.C., Riera-Knorrenschild, G., Schwertfeger, E., Bohmann, C., Spillner, G., and Schollmeyer, P. (1995). Dopaminergic and alpha-adrenergic control of neurotransmission in human right atrium. *J Cardiovasc Pharmacol* 26(3)**,** 462-470. doi: 10.1097/00005344-199509000-00017.

Rungarunlert, S., Techakumphu, M., Pirity, M.K., and Dinnyes, A. (2009). Embryoid body formation from embryonic and induced pluripotent stem cells: Benefits of bioreactors. *World J Stem Cells* 1(1)**,** 11-21. doi: 10.4252/wjsc.v1.i1.11.

Saini, H., Navaei, A., Van Putten, A., and Nikkhah, M. (2015). 3D cardiac microtissues encapsulated with the co-culture of cardiomyocytes and cardiac fibroblasts. *Adv Healthc Mater* 4(13)**,** 1961-1971. doi: 10.1002/adhm.201500331.

Saito-Diaz, K., Wu, H.F., and Zeltner, N. (2019). Autonomic Neurons with Sympathetic Character Derived From Human Pluripotent Stem Cells. *Curr Protoc Stem Cell Biol* 49(1)**,** e78. doi: 10.1002/cpsc.78.

Saito-Diaz, K., and Zeltner, N. (2019). Induced pluripotent stem cells for disease modeling, cell therapy and drug discovery in genetic autonomic disorders: a review. *Clin Auton Res* 29(4)**,** 367-384. doi: 10.1007/s10286-018-00587-4.

Sakai, K., Shimba, K., Ishizuka, K., Yang, Z., Oiwa, K., Takeuchi, A., et al. (2017). Functional innervation of human induced pluripotent stem cell-derived cardiomyocytes by co-culture with sympathetic neurons developed using a microtunnel technique. *Biochem Biophys Res Commun* 494(1-2)**,** 138-143. doi: 10.1016/j.bbrc.2017.10.065.

Sánchez-Danés, A., Richaud-Patin, Y., Carballo-Carbajal, I., Jiménez-Delgado, S., Caig, C., Mora, S., et al. (2012). Disease-specific phenotypes in dopamine neurons from human iPS-based models of genetic and sporadic Parkinson's disease. *EMBO Mol Med* 4(5)**,** 380-395. doi: 10.1002/emmm.201200215.

Sasaki, K., Makiyama, T., Yoshida, Y., Wuriyanghai, Y., Kamakura, T., Nishiuchi, S., et al. (2016). Patient-Specific Human Induced Pluripotent Stem Cell Model Assessed with Electrical Pacing Validates S107 as a Potential Therapeutic Agent for Catecholaminergic Polymorphic Ventricular Tachycardia. *PLOS ONE* 11(10)**,** e0164795. doi: 10.1371/journal.pone.0164795.

Scadden, D.T. (2006). The stem-cell niche as an entity of action. *Nature* 441(7097)**,** 1075-1079. doi: 10.1038/nature04957.

Schächinger, V., Erbs, S., Elsässer, A., Haberbosch, W., Hambrecht, R., Hölschermann, H., et al. (2006). Intracoronary Bone Marrow–Derived Progenitor Cells in Acute Myocardial Infarction. *New England Journal of Medicine* 355(12)**,** 1210-1221. doi: 10.1056/NEJMoa060186.

Scherlag, B.J., and Po, S. (2006). The intrinsic cardiac nervous system and atrial fibrillation. *Current opinion in cardiology* 21(1)**,** 51-54. doi: 10.1097/01.hco.0000198980.40390.e4.

Scheven, B.A., Visser, J.W., and Nijweide, P.J. (1986). In vitro osteoclast generation from different bone marrow fractions, including a highly enriched haematopoietic stem cell population. *Nature* 321(6065)**,** 79-81. doi: 10.1038/321079a0.

Schmidt, A., Ladage, D., Steingen, C., Brixius, K., Schinkothe, T., Klinz, F.J., et al. (2006). Mesenchymal stem cells transmigrate over the endothelial barrier. *Eur J Cell Biol* 85(11)**,** 1179-1188. doi: 10.1016/j.ejcb.2006.05.015.

Seibler, P., Graziotto, J., Jeong, H., Simunovic, F., Klein, C., and Krainc, D. (2011). Mitochondrial Parkin recruitment is impaired in neurons derived from mutant PINK1 induced pluripotent stem cells. *J Neurosci* 31(16)**,** 5970-5976. doi: 10.1523/jneurosci.4441-10.2011.

Shcherbakova, O.G., Hurt, C.M., Xiang, Y., Dell'Acqua, M.L., Zhang, Q., Tsien, R.W., et al. (2007). Organization of beta-adrenoceptor signaling compartments by sympathetic innervation of cardiac myocytes. *J Cell Biol* 176(4)**,** 521-533. doi: 10.1083/jcb.200604167.

Shen, M.J., and Zipes, D.P. (2014a). Role of the autonomic nervous system in modulating cardiac arrhythmias. *Circ Res* 114(6)**,** 1004-1021. doi: 10.1161/CIRCRESAHA.113.302549.

Shen, M.J., and Zipes, D.P. (2014b). Role of the Autonomic Nervous System in Modulating Cardiac Arrhythmias. *Circulation Research* 114(6)**,** 1004-1021. doi: 10.1161/CIRCRESAHA.113.302549.

Shimizu, W., and Antzelevitch, C. (1998). Cellular basis for the ECG features of the LQT1 form of the long-QT syndrome: effects of beta-adrenergic agonists and antagonists and sodium channel blockers on transmural dispersion of repolarization and torsade de pointes. *Circulation* 98(21)**,** 2314-2322. doi: 10.1161/01.cir.98.21.2314.

Si-Tayeb, K., Noto, F.K., Sepac, A., Sedlic, F., Bosnjak, Z.J., Lough, J.W., et al. (2010). Generation of human induced pluripotent stem cells by simple transient transfection of plasmid DNA encoding reprogramming factors. *BMC Dev Biol* 10**,** 81. doi: 10.1186/1471-213X-10-81.

Singh, C., and Roy-Chowdhuri, S. (2016). "Quantitative Real-Time PCR: Recent Advances," in *Clinical Applications of PCR,* eds. R. Luthra, R.R. Singh & K.P. Patel. (New York, NY: Springer New York), 161-176.

Singh, S., Johnson, P.I., Lee, R.E., Orfei, E., Lonchyna, V.A., Sullivan, H.J., et al. (1996). Topography of cardiac ganglia in the adult human heart. *J Thorac Cardiovasc Surg* 112(4)**,** 943-953. doi: 10.1016/s0022-5223(96)70094-6.

Sirabella, D., Cimetta, E., and Vunjak-Novakovic, G. (2015). "The state of the heart": Recent advances in engineering human cardiac tissue from pluripotent stem cells. *Exp Biol Med (Maywood)* 240(8)**,** 1008-1018. doi: 10.1177/1535370215589910.

Smolich, J. (1995). Ultrastructural and functional features of the developing mammalian heart – A brief overview. *Reproduction, fertility, and development* 7**,** 451-461. doi: 10.1071/RD9950451.

Snir, M., Kehat, I., Gepstein, A., Coleman, R., Itskovitz-Eldor, J., Livne, E., et al. (2003). Assessment of the ultrastructural and proliferative properties of human embryonic stem cell-derived cardiomyocytes. *Am J Physiol Heart Circ Physiol* 285(6)**,** H2355-2363. doi: 10.1152/ajpheart.00020.2003.

Sommer, C.A., and Mostoslavsky, G. (2010). Experimental approaches for the generation of induced pluripotent stem cells. *Stem Cell Res Ther* 1(3)**,** 26. doi: 10.1186/scrt26.

Sosunov, A.A., Hassall, C.J.S., Loesch, A., Turmaine, M., Fehér, E., and Burnstock, G. (1997). Neuropeptide Y-immunoreactive intracardiac neurones, granule-containing cells and nerves associated with ganglia and blood vessels in rat and guinea-pig heart. *Cell and Tissue Research* 289(3)**,** 445-454. doi: 10.1007/s004410050890.

Stadtfeld, M., and Hochedlinger, K. (2010). Induced pluripotency: history, mechanisms, and applications. *Genes Dev* 24(20)**,** 2239-2263. doi: 10.1101/gad.1963910.

Stadtfeld, M., Maherali, N., Breault, D.T., and Hochedlinger, K. (2008). Defining molecular cornerstones during fibroblast to iPS cell reprogramming in mouse. *Cell Stem Cell* 2(3)**,** 230-240. doi: 10.1016/j.stem.2008.02.001.

Staerk, J., Dawlaty, M.M., Gao, Q., Maetzel, D., Hanna, J., Sommer, C.A., et al. (2010). Reprogramming of human peripheral blood cells to induced pluripotent stem cells. *Cell Stem Cell* 7(1)**,** 20-24. doi: 10.1016/j.stem.2010.06.002.

Standish, A., Enquist, L.W., Escardo, J.A., and Schwaber, J.S. (1995). Central neuronal circuit innervating the rat heart defined by transneuronal transport of pseudorabies virus. *J Neurosci* 15(3 Pt 1)**,** 1998-2012. doi: 10.1523/jneurosci.15-03-01998.1995.

Steinbeck, G., Andresen, D., Bach, P., Haberl, R., Oeff, M., Hoffmann, E., et al. (1992). A comparison of electrophysiologically guided antiarrhythmic drug therapy with beta-blocker therapy in patients with symptomatic, sustained ventricular tachyarrhythmias. *N Engl J Med* 327(14)**,** 987-992. doi: 10.1056/nejm199210013271404.

Steinhauser, M.L., and Lee, R.T. (2011). Regeneration of the heart. *EMBO molecular medicine* 3(12)**,** 701-712. doi: 10.1002/emmm.201100175.

Stieber, J., Herrmann, S., Feil, S., Löster, J., Feil, R., Biel, M., et al. (2003). The hyperpolarization-activated channel HCN4 is required for the generation of pacemaker action potentials in the embryonic heart. *Proc Natl Acad Sci U S A* 100(25)**,** 15235-15240. doi: 10.1073/pnas.2434235100.

Streckfuss-Bomeke, K., Wolf, F., Azizian, A., Stauske, M., Tiburcy, M., Wagner, S., et al. (2013). Comparative study of human-induced pluripotent stem cells derived from bone marrow cells, hair keratinocytes, and skin fibroblasts. *Eur Heart J* 34(33)**,** 2618-2629. doi: 10.1093/eurheartj/ehs203.

Takahashi, K., Tanabe, K., Ohnuki, M., Narita, M., Ichisaka, T., Tomoda, K., et al. (2007). Induction of pluripotent stem cells from adult human fibroblasts by defined factors. *Cell* 131(5)**,** 861-872. doi: 10.1016/j.cell.2007.11.019.

Takahashi, K., and Yamanaka, S. (2006). Induction of pluripotent stem cells from mouse embryonic and adult fibroblast cultures by defined factors. *Cell* 126(4)**,** 663-676. doi: 10.1016/j.cell.2006.07.024.

Takayama, Y., and Kida, Y.S. (2016). In Vitro Reconstruction of Neuronal Networks Derived from Human iPS Cells Using Microfabricated Devices. *PloS one* 11(2)**,** e0148559-e0148559. doi: 10.1371/journal.pone.0148559.

Takayama, Y., Kushige, H., Akagi, Y., Suzuki, Y., Kumagai, Y., and Kida, Y.S. (2020). Selective Induction of Human Autonomic Neurons Enables Precise Control of Cardiomyocyte Beating. *Sci Rep* 10(1)**,** 9464. doi: 10.1038/s41598-020-66303-3.

Takeuchi, A., Mori, M., Kitagawa, K., Shimba, K., Takayama, Y., Moriguchi, H., et al. (2011a). Autonomic nervous system driven cardiomyocytes in vitro. *Conf Proc IEEE Eng Med Biol Soc* 2011**,** 1945-1948. doi: 10.1109/IEMBS.2011.6090549.

Takeuchi, A., Nakafutami, S., Tani, H., Mori, M., Takayama, Y., Moriguchi, H., et al. (2011b). Device for co-culture of sympathetic neurons and cardiomyocytes using microfabrication. *Lab Chip* 11(13)**,** 2268-2275. doi: 10.1039/c0lc00327a.

Takeuchi, A., Shimba, K., Mori, M., Takayama, Y., Moriguchi, H., Kotani, K., et al. (2012). Sympathetic neurons modulate the beat rate of pluripotent cell-derived cardiomyocytes in vitro. *Integr Biol (Camb)* 4(12)**,** 1532-1539. doi: 10.1039/c2ib20060k.

Takeuchi, A., Shimba, K., Takayama, Y., Kotani, K., Lee, J.K., Noshiro, M., et al. (2013). Microfabricated device for co-culture of sympathetic neuron and iPS-derived cardiomyocytes. *Conf Proc IEEE Eng Med Biol Soc* 2013**,** 3817-3820. doi: 10.1109/EMBC.2013.6610376.

Takigawa, M., Noda, T., Shimizu, W., Miyamoto, K., Okamura, H., Satomi, K., et al. (2008). Seasonal and circadian distributions of ventricular fibrillation in patients with Brugada syndrome. *Heart Rhythm* 5(11)**,** 1523-1527. doi: 10.1016/j.hrthm.2008.08.022.

Tan, A.Y., Li, H., Wachsmann-Hogiu, S., Chen, L.S., Chen, P.S., and Fishbein, M.C. (2006). Autonomic innervation and segmental muscular disconnections at the human pulmonary vein-atrial junction: implications for catheter ablation of atrial-pulmonary vein junction. *J Am Coll Cardiol* 48(1)**,** 132-143. doi: 10.1016/j.jacc.2006.02.054.

Tanaka, A., Yuasa, S., Mearini, G., Egashira, T., Seki, T., Kodaira, M., et al. Endothelin-1 Induces Myofibrillar Disarray and Contractile Vector Variability in Hypertrophic Cardiomyopathy–Induced Pluripotent Stem Cell–Derived Cardiomyocytes. *Journal of the American Heart Association* 3(6)**,** e001263. doi: 10.1161/JAHA.114.001263.

Tanaka, A., Yuasa, S., Node, K., and Fukuda, K. (2015). Cardiovascular Disease Modeling Using Patient-Specific Induced Pluripotent Stem Cells. *Int J Mol Sci* 16(8)**,** 18894-18922. doi: 10.3390/ijms160818894.

Tang, B.L. (2020). Maturing iPSC-Derived Cardiomyocytes. *Cells* 9(1). doi: 10.3390/cells9010213.

Tao, H., Han, Z., Han, Z.C., and Li, Z. (2016). Proangiogenic Features of Mesenchymal Stem Cells and Their Therapeutic Applications. *Stem Cells Int* 2016**,** 1314709. doi: 10.1155/2016/1314709.

Tao, Y., and Zhang, S.C. (2016). Neural Subtype Specification from Human Pluripotent Stem Cells. *Cell Stem Cell* 19(5)**,** 573-586. doi: 10.1016/j.stem.2016.10.015.

Terrenoire, C., Wang, K., Tung, K.W., Chung, W.K., Pass, R.H., Lu, J.T., et al. (2013). Induced pluripotent stem cells used to reveal drug actions in a long QT syndrome family with complex genetics. *J Gen Physiol* 141(1)**,** 61-72. doi: 10.1085/jgp.201210899.

Thaemert, J.C. (1966). Ultrastructure of cardiac muscle and nerve contiguities. *The Journal of cell biology* 29(1)**,** 156-162. doi: 10.1083/jcb.29.1.156.

Thaemert, J.C. (1970). Atrioventricular node innervation in ultrastructural three dimensions. *Am J Anat* 128(2)**,** 239-263. doi: 10.1002/aja.1001280209.

Thiene, G., Nava, A., Corrado, D., Rossi, L., and Pennelli, N. (1988). Right ventricular cardiomyopathy and sudden death in young people. *N Engl J Med* 318(3)**,** 129-133. doi: 10.1056/nejm198801213180301.

Ting, S., Chen, A., Reuveny, S., and Oh, S. (2014). An intermittent rocking platform for integrated expansion and differentiation of human pluripotent stem cells to cardiomyocytes in suspended microcarrier cultures. *Stem Cell Res* 13(2)**,** 202-213. doi: 10.1016/j.scr.2014.06.002.

Tiveron, M.C., Hirsch, M.R., and Brunet, J.F. (1996). The expression pattern of the transcription factor Phox2 delineates synaptic pathways of the autonomic nervous system. *J Neurosci* 16(23)**,** 7649-7660.

Tohyama, S., Hattori, F., Sano, M., Hishiki, T., Nagahata, Y., Matsuura, T., et al. (2013). Distinct metabolic flow enables large-scale purification of mouse and human pluripotent stem cell-derived cardiomyocytes. *Cell Stem Cell* 12(1)**,** 127-137. doi: 10.1016/j.stem.2012.09.013.

Tomaselli, G.F., and Zipes, D.P. (2004). What causes sudden death in heart failure? *Circ Res* 95(8)**,** 754-763. doi: 10.1161/01.RES.0000145047.14691.db.

Tomita, T., Takei, M., Saikawa, Y., Hanaoka, T., Uchikawa, S., Tsutsui, H., et al. (2003). Role of autonomic tone in the initiation and termination of paroxysmal atrial fibrillation in patients without structural heart disease. *J Cardiovasc Electrophysiol* 14(6)**,** 559-564. doi: 10.1046/j.1540-8167.2003.02462.x.

Turnbull, I.C., Mayourian, J., Murphy, J.F., Stillitano, F., Ceholski, D.K., and Costa, K.D. (2018). Cardiac Tissue Engineering Models of Inherited and Acquired Cardiomyopathies. *Methods Mol Biol* 1816**,** 145-159. doi: 10.1007/978-1-4939-8597-5_11.

Urbán, N., and Guillemot, F. (2014). Neurogenesis in the embryonic and adult brain: Same regulators, different roles. *Frontiers in Cellular Neuroscience* 8(NOV). doi: 10.3389/fncel.2014.00396.

Vacanti, C.A. (2006). The history of tissue engineering. *J Cell Mol Med* 10(3)**,** 569-576. doi: 10.1111/j.1582-4934.2006.tb00421.x.

Vacanti, C.A., and Vacanti, J.P. (1991). Functional Organ Replacement, The New Technology of Tissue Engineering. *Surg Technol Int* I**,** 43-49.

Vanhoutte, P.M., and Levy, M.N. (1980). Prejunctional cholinergic modulation of adrenergic neurotransmission in the cardiovascular system. *Am J Physiol* 238(3)**,** H275-281. doi: 10.1152/ajpheart.1980.238.3.H275.

VanPatten, S., and Al-Abed, Y. (2017). The challenges of modulating the 'rest and digest' system: acetylcholine receptors as drug targets. *Drug Discov Today* 22(1)**,** 97-104. doi: 10.1016/j.drudis.2016.09.011.

Vats, A., Bielby, R.C., Tolley, N., Dickinson, S.C., Boccaccini, A.R., Hollander, A.P., et al. (2006). Chondrogenic differentiation of human embryonic stem cells: the effect of the micro-environment. *Tissue Eng* 12(6)**,** 1687-1697. doi: 10.1089/ten.2006.12.1687.

Veerman, C.C., Kosmidis, G., Mummery, C.L., Casini, S., Verkerk, A.O., and Bellin, M. (2015). Immaturity of human stem-cell-derived cardiomyocytes in culture: fatal flaw or soluble problem? *Stem Cells Dev* 24(9)**,** 1035-1052. doi: 10.1089/scd.2014.0533.

Verrier, R.L., and Antzelevitch, C. (2004). Autonomic aspects of arrhythmogenesis: the enduring and the new. *Curr Opin Cardiol* 19(1)**,** 2-11. doi: 10.1097/00001573-200401000-00003.

Verrier, R.L., and Josephson, M.E. (2009). Impact of sleep on arrhythmogenesis. *Circ Arrhythm Electrophysiol* 2(4)**,** 450-459. doi: 10.1161/circep.109.867028.

Vieira, M.S., Santos, A.K., Vasconcellos, R., Goulart, V.A.M., Parreira, R.C., Kihara, A.H., et al. (2018). Neural stem cell differentiation into mature neurons: Mechanisms of regulation and biotechnological applications. *Biotechnol Adv* 36(7)**,** 1946-1970. doi: 10.1016/j.biotechadv.2018.08.002.

Virág, L., Iost, N., Opincariu, M., Szolnoky, J., Szécsi, J., Bogáts, G., et al. (2001). The slow component of the delayed rectifier potassium current in undiseased human ventricular myocytes. *Cardiovasc Res* 49(4)**,** 790-797. doi: 10.1016/s0008-6363(00)00306-0.

Wang, B., Zhao, M.Z., Cui, N.P., Lin, D.D., Zhang, A.Y., Qin, Y., et al. (2015). Kruppel-like factor 4 induces apoptosis and inhibits tumorigenic progression in SK-BR-3 breast cancer cells. *FEBS Open Bio* 5**,** 147-154. doi: 10.1016/j.fob.2015.02.003.

Wang, T., Kang, W., Du, L., and Ge, S. (2017). Rho-kinase inhibitor Y-27632 facilitates the proliferation, migration and pluripotency of human periodontal ligament stem cells. *Journal of cellular and molecular medicine* 21(11)**,** 3100-3112. doi: 10.1111/jcmm.13222.

Wang, W., Lin, C., Lu, D., Ning, Z., Cox, T., Melvin, D., et al. (2008). Chromosomal transposition of PiggyBac in mouse embryonic stem cells. *Proc Natl Acad Sci U S A* 105(27)**,** 9290-9295. doi: 10.1073/pnas.0801017105.

Wang, Y., Liu, J., Tan, X., Li, G., Gao, Y., Liu, X., et al. (2013). Induced pluripotent stem cells from human hair follicle mesenchymal stem cells. *Stem Cell Rev Rep* 9(4)**,** 451-460. doi: 10.1007/s12015-012-9420-5.

Wanjare, M., and Huang, N.F. (2017). Regulation of the microenvironment for cardiac tissue engineering. *Regen Med* 12(2)**,** 187-201. doi: 10.2217/rme-2016-0132.

Warren, L., Manos, P.D., Ahfeldt, T., Loh, Y.H., Li, H., Lau, F., et al. (2010). Highly efficient reprogramming to pluripotency and directed differentiation of human cells with synthetic modified mRNA. *Cell Stem Cell* 7(5)**,** 618-630. doi: 10.1016/j.stem.2010.08.012.

Weick, J.P., Held, D.L., Bonadurer, G.F., 3rd, Doers, M.E., Liu, Y., Maguire, C., et al. (2013). Deficits in human trisomy 21 iPSCs and neurons. *Proc Natl Acad Sci U S A* 110(24)**,** 9962-9967. doi: 10.1073/pnas.1216575110.

Weinberger, F., Mannhardt, I., and Eschenhagen, T. (2017). Engineering Cardiac Muscle Tissue: A Maturating Field of Research. *Circ Res* 120(9)**,** 1487-1500. doi: 10.1161/CIRCRESAHA.117.310738.

Wernig, M., Lengner, C.J., Hanna, J., Lodato, M.A., Steine, E., Foreman, R., et al. (2008). A drug-inducible transgenic system for direct reprogramming of multiple somatic cell types. *Nat Biotechnol* 26(8)**,** 916-924. doi: 10.1038/nbt1483.

Wichter, T., Borggrefe, M., Haverkamp, W., Chen, X., and Breithardt, G. (1992). Efficacy of antiarrhythmic drugs in patients with arrhythmogenic right ventricular disease. Results in patients with inducible and noninducible ventricular tachycardia. *Circulation* 86(1)**,** 29-37. doi: 10.1161/01.cir.86.1.29.

Wichter, T., Matheja, P., Eckardt, L., Kies, P., Schäfers, K., Schulze-Bahr, E., et al. (2002). Cardiac autonomic dysfunction in Brugada syndrome. *Circulation* 105(6)**,** 702-706. doi: 10.1161/hc0602.103677.

Wichter, T., Schäfers, M., Rhodes, C.G., Borggrefe, M., Lerch, H., Lammertsma, A.A., et al. (2000). Abnormalities of cardiac sympathetic innervation in arrhythmogenic right ventricular cardiomyopathy : quantitative assessment of presynaptic norepinephrine reuptake and postsynaptic beta-adrenergic receptor density with positron emission tomography. *Circulation* 101(13)**,** 1552-1558. doi: 10.1161/01.cir.101.13.1552.

Wijffels, M.C., Kirchhof, C.J., Dorland, R., and Allessie, M.A. (1995). Atrial fibrillation begets atrial fibrillation. A study in awake chronically instrumented goats. *Circulation* 92(7)**,** 1954-1968. doi: 10.1161/01.cir.92.7.1954.

Wilde, A.A., Antzelevitch, C., Borggrefe, M., Brugada, J., Brugada, R., Brugada, P., et al. (2002). Proposed diagnostic criteria for the Brugada syndrome: consensus report. *Circulation* 106(19)**,** 2514-2519. doi: 10.1161/01.cir.0000034169.45752.4a.

Willardsen, M.I., and Link, B.A. (2011). Cell biological regulation of division fate in vertebrate neuroepithelial cells. *Dev Dyn* 240(8)**,** 1865-1879. doi: 10.1002/dvdy.22684.

Winbo, A., Ramanan, S., Eugster, E., Jovinge, S., Skinner, J.R., and Montgomery, J.M. (2020). Functional coculture of sympathetic neurons and cardiomyocytes derived from human-induced pluripotent stem cells. *Am J Physiol Heart Circ Physiol* 319(5)**,** H927-h937. doi: 10.1152/ajpheart.00546.2020.

Wu, H.F., and Zeltner, N. (2019). Overview of Methods to Differentiate Sympathetic Neurons from Human Pluripotent Stem Cells. *Curr Protoc Stem Cell Biol* 50(1)**,** e92. doi: 10.1002/cpsc.92.

Wu, H.F., and Zeltner, N. (2020). Efficient Differentiation of Postganglionic Sympathetic Neurons using Human Pluripotent Stem Cells under Feeder-free and Chemically Defined Culture Conditions. *J Vis Exp* (159). doi: 10.3791/60843.

Xu, X.Q., Soo, S.Y., Sun, W., and Zweigerdt, R. (2009). Global expression profile of highly enriched cardiomyocytes derived from human embryonic stem cells. *Stem Cells* 27(9)**,** 2163-2174. doi: 10.1002/stem.166.

Yagi, T., Ito, D., Okada, Y., Akamatsu, W., Nihei, Y., Yoshizaki, T., et al. (2011). Modeling familial Alzheimer's disease with induced pluripotent stem cells. *Hum Mol Genet* 20(23)**,** 4530-4539. doi: 10.1093/hmg/ddr394.

Yang, L., Soonpaa, M.H., Adler, E.D., Roepke, T.K., Kattman, S.J., Kennedy, M., et al. (2008). Human cardiovascular progenitor cells develop from a KDR+ embryonic-stem-cell-derived population. *Nature* 453(7194)**,** 524-528. doi: 10.1038/nature06894.

Yang, X., Pabon, L., and Murry, C.E. (2014). Engineering adolescence: maturation of human pluripotent stem cell-derived cardiomyocytes. *Circ Res* 114(3)**,** 511-523. doi: 10.1161/CIRCRESAHA.114.300558.

Yanowitz, F., Preston, J.B., and Abildskov, J.A. (1966). Functional distribution of right and left stellate innervation to the ventricles. Production of neurogenic electrocardiographic changes by unilateral alteration of sympathetic tone. *Circ Res* 18(4)**,** 416-428. doi: 10.1161/01.res.18.4.416.

Yazawa, M., Hsueh, B., Jia, X., Pasca, A.M., Bernstein, J.A., Hallmayer, J., et al. (2011). Using induced pluripotent stem cells to investigate cardiac phenotypes in Timothy syndrome. *Nature* 471(7337)**,** 230-234. doi: 10.1038/nature09855.

Yoshida, Y., and Yamanaka, S. (2017). Induced Pluripotent Stem Cells 10 Years Later: For Cardiac Applications. *Circ Res* 120(12)**,** 1958-1968. doi: 10.1161/CIRCRESAHA.117.311080.

Young, Richard A. (2011). Control of the Embryonic Stem Cell State. *Cell* 144(6)**,** 940-954. doi: https://doi.org/10.1016/j.cell.2011.01.032.

Yu, J., Hu, K., Smuga-Otto, K., Tian, S., Stewart, R., Slukvin, II, et al. (2009). Human induced pluripotent stem cells free of vector and transgene sequences. *Science* 324(5928)**,** 797-801. doi: 10.1126/science.1172482.

Yu, J., Vodyanik, M.A., Smuga-Otto, K., Antosiewicz-Bourget, J., Frane, J.L., Tian, S., et al. (2007). Induced pluripotent stem cell lines derived from human somatic cells. *Science* 318(5858)**,** 1917-1920. doi: 10.1126/science.1151526.

Zaccolo, M., and Pozzan, T. (2002). Discrete microdomains with high concentration of cAMP in stimulated rat neonatal cardiac myocytes. *Science* 295(5560)**,** 1711-1715. doi: 10.1126/science.1069982.

Zaglia, T., Di Bona, A., and Mongillo, M. (2019). A Light Wand to Untangle the Myocardial Cell Network. *Methods and Protocols* 2(2). doi: 10.3390/mps2020034.

Zaglia, T., and Mongillo, M. (2017). Cardiac sympathetic innervation, from a different point of (re)view. *The Journal of physiology* 595(12)**,** 3919-3930. doi: 10.1113/JP273120.

Zamani, M., Karaca, E., and Huang, N.F. (2018). Multicellular Interactions in 3D Engineered Myocardial Tissue. *Front Cardiovasc Med* 5**,** 147. doi: 10.3389/fcvm.2018.00147.

Zeltner, N., Fattahi, F., Dubois, N.C., Saurat, N., Lafaille, F., Shang, L., et al. (2016). Capturing the biology of disease severity in a PSC-based model of familial dysautonomia. *Nat Med* 22(12)**,** 1421-1427. doi: 10.1038/nm.4220.

Zeltner, N., Lafaille, F.G., Fattahi, F., and Studer, L. (2014). Feeder-free derivation of neural crest progenitor cells from human pluripotent stem cells. *J Vis Exp* (87). doi: 10.3791/51609.

Zhang, J., Klos, M., Wilson, G.F., Herman, A.M., Lian, X., Raval, K.K., et al. (2012a). Extracellular matrix promotes highly efficient cardiac differentiation of human pluripotent stem cells: the matrix sandwich method. *Circ Res* 111(9)**,** 1125-1136. doi: 10.1161/CIRCRESAHA.112.273144.

Zhang, J., Wilson, G.F., Soerens, A.G., Koonce, C.H., Yu, J., Palecek, S.P., et al. (2009). Functional cardiomyocytes derived from human induced pluripotent stem cells. *Circ Res* 104(4)**,** e30-41. doi: 10.1161/CIRCRESAHA.108.192237.

Zhang, M., Schulte, J.S., Heinick, A., Piccini, I., Rao, J., Quaranta, R., et al. (2015). Universal cardiac induction of human pluripotent stem cells in two and three-dimensional

formats: implications for in vitro maturation. *Stem Cells* 33(5)**,** 1456-1469. doi: 10.1002/stem.1964.

Zhang, N., An, M.C., Montoro, D., and Ellerby, L.M. (2010). Characterization of Human Huntington's Disease Cell Model from Induced Pluripotent Stem Cells. *PLoS Curr* 2**,** Rrn1193. doi: 10.1371/currents.RRN1193.

Zhang, P., Su, J., and Mende, U. (2012b). Cross talk between cardiac myocytes and fibroblasts: from multiscale investigative approaches to mechanisms and functional consequences. *Am J Physiol Heart Circ Physiol* 303(12)**,** H1385-1396. doi: 10.1152/ajpheart.01167.2011.

Zhou, H., Wu, S., Joo, J.Y., Zhu, S., Han, D.W., Lin, T., et al. (2009). Generation of induced pluripotent stem cells using recombinant proteins. *Cell Stem Cell* 4(5)**,** 381-384. doi: 10.1016/j.stem.2009.04.005.

Zhou, S., Chen, L.S., Miyauchi, Y., Miyauchi, M., Kar, S., Kangavari, S., et al. (2004). Mechanisms of cardiac nerve sprouting after myocardial infarction in dogs. *Circ Res* 95(1)**,** 76-83. doi: 10.1161/01.RES.0000133678.22968.e3.

Zhou, Y., Wang, L., Liu, Z., Alimohamadi, S., Yin, C., Liu, J., et al. (2017). Comparative Gene Expression Analyses Reveal Distinct Molecular Signatures between Differentially Reprogrammed Cardiomyocytes. *Cell Rep* 20(13)**,** 3014-3024. doi: 10.1016/j.celrep.2017.09.005.

Zhou, Y.Y., and Zeng, F. (2013). Integration-free methods for generating induced pluripotent stem cells. *Genomics Proteomics Bioinformatics* 11(5)**,** 284-287. doi: 10.1016/j.gpb.2013.09.008.

Zipes, D.P. (1991). The long QT interval syndrome. A Rosetta stone for sympathetic related ventricular tachyarrhythmias. *Circulation* 84(3)**,** 1414-1419. doi: 10.1161/01.cir.84.3.1414.

ZIPES, D.P., FESTOFF, B., SCHAAL, S.F., COX, C., SEALY, W.C., and WALLACE, A.G. (1968). Treatment of Ventricular Arrhythmia by Permanent Atrial Pacemaker and Cardiac Sympathectomy. *Annals of Internal Medicine* 68(3)**,** 591-597. doi: 10.7326/0003-4819-68-3-591.

Zuppinger, C. (2019). 3D Cardiac Cell Culture: A Critical Review of Current Technologies and Applications. *Front Cardiovasc Med* 6**,** 87. doi: 10.3389/fcvm.2019.00087.